August 2013

Ph.D. Dissertation

Expression of Cowpea Chlorotic Mottle Virus Capsids in *Pichia pastoris* and their Application in Nanotechnology

Graduate School of Chosun University

Department of Chemical Engineering

Yuanzheng Wu

Expression of Cowpea Chlorotic Mottle Virus Capsids in *Pichia pastoris* and their Application in Nanotechnology

23rd August 2013

Graduate School of Chosun University

Department of Chemical Engineering

Yuanzheng Wu

Expression of Cowpea Chlorotic Mottle Virus Capsids in *Pichia pastoris* and their Application in Nanotechnology

Advisor: Prof. Hyun-Jae Shin

This dissertation is submitted to the Department of Chemical Engineering and the Graduate School of Chosun University in fulfilment of the requirements for the degree of Doctor of Philosophy

April 2013

Graduate School of Chosun University

Department of Chemical Engineering

Yuanzheng Wu

This is to certify that the Ph.D. dissertation of Yuanzheng Wu has successfully met the dissertation requirements of Chosun University.

Chairman : Prof. Jung-Gyu Kim .....

Committee Member : Prof. Jung-Heon Lee .....

Committee Member : Prof. Young-Jin Jeon .....

Committee Member : Prof. Geun-Joong Kim .....

Committee Member : Prof. Hyun-Jae Shin .....

June 2013

Graduate School of Chosun University

Contents

List of Tables

Chapter 3

Chapter 6

Appendix II

List of Figures

Chapter 1

Chapter 2

Chapter 3

Chapter 4

Chapter 5

Appendix I

Appendix II

Abstract

Expression of Cowpea Chlorotic Mottle Virus Capsids in *Pichia pastoris* and their Application in Nanotechnology

Yuanzheng Wu

Advisor: Prof. Hyun-Jae Shin, Ph.D.

Department of Chemical Engineering

Graduate School of Chosun University

Viruses and noninfectious virus-like particles (VLPs) exhibit the characteristics of ideal building blocks with highly symmetrical, polyvalent, and monodisperse structures for their utilization in nanotechnology. Cowpea chlorotic mottle virus (CCMV) is icosahedral virus with a diameter of 28 nm which has been a model system for virus studies for over 40 years. Recently CCMV has been considered to be a perfect candidate as nanoplatform for applications in materials science and medicine. The ability of CCMV to self-assemble into VLPs *in vitro* makes it suitable reaction vessel for nanomaterial encapsulation and modification.

Chapter-1 of this thesis is the general introduction of virus and virus capsids, and their applications in nanotechnology.

Chapter-2 is the backgrounds and objectives concerning the originality of the thesis.

In Chapter-3, the coat protein (CP) gene of CCMV was firstly optimized according to codon perference and expressed in *Pichia pastoris* GS115. The synthesized CP gene (573 bp) was cloned into *Pichia* shuttle vector pPICZ A under the alcohol oxidase I (AOX1) promoter. The recombinant plasmid pPICZ A-CPsyns was transformed into *P. pastoris* GS115 by electroporation. The resulting yeast colonies were screened by PCR and analyzed for protein expression by SDS-PAGE. Transformant GS115-27-6 was selected for scale-up fermentation in 5-L fermenter and CCMV CP yields reached up to 4.8 mg/mL. The CCMV VLPs were purified by modified poly(ethylene glycol) (PEG) precipitation followed by cesium chloride density gradient ultracentrifugation. The assembled CCMV VLPs were analyzed by UV spectrometry and transmission electron microscopy (TEM). The resulting data indicated the production of CCMV capsids by *P. pastoris* fermentation available for utilization in pharmacology or nanotechnology fields.

In Chapter-4, CCMV capsids were employed to encapsulate Prussian blue (PB, $MFe^{III}[Fe^{II}(CN)_6]$ (M = NH_4, Li, Na, K)) particles based on electrostatic interaction. A negatively charged metal complex, hexacyanoferrate (III), was entrapped inside the capsids through the disassembly/reassembly process under pH change from 7.5 to 5.2. The loaded capsids acted as nanoreactors because the metal complex could react with a second metal ion, iron (II), to fabricate PB particles in protein cages. The synthesis of PB in CCMV capsids was confirmed by unique colour transition of Prussian blue, UV-vis spectrum at 710 nm, and size exclusion fast protein liquid chromatography (FPLC). TEM image PB-CCMV biohybrids presented discrete spherical particles with relatively homogeneous size. The hydrodynamic diameters of PB-CCMV were measured by dynamic light scattering (DLS) showing two peaks of 29.2±1.7 nm corresponding to $T = 3$ particles, and 17.5±1.2 nm corresponding to pseudo $T = 2$ particles. The encapsulation and synthesis of PB in CCMV

provided a fast and efficient method for the self-organization of homo- and heterobimetallic nanoparticles.

In Chapter-5, copper(I)-catalyzed azide-alkyne cycloaddition (CuAAC) reaction was exploited to the exterior surface of CCMV for the first time. The exposed carboxyl residues of CCMV were addressed with alkyne and further modified with azide through triazole connection in the presence of $CuSO_4$, TCEP, and BCDS. Fluorogenic coumarin was successfully grafted on CCMV and monitored by FPLC and UV irradiated SDS-PAGE. Oligo-ethylene glycol (OEG) short chain and RGD (Arg-Gly-Asp) peptide were also installed on CCMV via CuAAC reaction. FPLC, TEM, and DLS analysis verified the modification and integrity of viral capsids. Interestingly OEG-CCMV displayed a distinct phenomenon of connected bridges with the intact capsids cross-linked with each other. Wild type CCMV, OEG-CCMV, and RGD-CCMV were absorbed onto APTES slides for the cell binding with HeLa cells. The opposite adhesion behaviors between OEG-CCMV and RGD-CCMV indicated the inhibition effect of OEG and promotion effect of RGD on cell attachment. As the most widely recognized example of click chemistry, CuAAC reaction paved a brilliant way for the design of bionanoparticle-based nanosensor, drug delivery carrier, and tissue engineering materials.

In the appendix I, *Heterocapsa circularisquama* RNA virus (HcRNAV) 109 CP gene was expressed in *P. pastoris* using the same strategy as CCMV. The encapsulation of fluorescence dye-labeled myoglobin by self-assembled HcRNAV capsids demonstrated potential application in the harmful algae blooms (HABs) control. The co-expression of HcRNAV CP and algicidal peptide PMAP-23-D7 was also accomplished with a structure transition from polyhedral to rod-like particles which might stem from the insertion of PMAP-23-D7 at N-terminus of HcRNAV CP.

In the appendix II, an efficient method for *Pichia* cell disruption that employed aminopropyl magnesium phyllosilicate (AMP) clay-assisted glass beads mill was presented. AMP clay is functionalized nanocomposite resembling the talc parent structure $Si_8Mg_6O_{20}(OH)_4$. The total protein concentration reached 4.24 mg/mL after 4 minutes treatment by glass beads mill combined with 0.2 % AMP clay, which was 11.2 % higher compared to glass beads mill only and the time was half shortened. The stability of purified CCMV VLPs illustrated it could be a reliable method for the disruption of yeast cell.

In conclusion, the expression of virus capsids in *P. pastoris* was established as a simple and efficient approach. The encapsulation and modification of the capsids were achieved for their applications in pharmaceutics and nanotechnology.

Chapter 1. Introduction

Bionanotechnology or nanobiotechnology has become a rapidly developing area of science research for its tremendous potential applications [Soto and Ratna, 2010; Wu et al., 2013]. Biological materials that display an astonishing variety of highly sophisticated architectures are appropriate nanostructures for new material development [Uchida et al., 2007]. Their prescribed shape together with the chemical and physical functionality provides huge advantages over other inorganic and organic substances [Sotiropoulou et al., 2008]. The self-assembled natural protein complexes, such as viruses and virus-based nanoparticles (VNPs), ferritins [Meldrum et al., 1991], small heat shock protein [Kim et al., 1998], and enzyme complexes [Domingo et al., 2001], have been employed as building blocks and templates in bionanotechnology since last decade. These bionanoparticles (BNPs) can form robust biosynthetic machineries while still being capable of modification by genetic and chemical approaches [Lee et al., 2009].

Recently there have been some detailed researches which summarize the remarkable progress of virus and virus capsids in biomedicine and anomaterial research. In this chapter, we present the general introduction on virus and virus capsids and their utilizations both in the encapsulation and surface modification with functional materials.

1.1 Virus and virus capsids

Virus is an infective agent that typically consists of a nucleic acid molecule in a protein coat, is too small to be seen by light microscopy, and is able to multiply only within the living cells of a host [Dimmock et al., 2009]. As the most abundant biological entities on earth, viruses play a key role in biological systems [Suttle, 2005]. Virus-like particles (VLPs) are multi-subunit protein complexes capable of self-assembly, forming structures that mimic the 3D conformation of native viruses. For lacking viral genetic material, VLPs are non-

infectious and unable to replicate [Edwards and Rohwer, 2005]. Viruses and VLPs exhibit the characteristics of ideal building blocks with highly symmetrical, polyvalent, and monodisperse structures which makes them widely used as emerging platforms in bionanotechnology [Rodríguez-Limas et al., 2013].

Virus capsid is the protein shell of a virus which is consisted of several oligomeric structural protein subunits (capsomeres) [Dimmock et al., 2009]. The capsid encloses genetic materials and protects them from ambient environments. According to their structure capsids are broadly classified into icosahedral, helical and complex structure [Nguyen et al., 2005]. Viruses exhibit a distinctive diversity of shapes and sizes ranging between 20 and 750 nanometers [Knipe et al., 2007]. Various viruses and VLPs that have been studied in the field of nanotechnology are shown in Fig. 1.1.

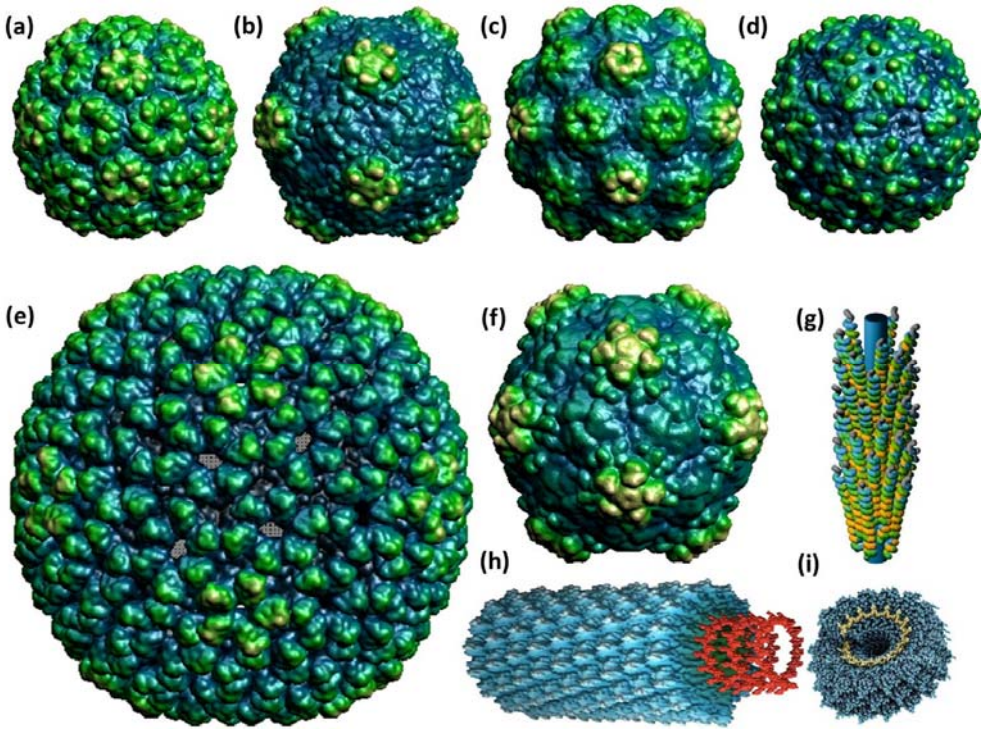

Fig. 1.1 Structures of virus particles used for nanotechnology. (a) Cowpea chlorotic mottle virus (CCMV), 28 nm in diameter; (b) Cowpea mosaic virus (CPMV), 30 nm in diameter; (c) Turnip yellow mosaic virus (TYMV), 30 nm in diameter; (d) Bacteriophage MS2, 26 nm in diameter; (e) Bacteriophage P22, 58 nm in diameter; (f) Red clover necrotic mosaic virus (RCNMV), 36 nm in diameter; (g) Bacteriophage M13, 6 nm in diameter and variable in length; (h) Tobacco mosaic virus (TMV), 18 nm in diameter and variable in length; (i) top view of TMV. Structures (a)-(f) were obtained from the VIPER, URL: http://www.viperdb.scripps.edu/; M13 image by Hemminga et al. *Eur. Biophys. J.* 39 (2010); TMV image by Jean-Yves Sgro, U. Wisconsin.

Icosahedral virus particles are nearly spherical in shape and exhibit icosahedral symmetry in their arrangement [Knipe et al., 2007; Dimmock et al., 2009]. The icosahedron is composed of equilateral triangles fused together into capsid, which generally has 20 facets and 12 vertices formed by one or several identical coat protein (CP) subunits. The spherical lattices are collections of two-, three-, and fivefold rotation axes (5:3:2 symmetry). The capsid usually assembles from 60- and 180-comma structures of pentamers and hexamers. The quasi-equivalence principle of protein subunits and their three-dimensional arrangement is illustrated by the triangulation number (*T*) which was originally proposed by Caspar and Klug [Caspar and Klug, 1962]. Icosahedral viruses can self-assemble spontaneously into capsids with diameter about 20–80 nm and the size of capsids depends on the size and number of capsomeres. The interior cavity of these cages offers the capacity to package genomic materials or encapsulate other particles. The widely studied icosahedral viruses include brome mosaic virus (BMV), cowpea chlorotic mottle virus (CCMV), cowpea mosaic virus (CPMV), red clover necrotic mosaic virus (RCNMV), turnip yellow mosaic virus (TYMV), bacteriophage MS2, and bacteriophage P22.

Helical viruses are comprised of a single type of capsomere stacked around a central axis to form a helical structure, which result in a central cavity or hollow tube [Knipe et al., 2007; Dimmock et al., 2009]. These viral helix arrangements are rod-shaped or filamentous, being either short and highly rigid or long and very flexible. The genetic material, generally single-stranded RNA (ssRNA), though ssDNA observed in some cases, is enmeshed by the protein helix through interactions between the negatively charged nucleic acid and positive charged protein [Hemminga et al., 2010]. Helical particles are typically about 15–30 nm in diameter, and their lengths may range from 300 to 500 nm depending on the genome size. Overall, the length of a helical capsid is determined by the length of the nucleic acid and the

diameter is dependent on the arrangement and dimensions of capsomeres. Bacteriophage M13 and tobacco mosaic virus (TMV) are the standing examples of helical viruses.

Complex viruses usually have a combination of icosahedral and helical shape and contain extra appendages and structures such as protein tails and/or complex exterior surfaces [Knipe et al., 2007; Dimmock et al., 2009]. The head–tail morphology structure comprising an icosahedral head bound to a helical tail is unique to bacteriophages that only infect bacteria. The bacteriophage uses its tail to attach to the bacterium and insert its viral genome into the cell like a molecular syringe. The poxvirus is one of the largest viruses in size and has a complex structure with an outer envelope with a thick layer of protein studded over its surface [Gubser et al., 2004].

Due to the well-defined structure and self-assembling system, a large number of viruses and virus capsids have been elaborated to function as constrained reaction vessels, imaging agents, drug/gene delivery vehicles, and other nanomaterials [Vriezema et al., 2005; Steinmetz and Evans, 2007]. Most VLPs used for encapsulation/modification in chemical/microbiological manner belong to the class of plant viruses. The reason behind this lies in their easy availability and non-pathogenic behavior towards humans.

1.1.1 CCMV

Cowpea chlorotic mottle virus (CCMV) is a model plant virus belonging to the *Bromovirus* group of *Bromoviradea* family [Bancroft et al., 1967]. The capsid consists of 180 copies of a single protein (20 kDa, 190 amino acids) that form an icosahedral shell with an outer diameter of 28 nm and an inner diameter of 18 nm ($T = 3$ symmetry) [Chen et al., 1990]. The low-resolution structure of CCMV has been determined by electron cryo-microscopy (cryo-EM) at 3.2 Å [Speir et al., 1993]. The most useful information that has been derived from these studies is the location of the epitopes and the relative orientation of the attached

molecules with respect to the viral capsid. The quaternary structure of CCMV displays 32 prominent capsomeres: 12 pentamers and 20 hexamers as shown in Fig. 1.2 [Speir, 1994].

CCMV was the first icosahedral virus to be reassembled *in vitro* into an infectious particle from wild-type purified components, i.e., the coat protein and genome RNA [Allison et al., 1988]. The most profound property of CCMV is that the viral capsid can undergo reversible structural transition depending on pH and ionic strength [Speir et al., 1995]. The capsid expands into a radially swollen state around 10 % when pH increases from 5 to 6.5 under low ionic strength ($I < 0.1$ M). The swelling capsid with 60 separate open pores of 2-nm diameter permits to ions diffuse freely into and out of the cavity. The capsid then disassembles into protein dimers and RNA under high pH (above 7) and ionic strength ($I \sim 1$ M). After removal of RNA and with a change in pH, the purified coat protein subunits will easily self-assemble and reform the empty capsids as presented in Fig. 1.3 [Tama and Brooks, 2002]. This characteristic provides a unique molecular gating mechanism for entrapment of organic or inorganic materials and release of entrapped materials.

In CCMV, the surface charge arises from the acidic amino acid residues, aspartic acid (Asp, D) and glutamic acid (Glu, E), which lie predominantly on the capsid exterior. In contrast most of the basic residues, lysine (Lys, K) and arginine (Arg, R), are near the amino terminus and project into the capsid interior [Gillitzer et al., 2002]. A simple calculation of the pH dependence of the charge on a CCMV capsid on the pH from the pK_a values of the isolated residues in which the contribution of the basic (largely interior) lysine and arginine residues is omitted-gives an isoelectric point (pI) of 3.6, which is essentially identical to that of CCMV [Johnson and Speir, 1997].

The high yield of CCMV capsid from natural infected leaf tissue (ca. 1–2 mg/g) capsid makes it suitable for the development of viral-based protein cage [Bancroft and Hiebert, 1967]. Furthermore, heterologous expression of the coat protein in *Escherichia coli* [Zhao et

al., 1995], *Pseudomonas fluorescens* [Phelps et al., 2007], and *Pichia pastoris* [Brumfield et al., 2004] allows genetic alteration by site-directed mutagenesis. The wild and mutant-type of CCMV capsids are tolerant of high temperatures and various pH's, stable in organic solvents (e.g., DMSO), and non-pathogenic for mammals. These conspicuous properties enhance a wide range of applications of CCMV capsids in nanotechnology from encapsulation to modification.

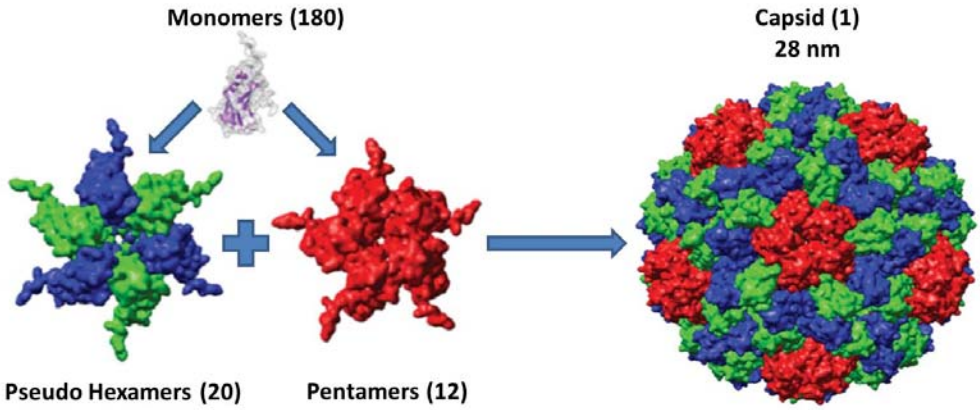

Fig. 1.2 Schematic representation of CCMV capsid formation by the coat protein monomers.

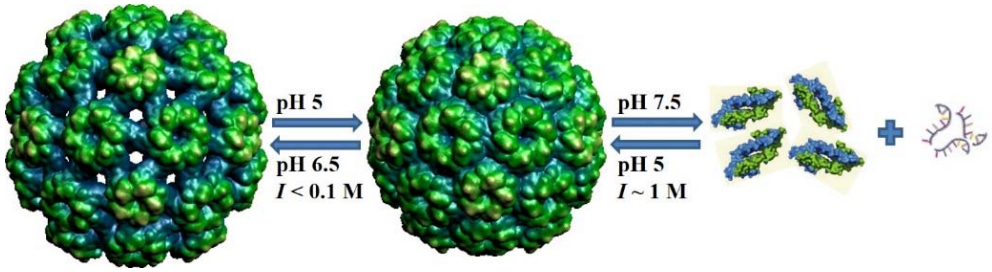

Fig. 1.3 Schematic representation of CCMV structure transition. With pH increasing from 5 to 6.5 under low ionic strength (I < 0.1 M), CCMV capsid expands into a swollen state; when pH increased to 7.5 under high ionic strength (*I* ~ 1 M), the capsid disassembles into protein dimers and viral RNA. With/without the removal of RNA and pH lowering to 5, the protein dimers can be reassembled into empty/intact capsid.

1.1.2 CPMV

CPMV is an icosahedral plant virus of the family *Comoviridae*, which infects black eyed pea plants (*Vigna unguiculata*) [van Kammen, 1967]. It can be easily purified in the range of 0.8–1.0 mg/g of leaves [Porta et al., 2003]. The capsid measuring 30 nm in diameter is composed of 60 copies of an asymmetric unit that is made of a small (S) and a large (L) subunit. The S and L subunits each are made up of a single polypeptide chain, which is folded into one and two jelly roll β sandwich domains, respectively [Lin et al., 1999]. CPMV is stable in a wide range of temperature, pH, and buffers, making this viral platform ideal for various bioconjugation methods and nanotechnological applications [Wang et al., 2002]. The CPMV surface-exposed lysines have been investigated extensively for attachment of molecules [Wang et al., 2002]. Furthermore, an azide-alkyne ‘‘click’’ conjugation has been employed on CPMV to more specifically and efficiently link ligands to the capsid surface [Wang et al., 2003; Gupta et al., 2005]. Together these techniques have provided many ways for conjugating various types of ligands to viral nanoparticles.

1.1.3 TMV

Tobacco mosaic virus (TMV), also known as tobamovirus, is a helical plant virus with a length of 300 nm and diameter of 18 nm [Kay, 1986]. TMV was the first virus to be discovered in the late 19th century. Its capsid is made from 2130 copies of coat protein arranged around the viral RNA. The rod-like spiraling structure (16.3 proteins per helix turn) shows a distinct inner channel of 4 nm [Klug, 1999]. Purified TMV coat protein undergoes a reversible states shift from micron-length rods in acetate buffer (pH 5.5) to double disks in phosphate buffer (pH 7.0). The internal and external surfaces of TMV capsid consist of repeated patterns of charged amino acid residues such as glutamate, aspartate, arginine, and lysine that are viable for chemical ligation and bioconjugation [Bruckman et al., 2008]. TMV can be purified from infected tobacco plants in kilogram quantities. The particle is

remarkably robust *in vitro*, remaining intact at temperatures up to 80 °C and pH values between 2 and 10. The assembled capsids have been used as templates to grow metal or metal oxide nanowires and coated conductive nanowires [Lee et al., 2012]. TMV based materials offer a wide variety in the field of nanoelectronics, energy storage, and light harvesting.

1.2 Surface modification of virus capsids

Virus can undergo a reversible disassembly/reassembly process *in vivo* and *in vitro* [Liu et al., 2012]. Chemical and genetic manipulations on the surface of viral protein cages confer unique properties to VLPs as programmable scaffolds in bionanotechnology.

The surface modification of virus capsids involve the coupling of synthetic molecules to native or artificial amino acid residues, typically yielding bioconjugates with chemical linkages that differ significantly from those that are produced biosynthetically [Francis and Carrico, 2010]. The exposed amino acid residues on the exterior surface of vial cages have been demonstrated to be applicable and addressable by different chemical reactions [Smith et al., 2013]. These residues include endogenous amino acids, such as lysines, glutamic or aspartic acids, and tyrosines, and the genetically introduced amino acids such as cysteines [Lee et al., 2009]. A variety of bioconjugation methods have been developed for the attachment of molecules to the exterior surface of virus capsids. It can be divided into three most commonly strategies based on chemical mechanisms (Fig. 1.4) [Koudelka and Manchester, 2010]. All these methods need solvent accessible VLPs surface residues which mean the position of individual residues is significant, and the availability of an atomic structure of the virus capsid is preferred.

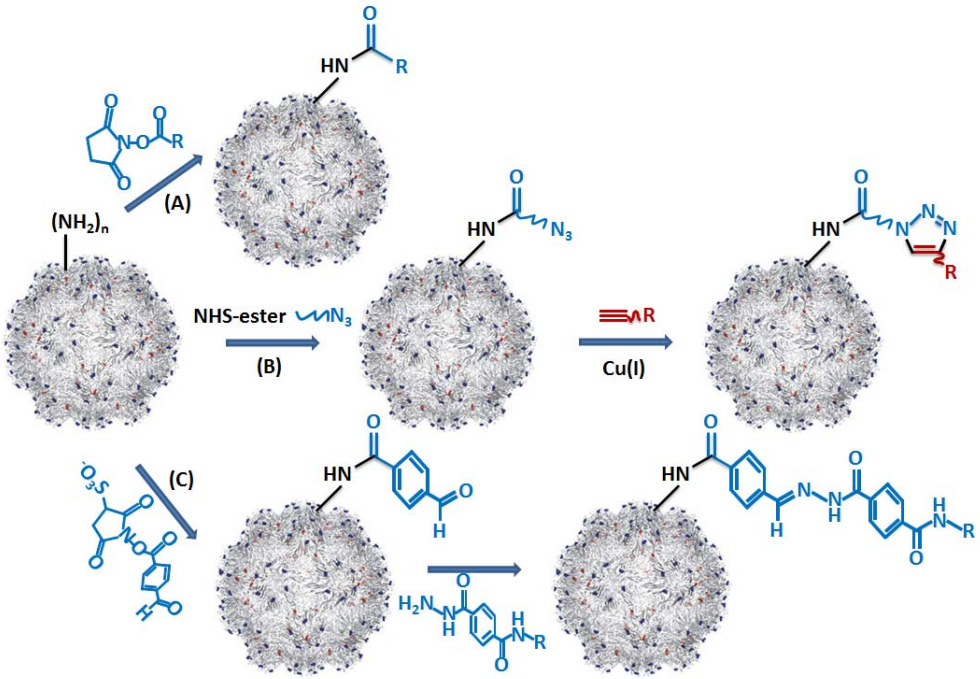

Fig. 1.4 Schematic diagram of different surface modification strategies by virus capsids. Methods of covalent modification of amino groups include: (A) NHS-ester acylation; (B) copper(I)-catalyzed azide-alkyne cycloaddition (CuAAC) reaction; (C) hydrazone ligation.

1.2.1 NHS-ester acylation

NHS-ester (N-Hydroxysuccinimide) acylation is the simplest and most common technique used for modification of exposed amines ($-NH_2$) on the capsid surface [Abello et al., 2007]. NHS esters are reactive groups formed by carbodiimide-activation of carboxylate molecules, which can crosslink with the nucleophilic amines. Wang et al. first introduced this concept through using NHS-esters of fluorescein or biotin to conjugate them to CPMV, establishing that VLPs could be used as "self-assembled dendrimers" or used similarly to metallic nanoparticles [Wang et al., 2002]. Fluorescent dyes or biotin were established to the reactive lysines on the surface of CPMV by NHS-ester acylation. They first illustrated the potential of viruses as scaffolds for bioconjugation. A variety of other residues and reactive groups including tyrosines, carboxylate groups, natural and genetically introduced cysteine residues, and binding ligands to introduced histidine tags were also modified following this same principle [Strable and Finn, 2009].

The other early example was small fluorescence molecules and peptides attached to the exterior-surface exposed carboxylate or amine functional groups of CCMV [Gillitzer et al., 2002]. The carboxylate groups were first activated by reaction with NHS and 1-ethyl-3-(3-dimethyl-aminopropyl)carbodiimide (EDC) to generate the succinimidyl esters, which were subsequently reacted with amine containing compounds. Based on the same reaction, surface exposed amine groups were derivatized using the succinimidyl esters of reactive carboxylic acid compounds. It was shown that using the above mentioned methods up to 540 amines and 560 carboxylic acids of CCMV could be labeled with fluorescent cargo.

1.2.2 CuAAC or click chemistry

A major advance in chemoselective ligation on virus surfaces is the copper(I)-catalyzed azide-alkyne cycloaddition (CuAAC) reaction first reported in 2002 [Rostovtsev et al.,

2002]. The CuAAC reaction, a member of the family of click chemistry, has emerged as an excellent tool to covalently fuse two different biological molecules together with relative ease. Both VLPs and the desired substrates can be specifically coupled in an orthogonal manner without the presence of protecting groups [Wang et al., 2003; Gupta et al., 2005]. The exclusive reactivity and selectivity of both azido and alkyne groups have placed this reaction among the favourites for protein coupling reactions due to its mild reaction conditions and high reaction rates. The azide or alkyne moiety can be attached to lysine, cysteine or tyrosine residues on the surface of virus using conventional conjugation chemistry. CuAAC is highly efficient and requires a significantly lower molar excess of substrate than NHS-ester based chemistry. Over past few years, this reaction has been expanded to conjugate various small molecules and cell-targeting moieties onto viruses [Hong et al., 2009].

CPMV was first exploited for the grafting of small fluorescent molecules *via* CuAAC reaction [Wang et al., 2003]. Further conjugation of the folic acid-PEG ligand to a mutant CPMV led to completely elimination of background binding of the virus with tumour cells while the attached folate moiety allowed CPMV-specific recognition of tumour cells bearing the folate receptor [Destito et al., 2007]. Another successful modification using CuAAC reaction was the attachment of oligo-ethylene glycol (OEG) short chain, coumarintriazole, and RGD-containing peptide on the exterior surface of TYMV [Zeng et al., 2011]. Different moieties resulted in different binding behaviors with mouse NIH-3T3 fibroblast cells. All these showed potential approaches in pharmaceutics and drug delivery.

1.2.3 Hydrazone ligation

Hydrazone ligation is a more recently chemoselective strategy. This method first derivatizes the VLPs with a benzaldehyde, which is then reacted with a substrate modified with a terminal hydrazido group [Dirksen and Dawson, 2008]. This approach has the advantages of

being both a chemoselective reaction that is highly efficient, and quantifiable by forming a product with absorbance near 350 nm. This method is also more feasible for bioconjugating VLPs and ligands that are relatively less stable to click chemistry conditions. Hydrazone ligation was applied to the assembly of CPMV nanoparticles with individually tunable levels of a VEGFR-1 ligand and a fluorescent PEGylated peptide [Brunel et al., 2010]. The nanoparticles recognized VEGFR-1 on endothelial cell lines and VEGFR1-expressing tumour xenografts in mice, validating targeted CPMV as a nanoparticle platform *in vivo*.

1.3 Encapsulation by virus capsids

The enclosed space in the interior of VLPs can be used to encapsulate and release various functional cargoes and the exterior surface can also be decorated by myriad moieties [Shen et al., 2011]. The genomic RNA or DNA of virus is generally packaged within the capsid through a simple assembly and disassembly process *in vivo*. Scientists have discovered that a variety of phages, plant, and animal viruses can be assembled *in vitro* from their molecular components: proteins, nucleic acid, and sometimes lipids [Douglas et al., 2002]. Bancroft et al. first revealed the electrostatic interaction as the driving force for efficient packaging and assembly by encapsulation of polyanions instead of ssRNA inside CCMV capsids [Bancroft et al., 1969]. The thermodynamic force during the assembly may include both specific and non-specific interactions between the capsid and the genome and there is no net delimitation to define these two mechanisms. The coat protein subunits themselves can spontaneously assemble into noninfectious VLPs under proper pH and ionic strength [Hu et al., 2008; Lin et al., 2012]. From the viewpoint of material science, the highly uniform VLPs can be regarded as organic nanoparticles. The principle regulating the encapsidation of the genetic materials can also be utilized to load functional cargoes. The encapsulation occurs simply by mixing the protein subunits with cargo particles at specific ionic strength, temperature, and pH ranges [Ng, 2010; Cadena-Nava et al., 2011]. The packaged functional cargoes include

polymers, enzymes, liquid droplets, nucleic-acid functionalized particles, and even ligand-coated particles [Siber et al., 2012]. According to the encapsulation mechanisms, there are three main strategies which will be discussed as following (Fig. 1.5).

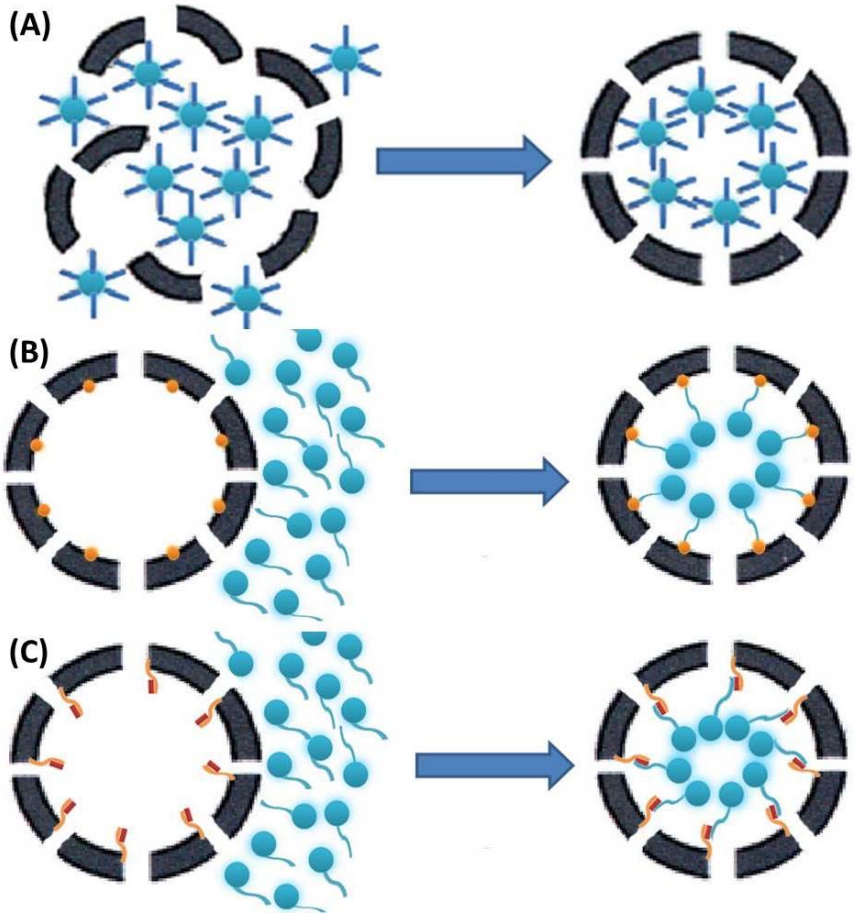

Fig. 1.5 Schematic diagram of different encapsulation mechanisms by virus capsids. (A) Electrostatic interaction, the negatively charged materials can act as the compressing genetic core to promote the assembly of a virus-like capsid as the natural type; (B) Chemical conjugation, the cargo molecules (blue) interact with the functional groups of amino acid residues on the interior of capsids (orange) by covalent bond such as peptide (amide) bonds; (C) Covalent attachment by genetic manipulation, the additional motifs (red) can be introduced inside virus cages by gene modification which are amenable to cargo molecules (blue) by specific chemical coupling.

1.3.1 Electrostatic interaction

The first strategy is to encapsulate the negatively charged species driven by electrostatic interaction [Zlotnick and Stray, 2003]. The foreign material, for example nanoparticles functionalized with anionic moieties or specific nucleic acid packaging signals and separated protein subunits, acts as the compressing genetic core to promote the assembly of a virus-like capsid like the natural type [Belyi and Muthukumar, 2006].

CCMV has been widely studied as a prominent example by several research groups for the ability to encapsulate various compounds [Douglas and Young, 2006]. A straightforward way to entrap negatively charged molecules inside CCMV is to reversibly alter the pH to induce swelling and contraction of the capsid to facilitate the entry and sequestering of the foreign material. CCMV could be disassembled into coat protein dimers at higher pH (pH 7.5) and reassembled by lowering the pH (pH 5). Taking advantage of this property, Douglas and Young demonstrated that CCMV capsids could be used to encapsulate and constrain anionic polyoxometalate (e.g., vanadate, molybdate and tungstate) by a mineralization process [Douglas and Young, 1998]. Cornelissen et al. also reported on the entrapment of negatively charged polyelectrolytes such as poly (styrene sulfonate) (PSS) [Comellas-Aragonès et al., 2009], polyferrocenylsilane (PFS) [Minten et al., 2009], poly[(2-methoxy-5-propyloxy sulfonate)-phenylene vinylene] (MPS-PPV) [Brasch and Cornelissen, 2012], and zinc phthalocyanine (ZnPc, a therapeutic agent) [Brasch et al., 2011]. The encapsidation can lead to monodisperse or polydisperse formation of $T = 1$, 2, and 3 VLPs. These approaches could be utilized for the encapsulation of negatively charged drug molecules for pharmaceutical applications in future.

Another interesting exploration of virus encapsulation is to incorporate individual horseradish peroxidase (HRP) in the inner cavity of CCMV capsid for single enzyme studies [Comellas-Aragonès et al., 2007]. HRP was loaded and immobilized in the capsid with only

one or no enzyme present per capsid. The fluorogenic substrate dihydrorhodamine 6G diffused in the HRP-containing CCMV capsid where HRP catalyzed the oxidation of this non-fluorescent substrate to produce rhodamine 6G. The release of fluorescent product through the pores on the capsid was easily monitored by confocal fluorescence microscope. The spatially confined virus capsid contributes to the understanding of the behavior and the interactions of enzymes at the single-molecule level.

1.3.2 Chemical conjugation

The second approach is to package the reagents or cargo molecules by chemical conjugation with the coat protein subunit [Cheung et al., 2006]. The foreign material is first transported and then sequestered inside the capsid by covalent bond such as peptide (amide) bonds between the carboxylate groups of amino acid residues and the amine groups of cargo molecules. The chemically well-defined local environment of the viral cavity provides the circumstance to directly synthesize inside the capsid [Aniagyei et al., 2008].

Francis et al. utilized rod-shaped TMV capsid as a robust and practical scaffold for the preparation of nanoscale materials [Schlick et al., 2005]. Both the exterior and the interior surface of the virus were attached with new functionality strategies separately. As for the inner cavity of TMV, the modification strategy focused on glutamate residues as targets for amide bond by a carbodiimide coupling reaction. Glu 97 exposed on the core surface was identified as the primary site of modification and Glu 106 was also found with appreciable reactivity, while there was no modification of exterior aspartic acids and carboxyl terminus observed. After disassembly/reassembly process, the internally modified TMV conjugates revealed rod-shape structures that were virtually identical to the native capsids. Importantly, the interior surface can also be doubly modified by rhodamine, yielding ~ 650 internal chromophores per 300 nm rod. This method positions the new functional groups as closely as 1 nm apart on the inside of TMV capsid.

More recently, the self-assembled rotavirus (RV) VLPs by the major structural protein VP6, were chemically conjugated with an anticancer drug doxorubicin (DOX) [Zhao et al., 2011]. The formation of amide bond between the carboxyl group of VP6 and the amine group of DOX was achieved in the presence of NHS and EDC. The DOX-loaded VLPs (DVLPs) were further linked with lactobionic acid (LA) as target for hepatocytes or hepatoma cells bearing asialoglycoprotein receptors (ASGPRs). LA-modified DVLPs (DVLPLAs) showed specific immunofluorescence in HepG2 cells *in vitro*. The chemically functionalized VLPs may find practical applications in biomedicine.

1.3.3 Covalent attachment by genetic manipulation

The third tactics is to integrate the cargo molecules based on covalent attachment with the site-specific residues on the capsid protein which is engineered through genetic manipulation [Huang et al., 2005]. The gene modification of coat protein results in the alteration of the amino acid residues displayed on interior of virus cage even the charge change of the interior surface, which then offers functional versatility amenable to the chemical coupling with target peptides or other cargoes [Yi et al., 2005].

Making use of heterodimeric coiled-coil linkers, Minten et al. reconstructed the interior cage of CCMV and encapsulated positively charged proteins inside it [Minten et al., 2009]. The K-coil $(KIAALKE)_3$ with positively charged lysine was introduced at the N-terminus of CCMV CP and E-coil $(EIAALEK)_3$ with negatively charged glutamic acid at the C-terminus of the enhanced green fluorescent protein (EGFP) and the modified proteins were expressed in *E. coli* respectively. Specific heterodimerization between K-coil and E-coil led to the formation of EGFP-CP complex. After the assembly of EGFP-CP complex with wild-type CP, EGFP-filled capsids were obtained. This provides a brand new approach of modification on virus capsids by gene manipulation.

Bacteriophage MS2 also presents a readily available scaffold for the construction of targeted delivery agents by genetic modification [Tong et al., 2009]. A cysteine residue was introduced at asparagine 87 (N87C). The mutation provided 180 sulfhydryl groups on the interior surface for cargo installation. Through the cysteine alkylation reaction, Alexa Fluor 488 maleimide was encapsulated as fluorescent label. A 41-nucleotide DNA aptamer was then installed on the outer surface of MS2 shell. The capsids bearing the cell-targeting sequence showed significant binding to Jurkat T cells. These suggested that aptamer-labeled capsids could be used as convenient and evolvable targeting groups for drug delivery.

1.4 Application of VLPs in nanotechnology

1.4.1 Drug delivery

With the property of excellent biocompatibility and biodegradability, there are various potential applications of functional self-assembled virus-based materials. Bentley's team has successfully utilized the hollow capsid of TMV as an RNAi carrier for gene delivery into mammalian and insect cells (Fig. 1.6.A) [Hung, 2008]. RNA interference (RNAi) is a process in which RNA molecules reduce gene expression by causing the destruction of specific mRNA molecules and usually involves two small RNA molecules: microRNA (miRNA) and small interfering RNA (siRNA). There is an origin of assembly sequence (OAS) within TMV genomic RNA which forms a unique hairpin structure and associates with coat protein to initiate the assembly. By incorporating TMV OAS into a siRNA which can program cells to destroy disease-causing proteins, the siRNA could assemble into "pseudo-virions" with coat protein. To deliver the siRNA to the targeted cells, pseudo virions are further modified with synthetic cell-penetrating peptides to facilitate cell endocytosis. The results showed pseudo virions targeting cyclin E (antisense cycE) were capable of arresting cells at G1 phase. This TMV-based siRNA packaging system protects the frail siRNA from degradation and provides a means of delivering RNAi constructs into

various host cells. Through changing the types of siRNA, multiple diseases from cancers to genetic disorders could be targeted and treated by this therapeutic agent in future.

A pH-dependent drug release system has been developed based on the human polyomavirus JC virus by Ijiro et al. (Fig. 1.6.B) [Ohtake et al., 2010]. Green fluorescence protein with N-terminal hexahistidine motif (His_6GFP) was fused to the N terminus of the inner core protein VP2 (His_6GFP-VP2) and co-expressed with the major coat protein VP1 in *E. coli*. VP1 and His_6GFP-VP2 associated with each other and formed His_6GFP-incorporated VLPs (His_6GFP-VLPs). Nitrilotriacetic acid-sulforhodamine (NTA-SR), containing both a His_6-tag-targeting NTA segment and a fluorescent sulforhodamine segment, could be encapsulated within His_6GFP-VLPs through the 1 nm holes at pH 7.4 and bind specifically to the His_6 tags. NTA was then released from the His_6GFP-VLPs at pH 5.0 due to a decrease in His_6-tag affinity, which has similar pH to the endosome and the lysosome. In this system, VP2 acted as an anchoring unit for the protonation of histidines, which could offer specific and reversible attachment of drug molecules. The feasibility of the encapsulation-release system can be used as a cell-specific drug delivery vehicle.

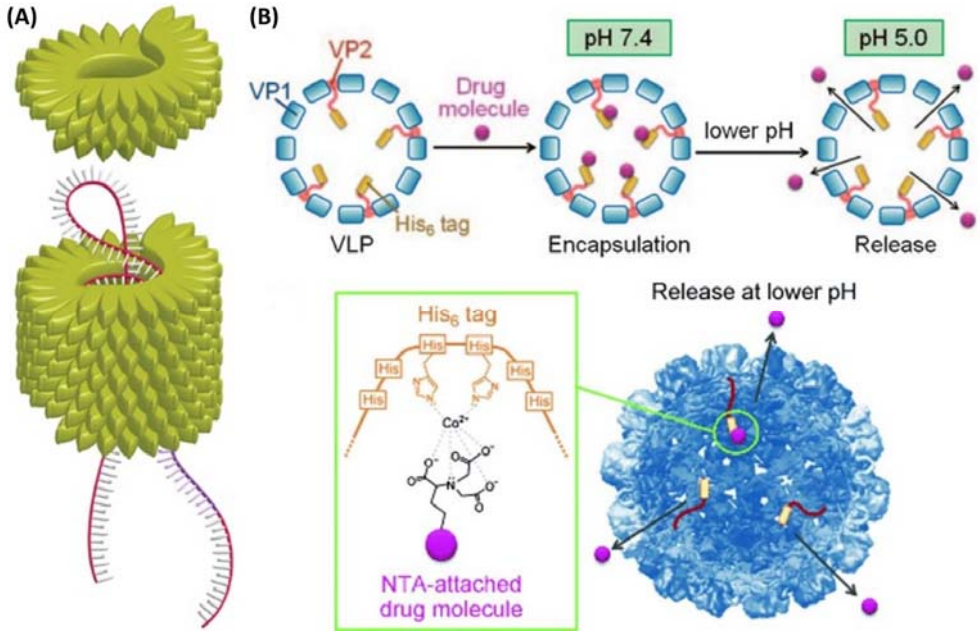

Fig. 1.6 Virus capsids used for drug delivery studies. (A) Schematic representation of TMV-based siRNA formation. (B) Schematic representation of pH-dependent drug release system based on human polyomavirus JC virus.

1.4.2 Single-enzyme nanoreactor

The virus capsid provides a well-defined structure to encapsidate the enzyme in a spatially confined way to observe the catalytic activity even in single-molecule level [Cardinale et al., 2012]. The entrapment of different enzymes by virus capsids has been done in CCMV and MS2. A precise number of enzyme *Pseudozyma antarctica* lipase B (PalB) loaded into the CCMV capsid were accomplished based on a coiled-coil linker and EGFP was co-encapsulated as a non-catalytic protein to investigate the reaction rate [Minten et al., 2011]. The apparent overall reaction rate increased upon encapsulation and was almost independent of the number of enzymes in the capsid. The encapsulated PalB seemed to have a higher activity than non-encapsulated PalB. It was more likely caused by extremely high confinement molarity (M_{conf} = ~ 1 mM) of the enzyme combined with an increased collision chance due to the spatial confinement leading to very rapid formation of the enzyme-substrate complex. These results highlight the importance of small volumes for efficient multi-enzyme cascade catalysis.

The RNA-removed MS2 capsids were also used to encapsulate *E. coli* alkaline phosphatase (PhoA) [Glasgow et al., 2012]. To increase the yield of encapsulation, PhoA was tagged with a 16 acidic peptide at C-terminus (PhoA-neg); Trimethyl amine N-oxide (TMAO) was added as an osmolyte to decrease protein unfolding and increase the thermal stability. Intact capsids were observed after incubation of PhoA-neg with disassembled coat protein dimers under presence of TMAO. Enzyme assay showed the value of K_m was equal to that of the free enzyme dimer and the K_{cat} was slightly reduced when the enzyme was encapsulated, possibly due to the constrained enzyme environment. This method provides a practical and potentially scalable way of studying the complex effects of encapsulating enzymes in protein-based compartments.

1.4.3 In vivo imaging

Near infrared (NIR) fluorescence imaging based upon virus capsids is particularly advantageous in optical imaging and therapy of disease. Indocyanine green (ICG), an FDA-approved NIR chromophore, was encapsulated into BMV for the utilization of mammalian intracellular optical imaging [Jung et al., 2011]. Instead of genomic RNA, the negatively charged ICG interacted with the positively charged arginine-rich motif in the N-terminus of BMV CP subunits to assemble into optical viral ghosts (OVGs). Human bronchial epithelial (HBE) cells were used to detect the intracellular optical imaging of OVGs, resulting that OVGs were internalized and localized at more than 90 % of the HBE cells after 3 h. These constructs may serve as a potentially nontoxic and multifunctional nanoplatform for site-specific deep-tissue optical imaging and therapy of disease.

1.4.4 Light-harvesting cells

A virus-based approach has been developed as light-harvesting systems through self-assembly. Recombinant TMV CP monomers with a reactive cysteine residue were constructed for the thiol-reactive chromophore attachment [Miller et al., 2007]. Three chromophores were installed on the interior surface of TMV including Oregon Green 488 maleimide as the primary donor, tetramethylrhodamine maleimide as an intermediate donor, and Alexa Fluor 594 maleimide as the acceptor. The conjugated TMV VLPs could be assembled into stacks of disks or rods under different buffers. Under both morphologies, there was efficient energy transfer (> 90 % overall efficiency) observed using fluorescence spectroscopy, from numbers of donor chromophores to a single acceptor. Later, multiple porphyrin arrays were accomplished similarly in TMV, in which Zn-porphyrin (ZnP) was coordinated as donor and free-base porphyrin (FbP) as acceptor [Endo et al., 2007]. CCMV capsids were also employed to package and synthesize TiO_2 nanoparticles, which showed similar structure to nanocrystalline anatase and photocatalytic activity [Klem et al., 2008]. This highly tunable method has emerged for the construction of photovoltaic devices.

1.5 Future directions

The ability to precisely encapsulate components into virus capsids, by self-assembly, chemical conjugation or genetic manipulation, has inspired the creation of complex systems with novel function [Singh et al., 2006; Yoshimura, 2006]. However, we should not just focus on one side of the coin. Today there are two main trends in the fabrication of modified virus capsids for nanotechnology: the surface modification and the encapsulation (Fig. 1.7) [Su and Wang, 2010]. As aforementioned, the combination of two methods turns out to be more delicate and efficient for the practical utilization. The chemical addressability of exterior and interior surface of virus capsids by covalent bioconjugation such as diazonium coupling and CuAAC reaction provides a diversity of functional moieties of versatile repertory [Fischlechner and Donath, 2007; Ma et al., 2012]. These dual modified VLPs can specifically recognize certain type of cells, attach with corresponding receptors, and deliver the packaged cargoes into the endosome.

Furthermore, quite a few of plant viruses such as CCMV, CPMV, TMV, and rod-like phages have been shown noninfectious to human and mammalian and will not induce obvious toxicity and immune response in human beings [Steinmetz, 2010]. CCMV showed broad tissue distribution and rapid clearance of in vivo both in naive and immunized mice [Kaiser et al., 2007]. TMV can be traced in the blood of most people from second-hand smoke and does not seem to cause irritation or obvious immune-system problems [Scholthof et al., 2011]. These will be quite promising nanocarriers with some issues concerning the toxicity and immunology be fully evaluated. Virus particles have presented distinguished stability and flexibility for pharmaceutical application, biomaterial fabrication, and photovoltaic construction. More light will be cast upon these elegant and elaborate creations in future.

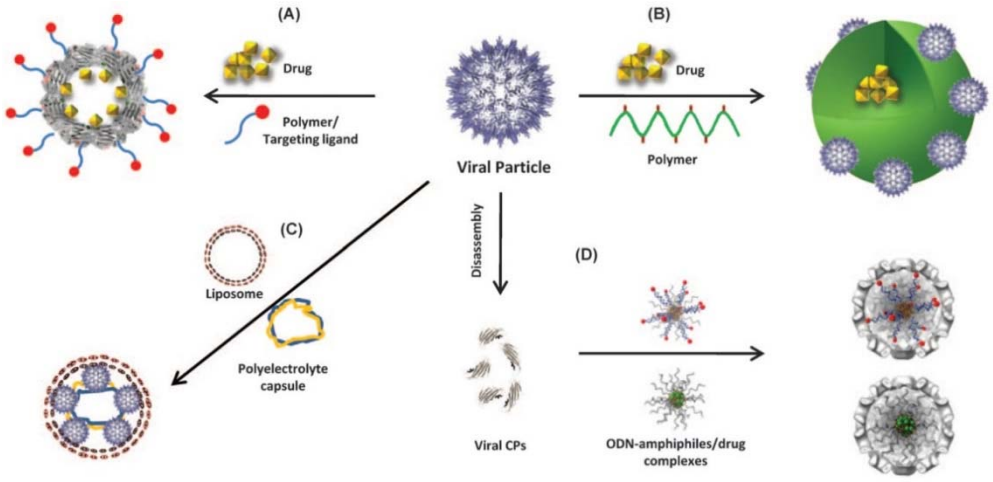

Fig. 1.7 Scheme of strategies available for the construction of virus-based nanomaterials. (A) Loading a viral particle with drugs and targeting motifs through bioconjugation reactions; (B) Loading hydrophobic drugs within a polymer–virus core–shell assembly;(C) Constructing a virus–polyelectrolyte–liposome complex; (D) Using DNA amphiphiles to induce the assembly of viral coat proteins to encapsulate drugs.

Chapter 2. Originality of Thesis

2.1 Backgrounds

Viruses used to be considered as the foes of human beings due to their pathogenicity [Breitbart and Rohwer, 2005]. As small infectious assemblies that can replicate only inside the living cells of an organism, viruses are described as "organisms at the edge of life" [Holmes, 2007]. They resemble organisms in some ways: possess genetic material, reproduce, and evolve through natural selection; however, they still lack key characteristics such as their own metabolism and cellular structures which are often seen as the basic unit of life. Opinions differ on whether viruses are a form of life, or organic structures that interact with living organisms [Wimmer et al., 2009]. From the viewpoint of material scientists, viruses provide another type of widely studied biological macromolecules in nanometer scale, i.e., organic nanoparticles, which are composed of nucleic acids, capsid proteins, and sometimes envelopes.

The essential nature of viruses is to infect a host cell, replicate, package its nucleic acid, and exit the cell. In the process, viruses have evolved to move through a broad range of biochemical environments [Douglas and Young, 2006]. During their journey, viruses exhibit a remarkable plasticity in their metastable structure and dynamics, including coordinated assembly and disassembly and target-specific delivery of cargo molecules. VLPs are the complexes consisted of multiple protein subunits that are capable of self-assembling and forming structures that mimic the 3D conformation of native viruses [Roy and Noad, 2009]. Without viral genetic material, VLPs are non-infectious and unable to replicate, making them safer than wild types based on attenuated or inactivated viruses. Due to their structural uniformity and complexity, viruses and VLPs are excellent scaffolds for nanomaterial research.

Viruses and VLPs have several characteristics that are suitable for nanomaterial fabrication and modification.

(i) They represent very stable and beautiful self-assembled architectures at the nanometer level with sizes ranging from a few tens to several hundreds of nanometers. Their small sizes are comparable to the size of nanoparticles and very difficult to make by standard synthetic methods in the laboratory [Manchester and Singh, 2006; Lee et al., 2009].

(ii) Viruses and VLPs have precise nanoscaled dimensions and sophisticated structures, in contrary to artificial nanomaterials prepared by top-down approaches. The structural and dimensional uniformity of viruses which can be characterized at near atomic resolution make them ideal for use as scaffolds [Liu et al., 2005; Singh et al., 2006].

(iii) Genetic information on the sequences of capsid proteins and nucleic acids has been revealed for years. The composition and surface properties of viruses and VLPs can be manipulated through genetic engineering, which can be easily performed using commercially available tool kits [Gazit, 2007; Lee et al., 2012].

(iv) Mass production of viruses and VLPs can be achieved easily and inexpensively by growing them in infected hosts or expressing capsid proteins in heterogonous expression systems that are sufficient for utilization in engineering applications [Bruton et al., 2005; Steinmetz and Evans, 2007].

Over the past few decades, viruses and VLPs have provided myriad platforms that can be used to manipulate and investigate the functions from material science to pharmaceutics research [Manchester and Singh, 2006; Ma et al., 2012]. The essence of viruses and VLPs are protein assemblies from repeating subunits which means chemical or genetic techniques that apply to biochemistry and molecular biology are also appropriate for these studies.

For about half of the known virus families, the capsid is “spherical” or icosahedral. The architectures of icosahedral viruses are composed of hundreds of copies of individual components that can assemble rapidly and reproducibly on a biological timescale [Suttle, 2005]. There are three important interfaces of these virus capsids that can be exploited: the exterior, the interior, and the interface between protein subunits making up the capsid (Fig. 2.1) [Douglas and Young, 2006].

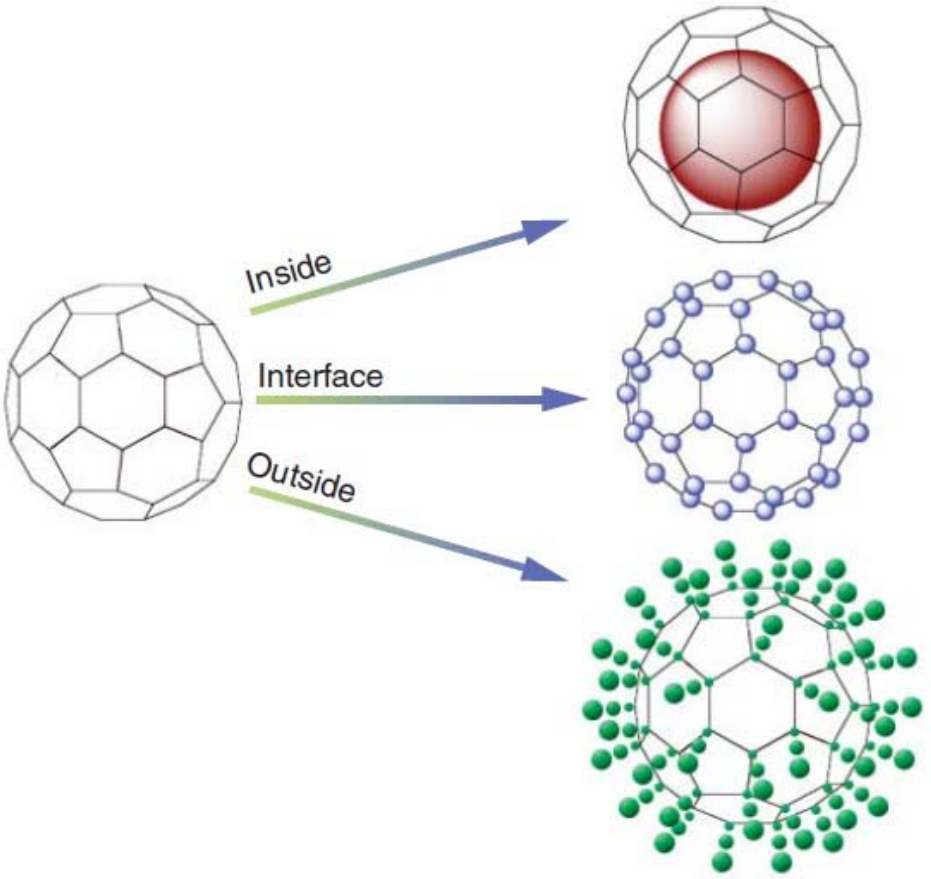

Fig. 2.1 Schematic representation of three approaches available for chemical and genetic manipulation of icosahedral virus capsids. The exterior, the interior, and the interface between subunits have all been used for the construction of multivalent, multifunctional viral cage-based materials.

The interior interface of the viral capsid architecture has been used for directing encapsulation and synthesis of both organic and inorganic materials. The principles that govern the packaging of viral nucleic acid can be applied to package nonviral cargoes within their capsid architecture [Belyi and Muthukumar, 2006]. In the case of CCMV, the interior interface presents a native positive-charge density or can be altered to negative-charge through genetic manipulation, which allows encapsulation or nucleation of the opposite charged cargoes inside the capsids.

The exterior surface of virus capsids has been demonstrated by bioconjugate reactions with chemical linkages between the exposed amino acid residues and functional moieties [Strable and Finn, 2009]. The natural or genetically introduced substrate-specific affinity enlarges the perspective of outer surface decoration. In the recent years there have been numerous progresses in covalent bioconjugation involved with virus capsids. CuAAC reaction is an extraordinary procedure for the ligation work [Amblard et al., 2009]. It has been proven there are plenty of amino acid residues protruded from CCMV capsids applicable. The modification of CCMV capsids with CuAAC reaction is showing brilliant prospect for application.

In addition the interface of viral capsids has been employed for electroless deposition (ELD) such as metal ions and poly(ethylene glycol) (PEG) grafted branched polymers [Bruton et al., 2005]. The interface acted as nucleation sites for the subsequent metal deposition from solution and formed the metallic coated nanoparticles by metallization process [Aljabali et al., 2010]. The electrostatically bounded virus capsid showed monodisperse and larger sphere which could allow further demonstration.

In summary, chemical modification and genetic manipulation on the outer surfaces and inner cavities of viruses and VLPs facilitate the development of new materials that could meet the requirements for bionanotechnology [Tu and Tirrell, 2004; Mateu, 2011]. The

biocompatibility, solubility and uptake efficiency of the capsids are attractive to assemble substances in a programmed pattern, to align small structured materials in a designer position, and to conjugate biomolecular substances with each other.

2.2 Objectives

Following the above-mentioned principles, the heterologous expressed CCMV was employed in the thesis for the demonstration of the capability to encapsulate foreign cargoes in the inner cavity and the modification of the exterior surface with functional molecules via CuAAC reaction. CCMV capsids were selected for their remarkable characteristic including the reversible structural transition, disassembly/reassembly property, and high stability under various temperatures, pH and organic solvents.

In the third chapter of the thesis, CCMV CP was firstly synthesized and expressed in *P. pastoris* and the appropriate assembly into VLPs was acquired through proper purification and treatment.

In the fourth chapter, the inner cavity of the capsid was exploited for the encapsulation and synthesis of Prussian blue nanoparticles based on electrostatic interaction, which lead to relatively homogeneous-sized spherical particles.

In the fifth chapter, the exterior surface was decorated with alkyne and further modified with azide through triazole connection via CuAAC reaction and the cell binding behavior of the modified capsids was determined using HeLa cells.

In the appendix I, *Heterocapsa circularisquama* RNA virus (HcRNAV) was also expressed in *P. pastoris* and self-assembled into VLPs. The co-expression of HcRNAV CP with algicidal peptide PMAP-23-D7 showed potential in the control of harmful algae blooms (HABs).

In the appendix II, a more efficient *Pichia* cell disruption was illustrated with the combination of aminopropyl magnesium phyllosilicate (AMP) clay, showing no side influence on VLPs assembly.

The structure of the thesis is summarized in Fig. 2.2.

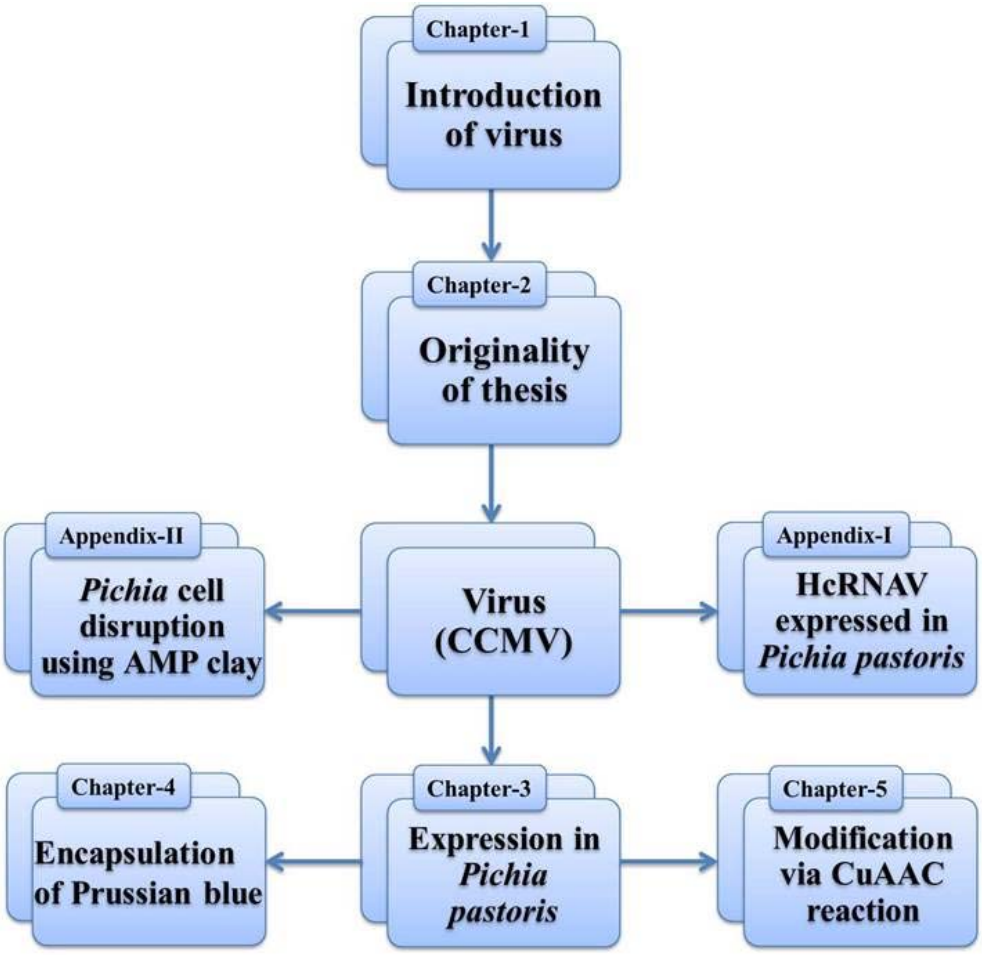

Fig. 2.2 Outline structure of the thesis.

Chapter 3. Expression and Self-assembly of CCMV in *Pichia pastoris*

3.1 Introduction

Virus particles consist of the genetic material of either DNA or RNA and the capsid that protects these genes, and in some cases an envelope of lipids surrounding the capsid. The capsids are typically composed of identical CP subunits that permit manipulation by genetic and chemical modifications [Zlotnick and Stray, 2003]. As nanoscale assemblies, viruses have sophisticated yet highly organized structural features. Therefore, viruses and VLPs offer a unique platform where functional motifs can be attached on their capsids precisely or encapsulated inside the cages, which is a big advantage over synthetic nanoparticles [Loo et al., 2008; Minten et al., 2010].

The utility of virus capsids has highlighted the need for large production systems. However, yield of virus particles from plant or animal hosts requires a long replication period and obtains a low output quantity [Jermutus et al., 1998]. Also some modifications to the coat protein may severely affect the process of viral packaging, accumulation and purification from hosts [Schneemann and Young, 2003]. To overcome these disadvantages, heterologous expression systems have been introduced to express virus CP in the absence of other viral components. A few of these expression systems have resulted in the assembly of VLPs. The first widely used is prokaryotic expression system such as *E. coli* and *P. fluorescens*. Baculovirus-based heterologous expression is also evaluated [Kost et al., 2005]. However, these systems have their limitations. *E. coli*-based expression often results in insoluble inclusion aggregates that do not self-assemble properly, and baculovirus-based expression is cumbersome and expensive.

The methylotropic yeast, *Pichia pastoris*, has been shown to be a suitable system for the heterologous expression of virus CP, which could then self-assemble into VLPs *in vitro*. *P. pastoris* can be genetically engineered to express proteins for both basic research and industrial use [Cereghino and Cregg, 2000]. Over 400 proteins, from human endostatin to spider dragline silk protein, have been produced in this yeast [Macauley-Patrick et al., 2005]. Coupled with the powerful genetic techniques, *P. pastoris* has been extensively utilized for the production of various recombinant proteins. The successful examples of virus CP expressed in *P. pastoris* include CCMV [Brumfield et al., 2004], hepatitis B virus (HBV) [Freivalds et al., 2011], human papillomavirus (HPV) [Bazan et al., 2009], and bacteriophage Qβ [Freivalds et al., 2006].

P. pastoris is uniquely suited for foreign protein expression for three key reasons [Cereghino et al., 2002]: it can be easily manipulated at the molecular genetic level, e.g. gene targeting, high-frequency DNA transformation, cloning by functional complementation; it can express proteins at high levels on a simple and inexpensive medium and reach high-density yields for both small experimental and large-scale industrial production; and it can perform many protein folding and post-translational modification such as glycosylation, disulfide-bond formation, and proteolytic processing, which is more suitable for eukaryotic protein expression (Fig. 3.1). Because of these characteristics some proteins that cannot be expressed efficiently in *E.coli*, *Saccharomyces cerevisiae* or baculovirus have been successfully produced in functionally active form in *P. pastoris* [Hohenblum et al., 2004]. Besides its ability to express foreign proteins at a high level, *P. pastoris* has a fermentation period of 4–5 days, much shorter compared to the plant hosts in which production took weeks.

The unusually efficient and tightly regulated promoter from the alcohol oxidase I (AOX1) gene is commonly used to drive the expression of the foreign gene [Higgins and Cregg,

1998]. The AOX1 promoter is strongly repressed in cells grown on glucose and most other carbon sources, but is induced over 1000-fold when cells are shifted to a medium containing methanol as a sole carbon source. Physiologically, *P. pastoris* prefers a respiratory rather than a fermentative mode of growth. Fermentation products include ethanol and acetic acid, which quickly reach toxic levels in the high cell density environment of a fermenter with strongly fermentative organisms [Li et al., 2007].

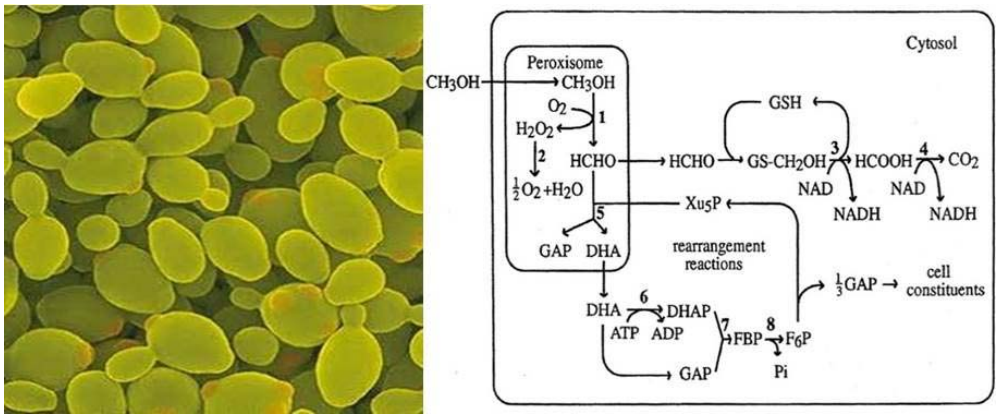

Fig. 3.1 The microscopic image of *Pichia pastoris* and its methanol metabolism pathway. *P. pastoris* has two alcohol oxidase genes, AOX1 and AOX2, under a strongly inducible promoter, which makes it use methanol as only carbon and energy source. Foreign gene is introduced under the control of AOX1 promoter and the production can reach over 90 % of total proteins induced by methanol (by Dennis Kunkel).

Following the scheme in Fig. 3.2, the gene of CCMV CP was optimized and synthesized for the expression in *P. pastoris* for the first time. The large scale fermentation and purification of the self-assembled CCMV VLPs were performed. Compared with the expression resulted insoluble inclusion aggregates in *E. coli* [Zhao et al., 1995; Fox et al., 1996] and relatively low expression level of wild type CCMV CP in *P. pastoris* [Brumfield et al., 2004], this expression and assembly system was simple, rapid, and potentially scalable which would provide a promising way to high yield of CCMV and other VLPs [Wu et al., 2011].

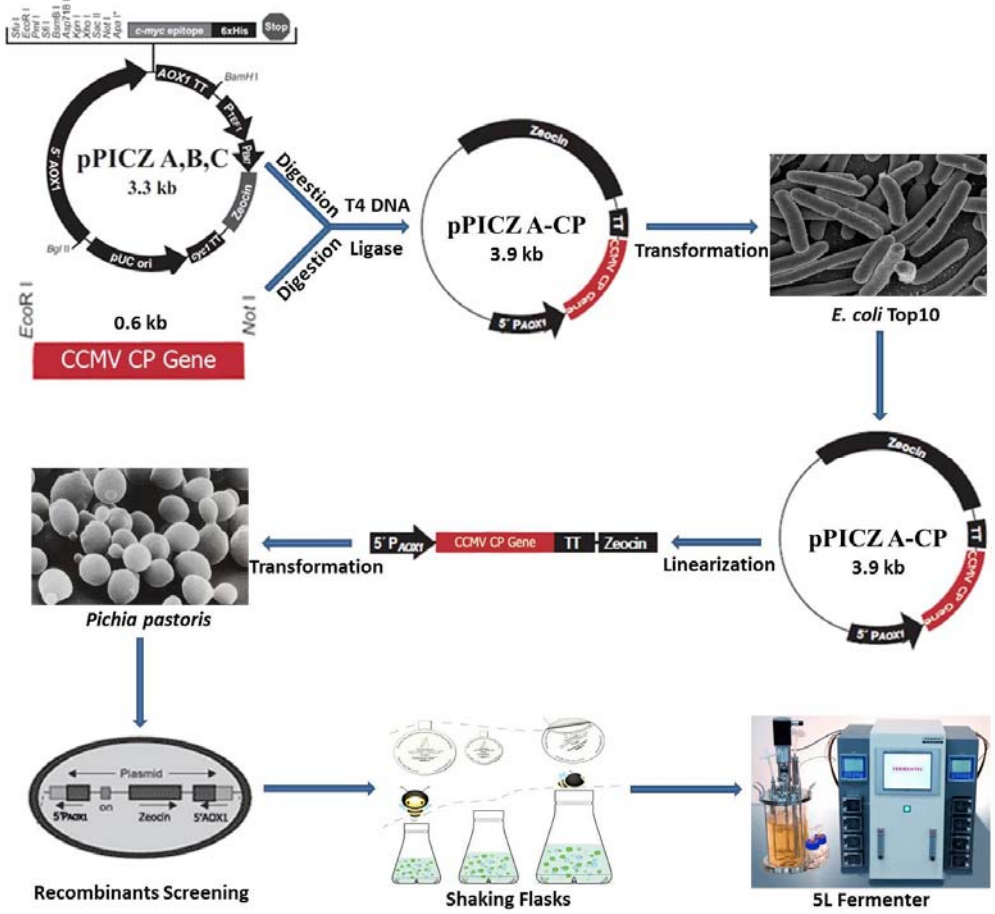

Fig. 3.2 Schematic diagram of synthesized gene encoding CCMV CP expressed in *P. pastoris*.

3.2 Materials and methods

3.2.1 Synthesis of P. pastoris codon-optimized CCMV CP

The gene sequence of CCMV coat protein, GenBank accession no. M28818 [Allison et al., 1998], was redesigned to substitute some amino acid codons seldom used in *P. pastoris* by frequently used codons [Sreekrishna et al., 1997]. Chemical synthesis of new CP gene (CPsyns) was accomplished by GenScript Co (USA). Two restriction sites of *Eco*RI (GAATTC) and *Not*I (GCGGCCGC) were added to upstream and downstream of CPsyns genes respectively. The plasmid pUC57-CPsyns was transformed into *E.coli* Top10 for amplification and preservation.

3.2.2 Construction of recombinant plasmid

The *P. pastoris* host strain GS115 (*his4*$^{-}$, histidine-requiring auxotroph) and intracellular expression vector pPICZ A were purchased from Invitrogen (San Diego, CA). According to the manual of EasySelect *Pichia* Expression Kit. for *in vivo* expression in *P. pastoris*, the 0.6 kb CPsyns gene was retrieved from the pUC57 vector as an *Eco*RI and *Not*I fragment and cloned into the corresponding *Eco*RI and *Not*I site of the *Pichia* integrative vector, pPICZ A. The resultant vector pPICZ A-CPsyns was then transformed into *E.coli* Top10 for its amplification.

3.2.3 Expression of CCMV CP in P. pastoris

Transformation and expression of the CPsyns gene into *P. pastoris* was carried out as described in Molecular Cloning [Sambrook and Russell, 2001]. The recombinant plasmid pPICZ A-CPsyns was linearized with *Sac*I and then used to transform *P. pastoris* GS115 by electroporation (Multiporator, Eppendorf). The transformed yeast cells were incubated in YPD agar containing Zeocin at 30 °C for 2–3 days. As the CPsyns gene was integrated into the 5' AOX1 locus on *Pichia* chromosome, all transformants should be His^{-} Mut^{+} phenotype.

The CPsyns gene of the transformed yeast cells was amplified by PCR using the CP primers and AOX1 primers.

More than ten verified transformants were grown in buffered glycerol-complex medium (BMGY) at 30 °C for 16–20 h. The yeast cells were harvested by centrifugation and resuspended in buffered methanol-complex medium (BMMY) with a concentration of 1.0 at OD_{600} (5×10^7 cells/mL). Incubation was continued for a further 96 h at 30 °C with 1 % methanol induction every 24 h. One mL of the expression medium was withdrawn every 12 h to determine the protein expression levels by sodium dodecyl sulfate polyacrylamide gel electrophoresis (SDS-PAGE) in a Bio-Rad MiniPROTEAN 4 gel electrophoresis cell. The original host *P. pastoris* GS115 and pPICZ A/GS115 transformants with the empty vector were also included as controls by same induction.

3.2.4 Scale-up fermentation

The scale-up fermentation of *Pichia* cells containing CCMV CP was carried out in the 5 liter fermenter XP 50 (Fermentec, Korea). A single colony of CCMV transformant was first inoculated in 250 mL BMGY at 30 °C for 16 h until OD_{600} reached 2–6, then transferred into the sterilized 2.5 L Fermentation Basal Salts medium (For 1 liter of FBSM, add aseptically 4.35 mL PTM_1 trace salts and adjust the pH to 5.0 with 28 % ammonium hydroxide). Set temperature to 30 °C, agitation to 600 rpm, and aeration to 0.1–1.0 vvm air. Dissolved Oxygen (DO) was used to monitor the growth of *P. pastoris*. DO would decrease from initial 100 % (Be sure to keep it above 20 % during all phases of fermentation) as the culture started to grow for the consumption of oxygen (*Pichia* Fermentation Process Guidelines). After the glycerol was completely consumed from the batch growth phase (18 to 24 hours) which was indicated by an increase in the DO to 100 %, the glycerol feed was initiated to increase the cell biomass with the feed rate to 18.15 mL/h/liter initial fermentation volume and continued for about four hours to get the maximum level of 4 %

glycerol. The methanol induction was carried out with the feed rate slowly rising from 3.6 mL/h/L for 2–4 hours, 7.3 mL/h/L for 2 hours, to final 10.9 mL/h/L maintained throughout the remainder of the fermentation. The entire methanol fed-batch phase lasted approximately 72 hours [Dietzsch et al., 2011]. After the fermentation, the yeast cells were collected as described in section 3.2.3 for further purification and analysis.

3.2.5 Purification of CCMV VLPs

A modified purification procedure of virus capsids, based on PEG precipitation and density gradient centrifugation was introduced to purify the soluble protein and then assembled CCMV VLPs [Ali and Roossinck, 2007]. The *Pichia* cells gathered by centrifugation at 4000× *g* for 30 min, were resuspended in five volumes of cells weight of breaking buffer (50 mM sodium phosphate, pH 5.5, 1 mM PMSF, 1 mM EDTA, 5 % glycerol) and disrupted by sonication (30 s on, 30 s off, 15 cycles, Sonics Vibra-cell VCX-750). Cell debris and insoluble aggregates were removed by centrifugation at 10,000× g for 30 min and PEG 6000 was added to the supernatant to a final concentration of 10 %. After incubation at 4 °C overnight, the solution was centrifuged at 10,000× g for 30 min and the resulting pellet was resuspended in assembly buffer (100 mM NaOAc, 1 mM EDTA, 5 mM DTT, 0.5 mM PMSF, pH 5.2). The resuspended PEG pellet was loaded onto 10–40 % cesium chloride gradient and centrifuged at 35,000× g for 2 h at 4 °C (SW55Ti rotor, OptimaL, Beckman Coulter, USA). The pellet was dissolved in NaOAc buffer for further investigations.

3.2.6 Analysis of purified CCMV VLPs

The purified CCMV VLPs were analyzed by UV spectrometry, and transmission electron microscopy (TEM). Absorption at 260 nm and 280 nm were measured on Scinco S-3100 UV spectrophotometer and A_{260}:A_{280} ratio was calculated. TEM images of negatively

stained VLPs with 2 % (w/v) uranyl acetate was obtained with a CM30 electron microscope (FEI/Philips) operated at 200 kV (Korea Basic Science Institute, Chunchon Center, Korea).

3.3 Results and discussion

3.3.1 Synthesis of P. pastoris codon preferred CCMV CP

Numerous heterologous proteins have been produced at greater than gram per liter levels in *P. pastoris*, using AOX1 promoter [Li et al., 2007]. The factors that drastically influence protein yields in this system include: copy number of the expression cassette, site and mode of chromosomal integration of the expression cassette, property of secretion signal and promoter, media and growth conditions, and fermentation parameters [Sreekrishna et al., 1997]. All these factors should be considered in designing an optimal production system even using the commercial expression system. When the prokaryotic gene is expressed in the eukaryotic system such as *P. pastoris*, some codons should be altered in order to acquire higher production. As far as CCMV CP is concerned, the seldom-used codons of arginine (CGG) and alanine (GCG) residues, which could lead to low efficiency of gene translation via early termination in *P. pastoris*, should be substituted with synonymous alterations i.e. CGG→AGA, GCG→GGT. A 573 bp CCMV CPsyns gene was synthesized according to the preference of *P. pastoris* (Fig. 3.3). In total 47 substitutes were introduced into CCMV CPsyns gene. The sequencing result showed 92 % nucleotide identity (527/574) and 100 % deduced amino acid identity with wild CCMV CP gene (M28818).

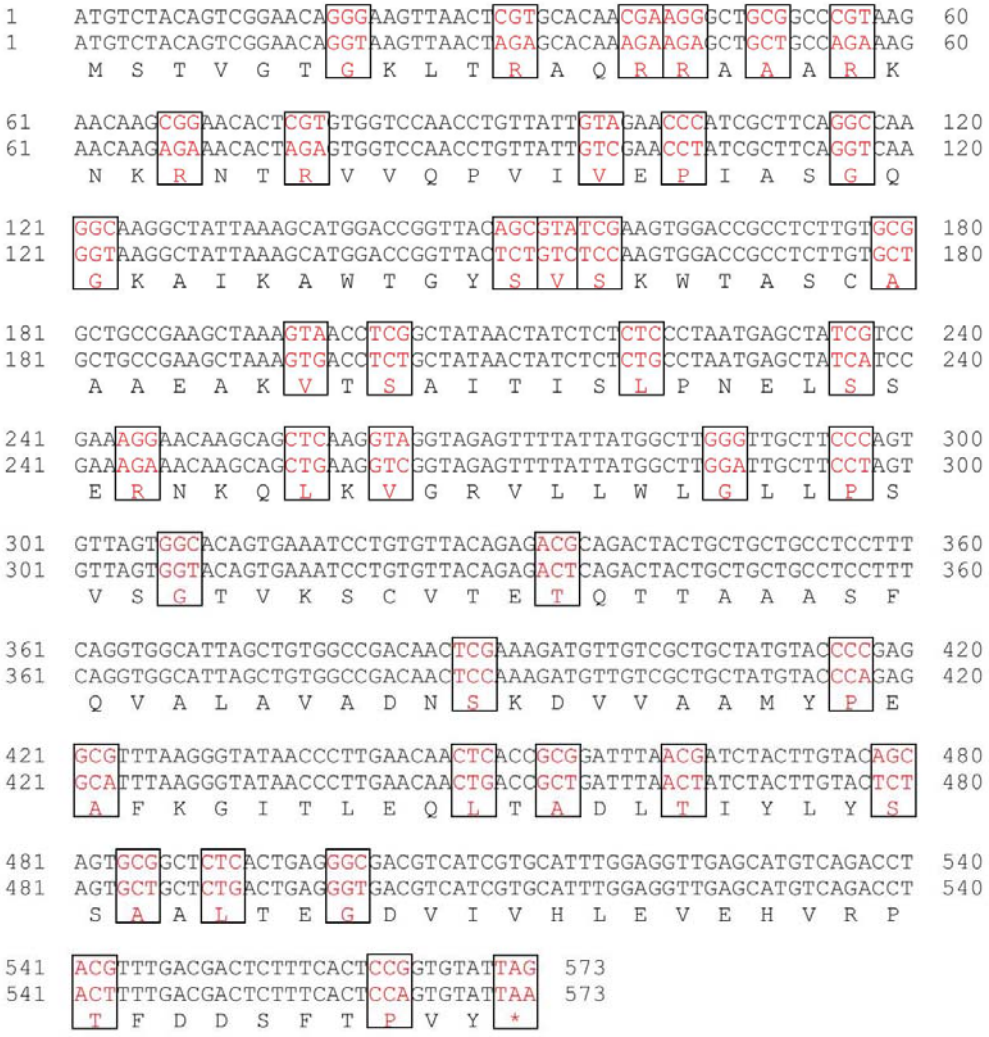

Fig. 3.3 Nucleotide and deduced amino acid sequence of CCMV CP gene and CCMV CPsyns gene. The alternations of nucleotide sequences were boxed as red.

3.3.2 Construction of recombinant plasmid

The digestion result of the recombinant plasmid pPICZ A-CPsyns by *EcoR*I and *Not*I showed two bands of 600 bp and 3.3 kb corresponding to CPsyns and pPICZ A separately, which indicated that pPICZ A-CPsyns was constructed successfully (Fig. 3.4).

PCR amplification was then done to confirm the transformation of CPsyns gene into the genome of *Pichia* cells using the CP primers and AOX1 primers. As shown in Fig. 3.5, there were significant bands of 600 bp in the all recombinants while there were no such ones in the controls.

The amplified gene was submitted to DNA sequencing by Genotech Co (Korea). The result showed the introduction of 47 substitutes in CCMV CPsyns was achieved successfully while the translated amino acid sequence remained identical to the wild-type CCMV CP (table 3.1).

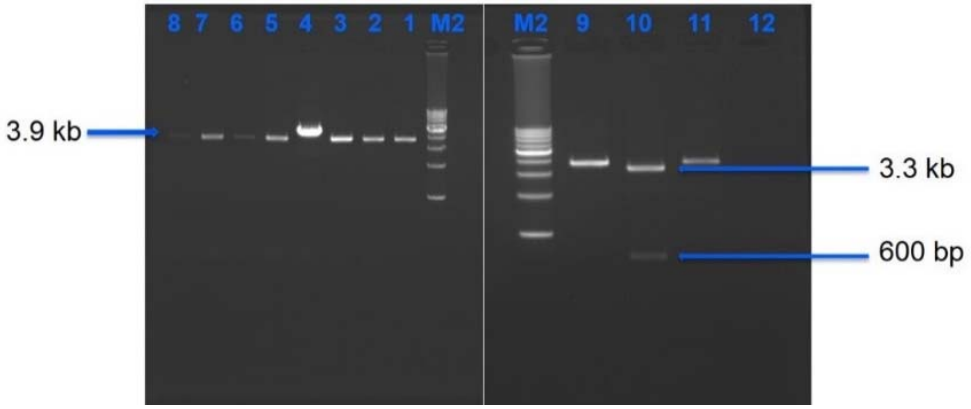

Fig. 3.4 Digestion results of pPICZ A-CPsyns by *EcoR*I and *Not*I. Lane 1-8, plasmid results of *E.coli* transformants; 9, pPICZ A-CPsyns plasmid; 10, double digestion result of pPICZ A-CPsyns with *EcoR*I and *Not*I; 11, single digestion result of pPICZ A-CPsyns with *EcoR*I; 12, control of ddH_2O; M2, Takara 1 kbp DNA ladder.

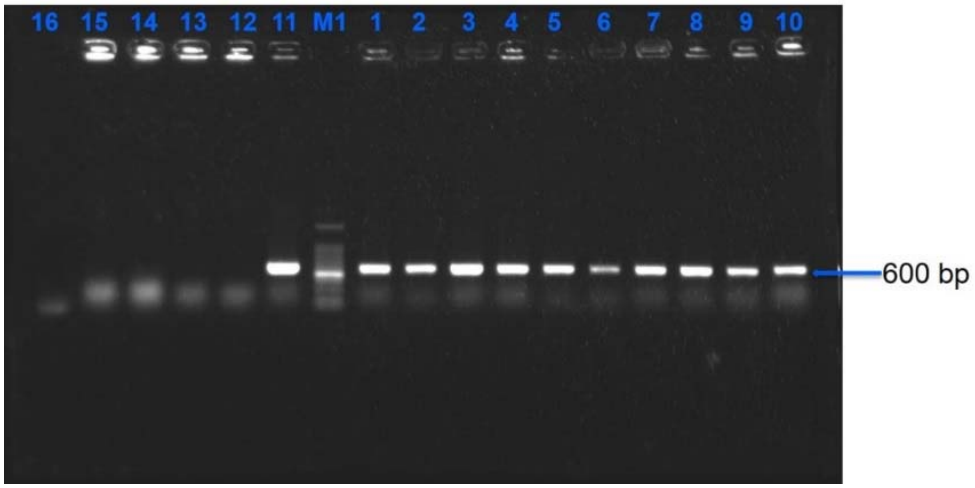

Fig. 3.5 PCR amplification results of *Pichia* recombinants. Lane 1-10, PCR results of recombinants; 11, control of pPICZ A-CP; 12, control of GS115-pPICZ A; 13, control of KM71-pPICZ A; 14, control of GS115; 15, control of KM71; 16, control of ddH_2O; M1, Takara 100 bp DNA ladder.

Table. 3.1 The sequence comparison of the synthesized CCMV CPsyns by NCBI blastp.

Score	Expect	Method	Identities	Positives	Gaps
387 bits (993)	5e-135	Compositional matrix adjust	190/190 (100 %)	190/190 (100 %)	0/190 (0 %)

Query 1 MSTVGTGKLTRAQRRAAARKNKRNTRVVQPVIVEPIASGQGKAIKAWTGYSVSKWTASCA 60

MSTVGTGKLTRAQRRAAARKNKRNTRVVQPVIVEPIASGQGKAIKAWTGYSVSKWTASCA

Sbjct 1 MSTVGTGKLTRAQRRAAARKNKRNTRVVQPVIVEPIASGQGKAIKAWTGYSVSKWTASCA 60

Query 61 AAEAKVTSAITISLPNELSSERNKQLKVGRVLLWLGLLPSVSGTVKSCVTETQTTAAASF 120

AAEAKVTSAITISLPNELSSERNKQLKVGRVLLWLGLLPSVSGTVKSCVTETQTTAAASF

Sbjct 61 AAEAKVTSAITISLPNELSSERNKQLKVGRVLLWLGLLPSVSGTVKSCVTETQTTAAASF 120

Query 121 QVALAVADNSKDVVAAMYPEAFKGITLEQLTADLTIYLYSSAALTEGDVIVHLEVEHVRP 180

QVALAVADNSKDVVAAMYPEAFKGITLEQLTADLTIYLYSSAALTEGDVIVHLEVEHVRP

Sbjct 121 QVALAVADNSKDVVAAMYPEAFKGITLEQLTADLTIYLYSSAALTEGDVIVHLEVEHVRP 180

Query 181 TFDDSFTPVY 190

TFDDSFTPVY

Sbjct 181 TFDDSFTPVY 190

3.3.3 Expression of CCMV CP in P. pastoris

Different *P. pastoris* transformants were induced by methanol and detected for their CCMV CPsyns expression. The supernatant samples were diluted ten times after cell were broken and five μL of each sample were loaded on SDS-PAGE (Fig. 3.6). All of them showed a band at 20 kDa which was the calculated molecular weight of CCMV monomers and transformant GS115-27-6 was screened out for further fermentation. After the optimization of the culture in shaking flasks, the yield of CCMV CP reached 0.78 mg/mL.

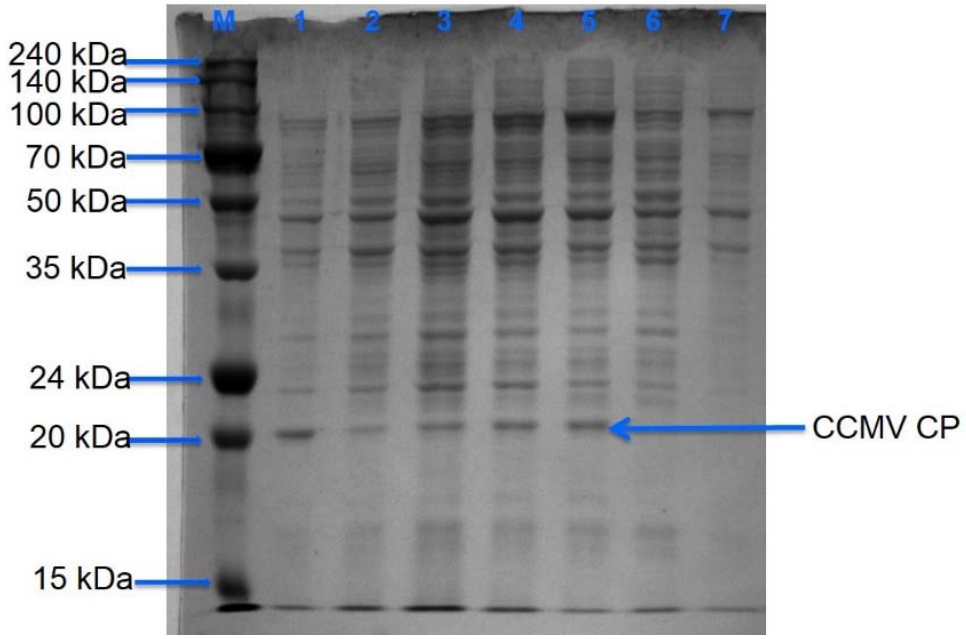

Fig. 3.6 SDS-PAGE results of *P. pastoris* transformants. Lane 1-5, soluble fractions of pPICZ A-CPsyns transformants after sonication; 6, control of pPICZ A/GS115; 7, control of GS115; M, DokDo-MARK^{TM} broad-range.

3.3.4 Scale-up fermentation

The fermentation of transformant GS115-27-6 in 5 liter fermenter was divided into 3 phases with a stepwise feeding strategy adopted from the reference [Dietzsch et al., 2011]. As the results presented in table 3.2 and Fig. 3.7, the wet cell weight attained 180.8 g/L after glycerol fed-batch, while the total protein concentration was 12.3 mg/mL. The maximum yield of soluble CCMV CP was obtained after 72-h methanol induction at the level of 4.8 mg/mL, which accounted 39.0 % of total protein. The increase of induced protein from methanol induction was 8.6 mg/mL for total protein, 3.9 mg/mL of which was contributed by CCMV CP and 4.7 mg/mL from other intracellular components. The reasonable explanation to this might be due to CCMV CP occurred synchronously together with other proteins as time went on. The mechanism of the foreign genes expressed intracellular usually were inserted in the chromosome DNA of *Pichia* which were also combined with other proteins under the promoter of AOX1 and AOX2 [Cereghino et al., 2002]. It's different with the foreign gene expressed in *E.coli* that existed as independent plasmid in cytoplasm.

Given the high yield of natural CCMV from infected leaf tissue (ca. 1–2 mg/g), the process was cumbersome and inefficient. And compared with other heterologous expression of CCMV CP in *E.coli* (0.1 mg/mL) [Zhao et al., 1995], *P. fluorescens* (2.6 mg/mL) [Phelps et al., 2007], and *P. pastoris* (wild type with non-optimal codon, 0.05–0.5 mg g^{-1} wet cell mass) [Brumfield et al., 2004], the yield presented here was one of the highest productions of viral coat protein reported to date.

Table. 3.2 Fermentation results of CCMV CP in fermenter during different cultivation phases

	Glycerol Batch	Glycerol Fed-Batch	Methanol Fed-Batch (mL/h/L)		
			3.6	7.3	10.9
Time of duration (h)	20	4	4	2	72
Wet cell weight (g/L)	135.6	179.5	180.8	180.8	180.2
Total protein (mg/mL)	2.8	3.5	3.7	4.3	12.3
CCMV CP (mg/mL)	--	--	0.9	1.5	4.8
Yield (%)	--	--	24.3	34.9	39.0

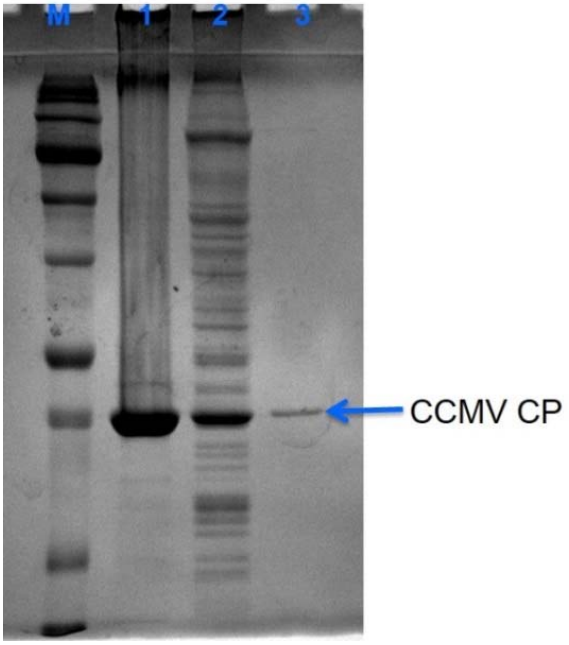

Fig. 3.7 SDS-PAGE results on 5L fermenter. Lane 1, PEG-precipitated CCMV CP pellets; 2, supernatant after sonication; 3, pellets after loading on FPLC; M, DokDo-MARKTM broad-range.

3.3.5 Purification of CCMV VLPs

PEG treatment to transformant GS115-27-6 supernatant preferentially precipitated CCMV CP with only little other proteins precipitated (Fig. 3.8). After CsCl ultracentrifugation, it was further purified to one band which indicated that the coat protein assembled into high molecular weight structures (CCMV CP). This provided a simple approach for the purification of virus capsids.

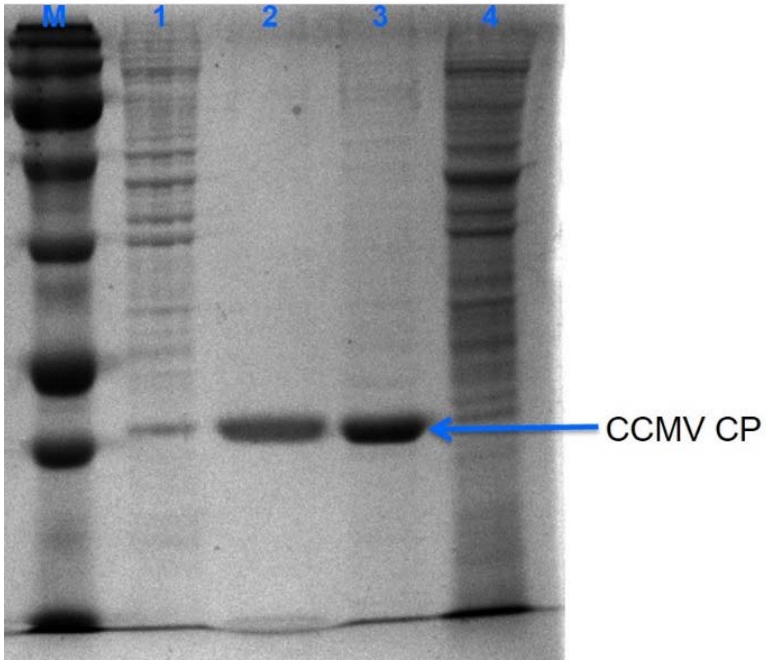

Fig. 3.8 Purification results of CCMV CP. Lane 1, soluble fractions of GS115-27-6 after sonication; 2, purified CCMV CP by CsCl ultracentrifugation; 3, pellets after PEG-precipitation; 4, supernatant after PEG-precipitation; M, DokDo-MARK^{TM} broad-range.

3.3.6 Analysis of purified CCMV VLPs

The obtained CCMV VLPs sample was analyzed by UV spectroscopy as shown Fig. 3.9. The assembled VLPs sometime could package the yeast RNAs *in vivo* although they usually prefer to encapsulate viral RNAs selectively during replication in plants [Annamalai et al., 2005]. The UV spectrum was dominated by the nucleic acid absorption maximum located at 260 nm, and the A_{260}:A_{280} ratio of 1.52 was similar to 1.56 which was observed for plant derived CCMV particles as reported [Lavelle et al., 2007]. This indicated that *P. pastoris* derived CCMV VLPs packaged the CP mRNA among with other host mRNAs during the assembly process.

The sample was also analyzed by TEM, which showed spherical particles of 28 nm in diameter with RNA entrapped inside the capsids and empty ones of 26 nm in diameter (Fig. 3.10).

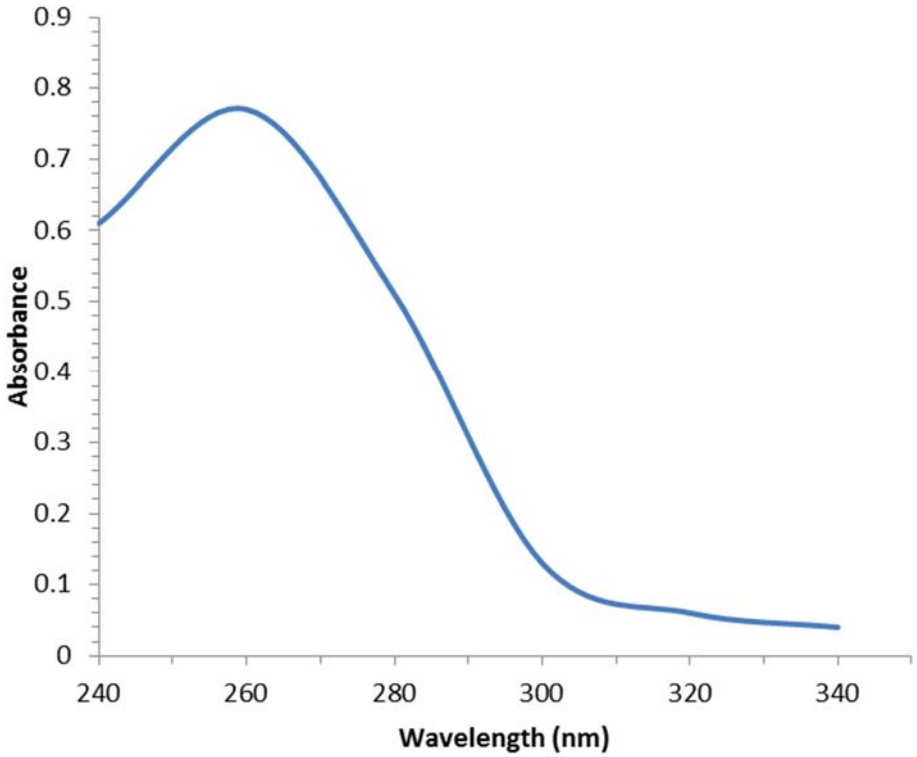

Fig. 3.9 UV profile of the CCMV VLPs in sodium acetate buffer.

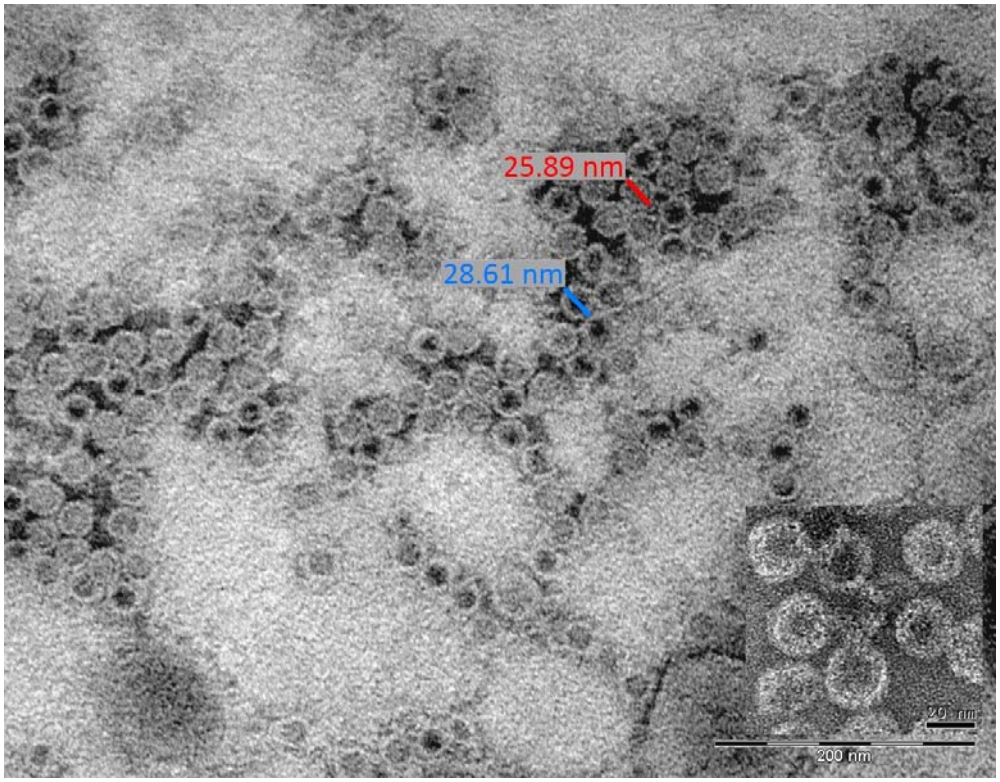

Fig. 3.10 TEM image of CCMV VLPs expressed in *P. pastoris*. Two types of capsids were observed: 28 nm in diameter with RNA entrapped, and empty ones of 26 nm in diameter; Size bar represents 200 nm. Insert was magnified TEM image of CCMV VLPs with size bar of 20 nm.

3.4 Summary

CCMV coat protein gene was optimized by *Pichia pastoris* codon preference to remove the low efficient codons and improve its expression level for the first time. The newly synthesized CPsyns was transformed into *P. pastoris* GS115 and soluble CCMV VLPs were obtained at high yield of 4.8 mg/mL. Our data suggested that proper codon optimization could be valuable for heterologous virus genes to be expressed in *P. pastoris* at an ample level. Except high expression, the *P. pastoris* system has been certified that it has advantages over other expression systems [Macauley-Patrick et al., 2005; Yokoyama, 2003]. The fermentation period, usually 4–5 days, was shorter compared to plant hosts which usually last several weeks. The VLPs attained were soluble and self-assembled, while prokaryotic hosts such as *E. coli* often resulted in insoluble inclusions.

TEM image of the assembled CCMV VLPs revealed that the VLPs derived from *P. pastoris* were similar to the wild type particles derived from plants. This work provided a promising tool for the preparation of large amount VLPs in gene therapy, vaccine development, and other applications.

Chapter 4. Encapsulation of Prussian Blue by CCMV

4.1 Introduction

As sophisticated biomolecular architectures, virus capsids can serve as nanoreactors or nanotemplates for encapsulations, crystallizations, and other reactions. Among the repertoire of biological scaffolds for nanotechnology, CCMV has been used as a nanoreaction vessel for the fabrication of nanoparticles [Vriezema et al., 2005; Fischlechner and Donath, 2007]. There are at least nine basic residues (arginine and lysine) to the interior of CCMV cavity [van der Graaf et al., 1991], which creates a positively charged interior cavity surface and provides an interface for inorganic crystal nucleation and growth. Taking the advantage of the reversible pH-dependent assembly/disassembly process, CCMV was employed for the entrapment of organic and inorganic materials governed by a unique molecular gating mechanism. Douglas and Young employed CCMV capsid for the encapsulation and crystallization of polyoxometallate species (e.g., vanadate, molybdate and tungstate) based on its positively charged interior surface [Douglas and Young, 1998]. The size and property of CCMV capsid confer it potential technological applications in a wide range of fields, including magnetic memory devices and magnetic resonance imaging.

Prussian blue (PB) is the historic name of an ancient pigment which is now recognized as a member of the transition metal hexacyanoferrate family [Ferlay et al., 1995; Sato et al., 1996]. These functional inorganic materials are possessed of an elegant and simple face-centred cubic (FCC) lattice of transition metal ion centres bridged by electron-rich cyanide groups; PB is the simplest representative for which the metal ion centres are both iron [de Tacconi et al., 2003; Dei, 2005]. There exist two well-known forms of the PB crystal: the insoluble PB with the formula $Fe^{III}_4[Fe^{II}(CN)_6]_3$ and the soluble $MFe^{III}[Fe^{II}(CN)_6]$ (M = NH_4, Li, Na, K). In fact both forms are completely insoluble in water and most common solvents.

The soluble form contains monovalent metal ion inclusions that can dissociate in aqueous media and lead to a net negative ionization on the crystal surface which allows a small and stable dispersion to be “soluble” [DeLongchamp and Hammond, 2004]. The reaction between hexacyanoferrate (III) and iron (II) leads to the synthesis of soluble PB nanoparticles is presented in Fig. 4.1. The variety of unique structures and magnetic properties of PB and its related metal hexacyanates have attracted intense interest because of their application as molecular magnets [Taguchi et al., 2005].

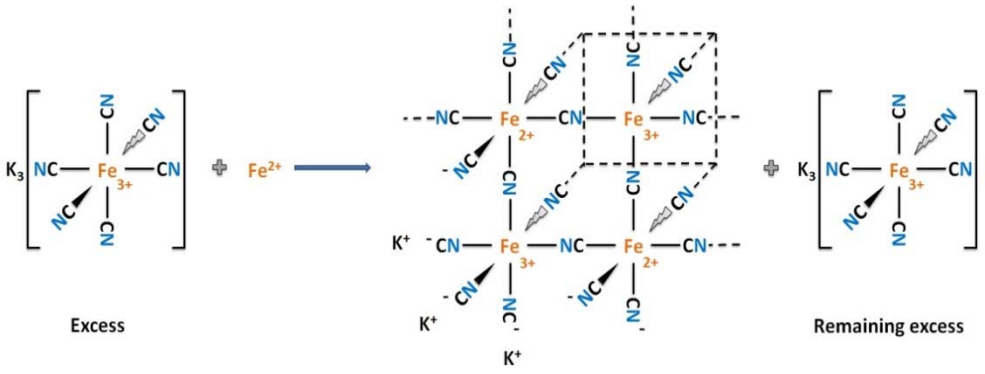

Fig. 4.1 Scheme of the synthesis of Prussian blue.

CCMV capsids have the positively charged amino acids of the N-terminus of CP that are protruding into the interior of the capsid which is essential for the package of the negatively charged genome. Thus the incorporation of the negatively charged iron complexes, Prussian blue particles, into viral cages is feasible and practical [Domínguez-Vera and Colacio, 2003; de la Escosura et al., 2008]. Following a similar strategy like this, we described the self-organization of PB-CCMV biohybrids and the properties of the nanoparticles for their potential applications (Fig. 4.2). The method presented here was more concise and explicit without the need for long-time irradiation by laser beam [de la Escosura et al., 2008].

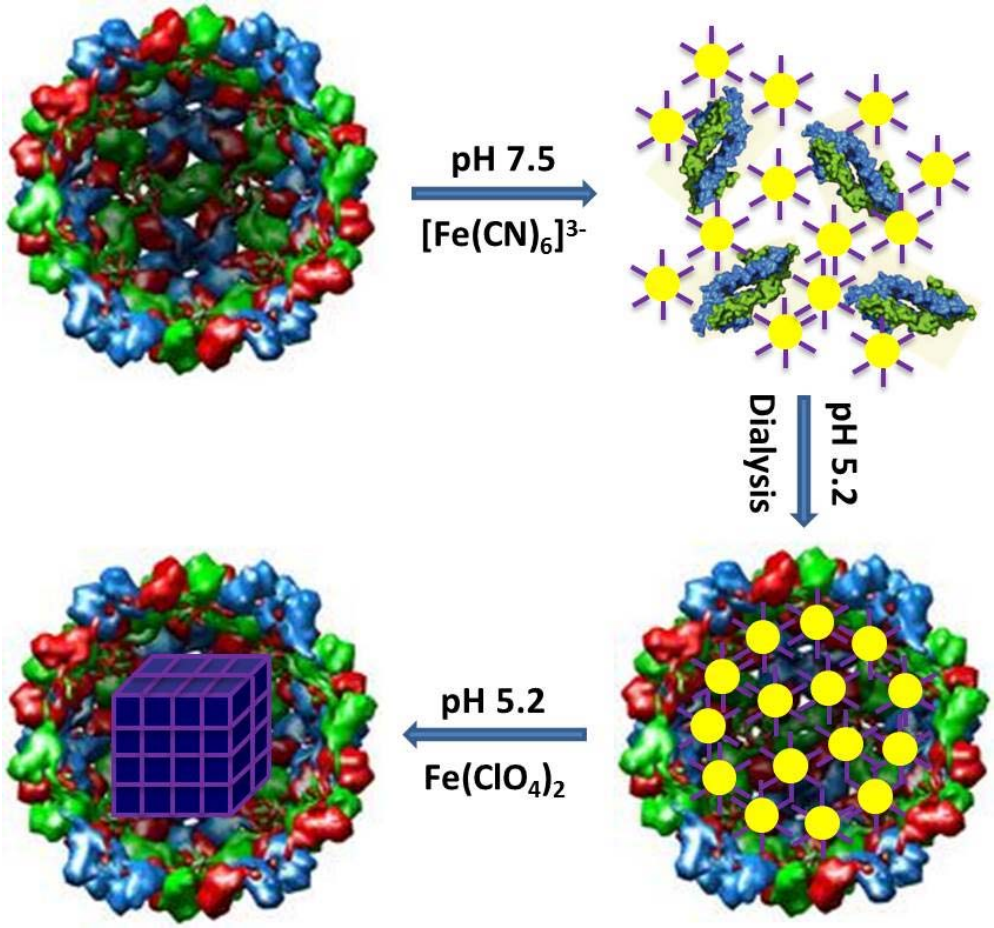

Fig. 4.2 Schematic diagram of the method employed to prepare PB nanoparticles inside the CCMV capsid.

4.2 Materials and methods

4.2.1 Preparation of disassembled CCMV solution

Unless otherwise stated, all reagents and chemicals were obtained from Sigma-Aldrich and Fluka and used without further purification. Buffers were prepared from ultrapure (Milli-Q) water and filtered through 0.22 μm filters (Millipore, Germany) for sterilization. The purified CCMV sample with the concentration of 2.5 mg/mL was prepared in assembly buffer as mentioned in Section 3.2.5. The solution was dialyzed against disassembly buffer (20 mM Tris-HCl, 1 M NaCl, 5 mM DTT, 0.5 mM PMSF, pH 7.5) over a period of 9 h with buffer changes every 3 h at 4 °C using a 12–14 kDa MWCO SnakeShin® Pleated Dialysis Tubing membrane (Thermo Scientific, USA). The sample was concentrated using centrifugal filter devices (Vivaspin 6 mL, Vivascience).

4.2.2 Encapsulation and synthesis of Prussian blue nanoparticles by CCMV

The disassembled CCMV solution (225 μL) was mixed with 100 mM precursor salt of potassium ferricyanide ($K_3[Fe(CN)_6]$, 25 μL) and incubated for 30 min. The resulted solution was then dialyzed against assembly buffer for the dimers to reassemble into intact capsids. The iron (II) chloride solution ($FeCl_2$) and iron (II) perchlorate hydrate solution ($Fe(ClO_4)_2$, 3 mM) were separately added to the dialyzed solution containing the hexacyanoferrate (III)-loaded CCMV slowly. The open pores of 2-nm diameter on CCMV capsids permit the ions to diffuse freely into and out of the cavity which will lead to the production of PB nanoparticles. The yielding of the immediate appearance of an intense blue colour was observed in the later one. The resulting PB-CCMV solution was dialyzed against assembly buffer over a period of 6 h with buffer changes every 3 h at 4 °C to remove the excess iron ion. The UV-vis spectrum at 710 nm was measured to confirm the presence of Prussian blue inside the capsid.

4.2.3 Purification of PB-CCMV by FPLC

Size-exclusion fast protein liquid chromatography (FPLC) was introduced to remove the non-encapsulated PB particles from access [Sheehan and O'Sullivan, 2003]. FPLC was performed on an Akta FPLC system (GE Healthcare Life Sciences) equipped with a Superose 6 PC 3.2/30 column (Amersham biosciences) at a flow rate 40 μL/min. The injection volume was 100 μL and the elution buffer composed of 50 mM sodium acetate, 500 mM NaCl, and 1 mM DTT at pH 5.0. The purified wild type CCMV (wt-CCMV) from Section 3.2.5 was used as a control for the elution time during FPLC purification. The purified PB-CCMV was concentrated with centrifugal filter devices for further analysis.

4.2.4 Analysis of the purified PB-CCMV

The purified PB-CCMV was subsequently examined by TEM to determine the size distribution of PB-CCMV biohybrids. Formvar-carbon coated grids were hydrophilized in a glow discharge apparatus and 5 μL of the sample was applied onto the grid. After leaving the sample air-dried for 1 minute, the excess of liquid was drained using a piece of filter paper. Uranyl acetate (5 μL, 2 % w/v) was then applied and the drying procedure was repeated. TEM image was obtained with a CM30 electron microscope (FEI/Philips) operated at 200 kV (Korea Basic Science Institute, Chunchon Center, Korea).

Dynamic light scattering (DLS) was employed to measure the hydrodynamic diameters of the formed nanoparticles at physiological pH (Malvern Zetasizer nano ZS spectrometer). The particle size distribution of scattering data was best fit using the Contin algorithm with the average of at least five measurements.

4.3 Results and discussion

4.3.1 Encapsulation and synthesis of Prussian blue nanoparticles by CCMV

The disassembly of CCMV capsid into protein dimers at pH 7.5 followed by its reassembly at pH 5.2 provided a strategy to entrap hexacyanoferrate (III) within the protein cage. Once CCMV reassembled in the presence of the negatively charged hexacyanoferrate (III), two types of hexacyanoferrate (III) could be detected: the one trapped by CCMV capsid and the free one outside the capsid. The resulting yellow solution was exhaustively dialyzed against four changes of buffer. After this treatment, the yellow colour within the dialysis bag rapidly decreased until it remained constant, indicating the existence of hexacyanoferrate (III) trapped by CCMV capsid in the reassembly process. The addition of the iron (II) salt $Fe(ClO_4)_2$ to this solution produced the immediate appearance of an intense blue colour of Prussian blue (Fig. 4.3). There are separate 2-nm pores presented on the interface of CCMV capsids through which the ions can diffuse into and out of the capsid to produce PB nanoparticles. As for the solution of $FeCl_2$, the reaction failed as expected which might be due to the presence of perchlorate hydrate ion attributed to the formation of PB particles in some way unknown for now [Culp et al., 2005]. The UV-vis spectrum showed a broad increase of absorption centred at around 710 nm, which was consistent with an intermetal charge transfer between Fe^{II} and Fe^{III} in PB (Fig. 4.4). All these clearly indicated the presence of Prussian blue inside CCMV capsid.

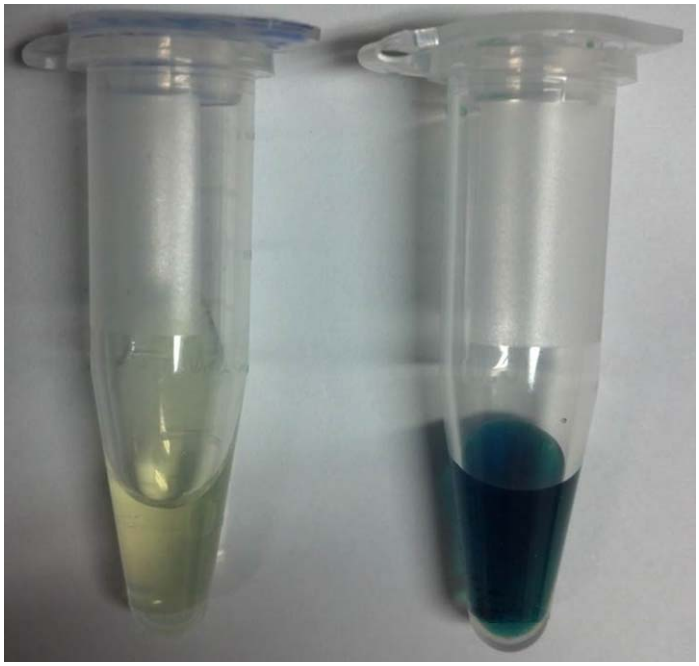

Fig. 4.3 The colour transition of Prussian blue encapsulated by CCMV capsid. The left one with yellow colour indicated hexacyanoferrate (III) trapped by CCMV capsids, the right one with blue colour after iron (II) salt $Fe(ClO_4)_2$ was added showing the appearance of an intense of Prussian blue.

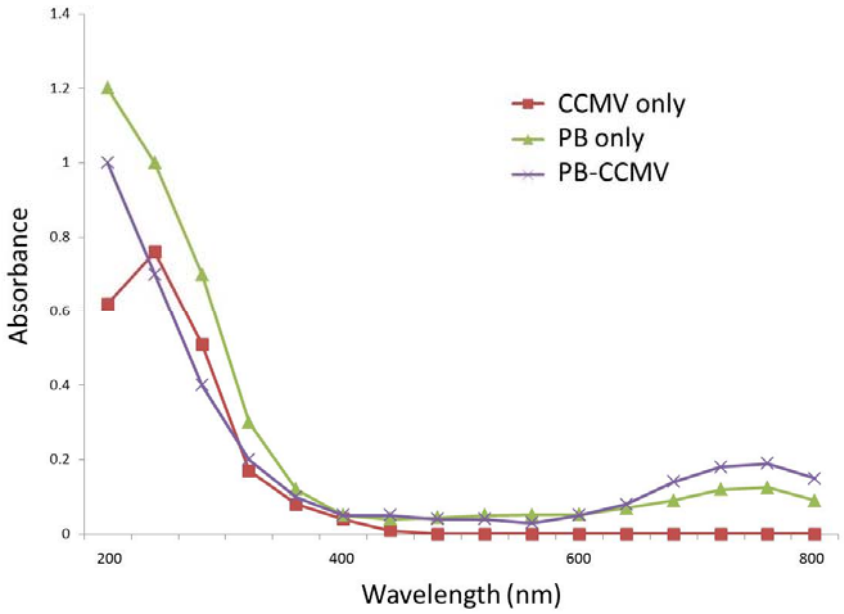

Fig. 4.4 UV-vis spectra of PB-CCMV. The red square represents CCMV only, green triangle represents PB only, and purple cross represents PB-CCMV.

4.3.2 Purification of PB-CCMV by FPLC

Purification of PB-CCMV and free PB particles using FPLC was verified by a very efficient separation, shortly after the column was loaded. As shown in Fig. 4.5, the FPLC chromatogram first presented an intense but broader peak at V = 1.6 mL at 280 nm which was similar to the control of wt-CCMV, while the remaining PB particles exhibited a second peak at V = 2.8 mL. As monitored at 710 nm, PB-CCMV showed two corresponding peaks for the existence of PB pigment and the wt-CCMV had no significant absorption.

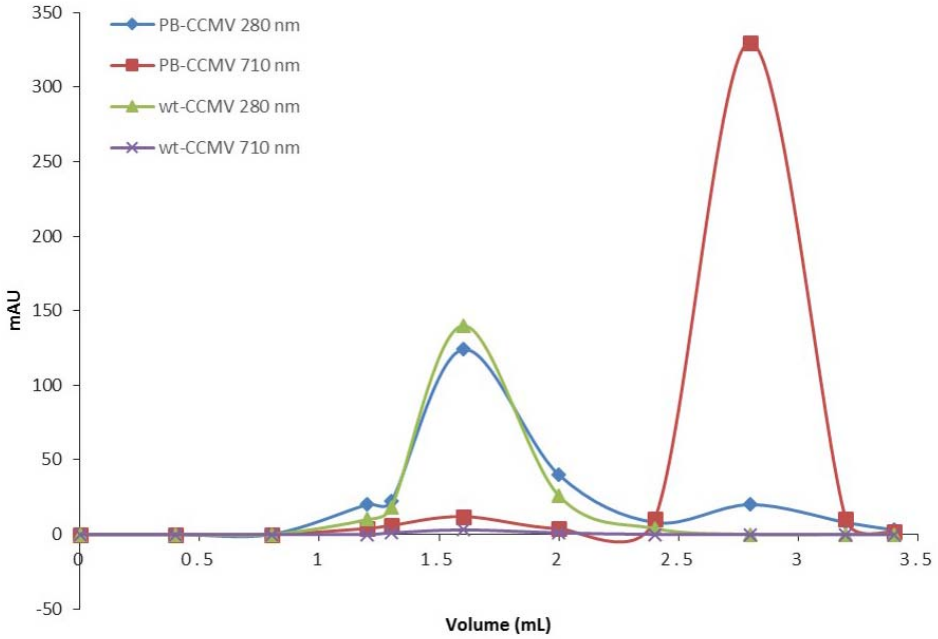

Fig. 4.5 Size-exclusion FPLC of PB-CCMV. The blue diamond represents PB-CCMV at 280 nm, red square represents PB-CCMV at 710 nm, green triangle represents wt-CCMV at 280 nm, and purple cross represents wt-CCMV at 710 nm. The peak at elution volume of 1.6 mL and 2.8 mL corresponded to PB-CCMV and free PB particles.

4.3.3 Analysis of the purified PB-CCMV

TEM images of the purified sample showed discrete spherical particles with relatively homogeneous size (Fig. 4.6). These capsids appeared as black dots surrounded by a bright shell compared to the wild type CCMV capsids, which can be attributed to the high electron density cores of Prussian blue. The spherical form, size, and composition of the non-aggregate particles validated the formation of PB inside the CCMV capsid. As expected, the reaction between hexacyanoferrate (III) and iron (II) did not lead to an infinite 3D well-ordered PB crystal structure but to a confined "PB-CCMV complex" according to the size limitation of CCMV capsid. Discrete rounded cubic particles were also observed.

The hydrodynamic diameters of the formed particles were measured by DLS (Fig. 4.7). The results showed the dots to be homogeneous, with two peaks of 29.2±1.7 nm corresponding to $T = 3$ particles (180 CP), and 17.5±1.2 nm corresponding to pseudo $T = 2$ particles (120 CP). Similar phenomenon was also reported by Daniel et al. that BMV capsids were utilized to encapsulate PEGylated gold nanoparticles and the size of formed hybrid VLPs varied from pseudo $T = 2$ to $T = 3$ capsids when 11.3-nm gold particles as the nucleating core for the capsids reassembly [Daniel et al., 2010]. This was in agreement accurately with the dimensions of the inner cavity of the CCMV capsid.

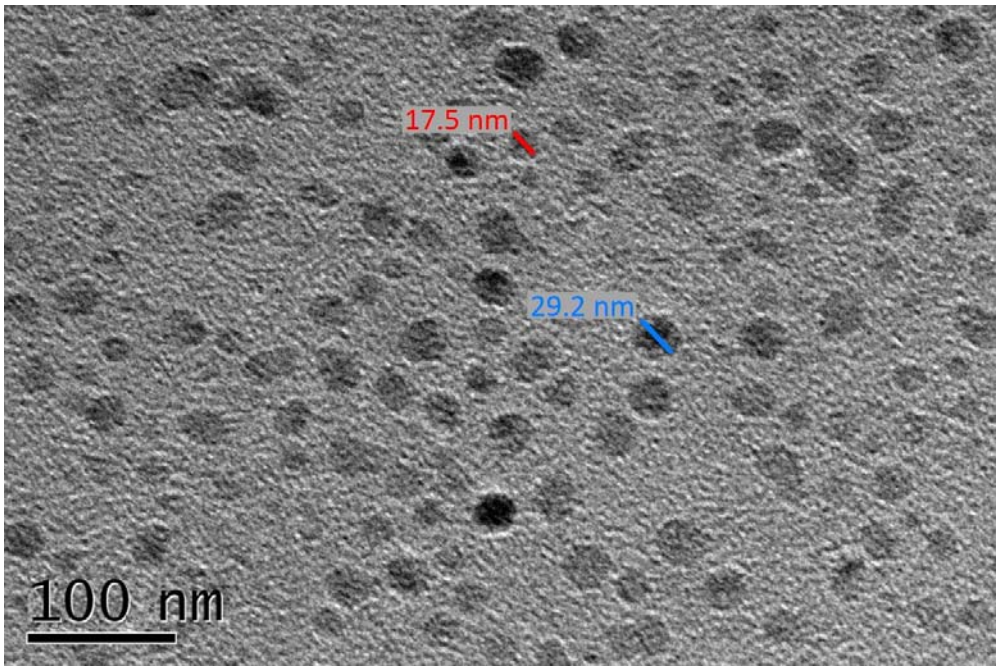

Fig. 4.6 TEM image of the PB-CCMV nanoparticles. Two types of capsids were observed: 29.2 nm corresponding to $T = 3$ particles, and 17.5 nm corresponding to pseudo $T = 2$ particles. Size bar represents 100 nm.

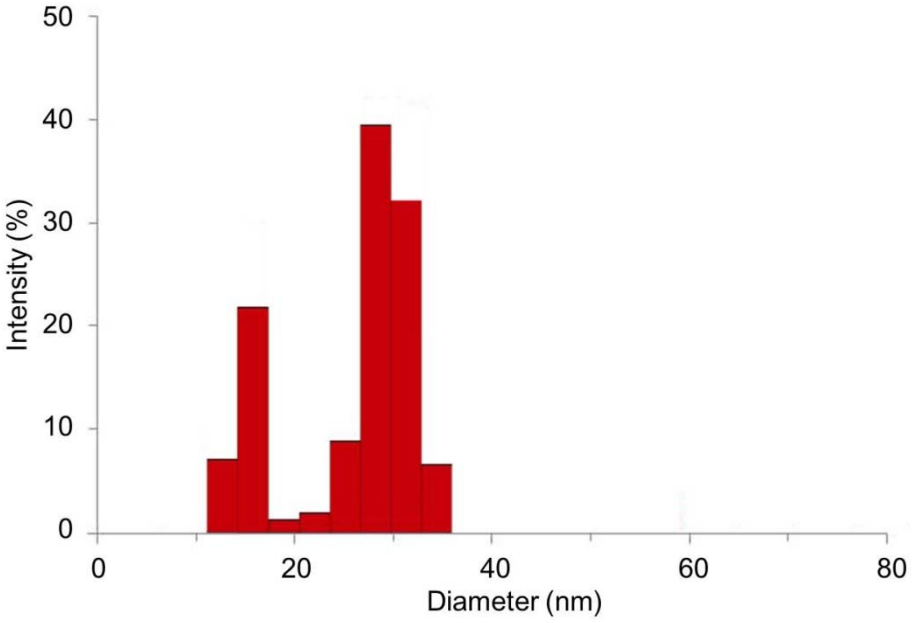

Fig. 4.7 DLS size distribution of PB-CCMV particles.

4.4 Summary

CCMV capsid is loaded with a negatively charged metal complex, hexacyanoferrate (III). The loaded capsid can act as a nanoreactor because the trapped metal complex is able to react with a second metal ion, iron (II), to fabricate a new material. The synthesized PB-CCMV biohybrids yield relatively homogeneous nanoparticles. With the omission of laser beam irradiation, the preparation method is much faster and more efficient, and the purification is easy to carry out.

This represents a novel route for the self-organization of homo- and heterobimetallic nanoparticles. Considering that the potential of magnetic nanoparticles in information storage devices and other magneto-optic applications, the properties of the system described here will be the subject of future research.

Chapter 5. Surface Modification of CCMV by CuAAC Reaction

5.1 Introduction

CCMV capsids provide a versatile platform for modification and multivalent presentation of ligands. Most research works used to focus on the constrained synthesis and encapsulation of both inorganic and organic materials taking the advantage of the structure transition of CCMV capsids [Bronstein, 2011]. There are few studies about the surface modification based on CCMV. As the assembly from 180 identical CP subunits, the outside surface of CCMV protrudes multiple, highly symmetrically arranged, native or engineered functional groups that can potentially be chemically modified for site specific attachment of a variety of ligands [Johnson and Speir, 1997]. Determined by the cryo-EM, each CP subunit presents up to 11 carboxylate groups (E63, E77, E81, E111, E148, E166, D128, D132, D153, D168, D183) exposed on the exterior surface (Fig. 5.1) [Reddy et al., 2001]. Similarly, there are up to six surface exposed amine groups (K54, K84, K87, K65, K106, K131) per subunit. This provides an estimate of up to 1980 and 1080 accessible sites for each of these functional groups, respectively, on the assembled capsid. Based on these information, Gillitzer et al. have successfully modified the exterior surface of CCMV with both fluorescent molecules and small peptides [Gillitzer et al., 2002]. The degree of surface modification was quantified *via* coupling of fluorophores to surface exposed amine (K), carboxylic acid (D and E), and engineered thiol residues (cysteine, C). A 24 amino acid peptide was also linked to the exterior surface of CCMV through exposed lysine and cysteine residues.

There have been a variety of bioconjugation methods developed for the attachment of ligands to the exterior surface of virus capsids. Among them, the copper(I)-catalyzed azide-alkyne cycloaddition (CuAAC) reaction, the most widely recognized example of click

chemistry, has been rapidly embraced for applications in myriad fields since its discovery by Finn and Sharpless, Scripps [Kolb et al., 2001; Rostovtsev et al., 2002; Tornøe et al., 2002]. As shown in Fig. 5.2, the selective reactivity between azides and alkynes (only with each other) has drawn tremendous attractiveness to this procedure (and its copper-free strained-alkyne variant). For the fragile nature and low concentrations of the manipulated biomolecules in practice, bioconjugation presents significant challenges for any ligation methodology. Several different CuAAC variants have been reported to address specific cases involving peptides, proteins, polynucleotides, and fixed cells [Hong et al., 2009]. CuAAC reaction provides a reliable method for coupling a wide range of molecules in a regiospecific fashion under relatively mild reaction conditions with little byproduct, which makes it a versatile and modular procedure for the modification of viral capsids. The Finn group has employed CuAAC reaction to conjugate both small molecules and macromolecules on the exterior surface of CPMV [Wang et al., 2003] and bacteriophage Qβ [Gupta et al., 2005]. The tyrosine residues on helical surface of TMV were coupled with chemoselective diazonium and azides *via* a sequential CuAAC reaction [Bruckman et al., 2008]. Different fluorescent coumarin and RGD-containing peptide were also grafted on the surface of TYMV by CuAAC reaction [Parrish et al., 2005; Zeng et al., 2011].

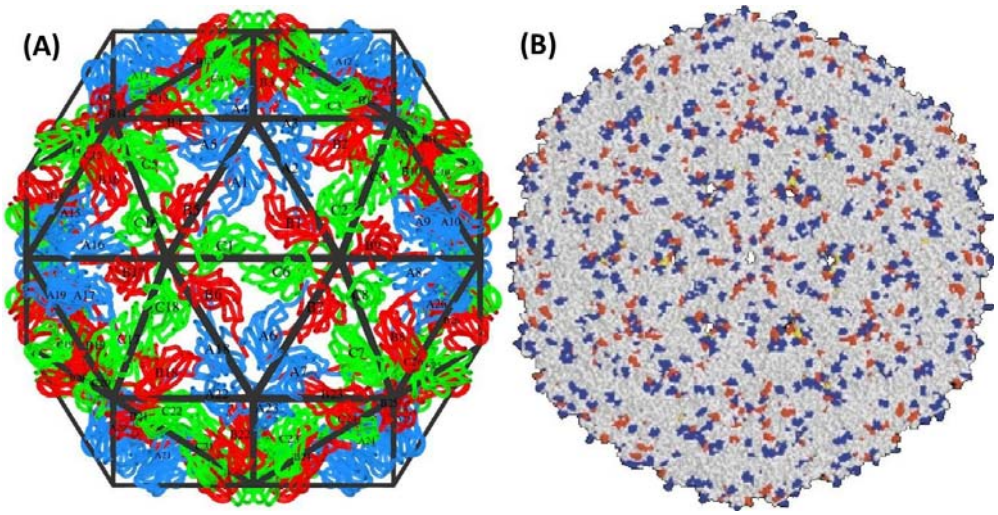

Fig. 5.1 Structure model of the exterior surface of CCMV. (A) *T* = 3 lattice model; (B) side view of the entire cage, lysines are indicated in red and carboxylates in blue.

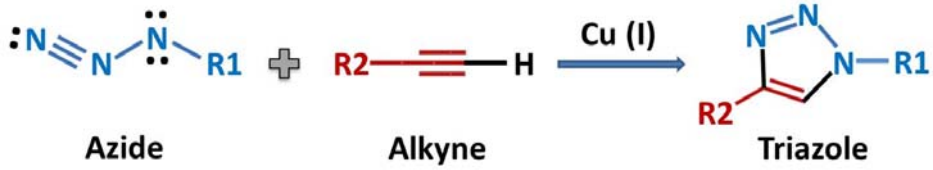

Fig. 5.2 Schematic diagram of the copper(I)-catalyzed azide-alkyne cycloaddition (CuAAC) reaction.

Although the exterior surface of CCMV capsid has been attached with fluorescent molecules and small peptides by NHS-ester acylation, there is no report about the modification of CCMV *via* CuAAC reaction. In this chapter, we first extended the CuAAC reaction to tailor CCMV capsid (Fig. 5.3). The surface exposed amine and carboxylate residues were efficiently addressable under wild conditions. The corresponding cell binding studies using decorated CCMV with relevant motifs showed a more cell-friendly environment with nanometer-scale surface features. This ligation methodology should be applicable to a wide variety of biomolecules, scaffolds, and cellular components, both *in vitro* and *in vivo*. The modified CCMV has potential applications in biosensors, nanoelectric devices, and drug targeting and delivery.

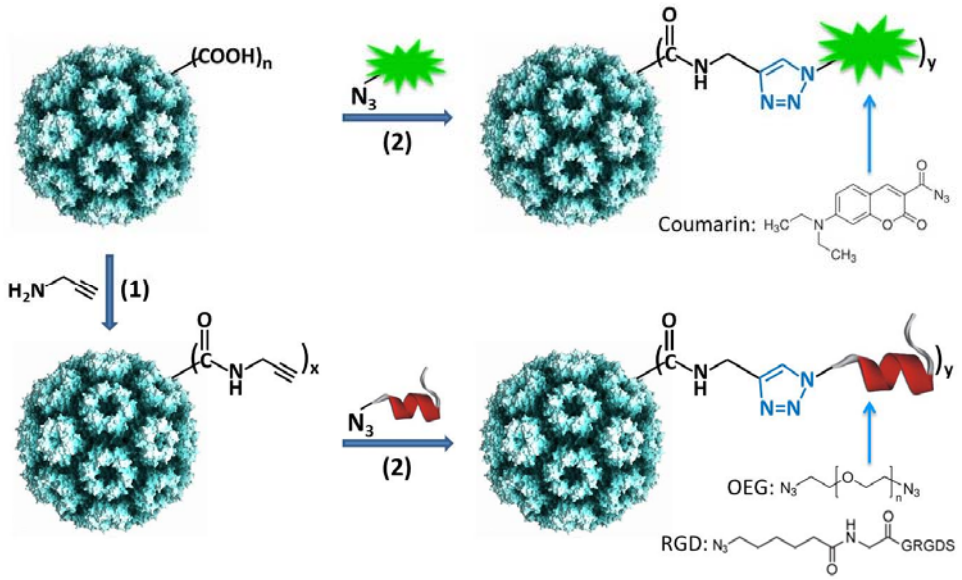

Fig. 5.3 Schematic diagram of bioconjugation on CCMV using CuAAC reaction. Fluorescent coumarintriazole (marked as green one), oligo-ethylene glycol short chain and RGD-containing peptide (marked as red one) were grafted on the surface of CCMV capsid *via* CuAAC reaction.

5.2 Materials and methods

5.2.1 Materials and instruments

Unless otherwise stated, all reagents and chemicals were obtained from commercial sources and used without further purification. 7-(Diethylamino)coumarin-3-carbonyl azide, oligo-ethylene glycol (OEG) bisazide, and azide-terminated RGD oligopeptide were purchased from Sigma-Aldrich or Invitrogen. APTES slides (3-aminopropyl-triethoxysilane-coated microscopy slides) were from Labscientific. The purified CCMV sample (1 mg/mL) was prepared in 80 % assembly buffer plus with 20 % dimethyl sulfoxide (DMSO) for the process. General desalting and removal of other small molecules from protein samples were achieved using centrifugal filter devices (Vivaspin 6 mL, Vivascience). Cesium chloride gradient ultracentrifugation, SDS-PAGE, TEM and DLS analyses were all performed as mentioned before. FPLC was performed on Biologic DuoFlow^{TM} Chromatography System (Bio-Rad, USA) with a Superose 6 PC 3.2/30 column (Amersham biosciences) at a flow rate 40 µL/min. Fluorescently labeled CCMV was visualized with ImageQuant 300 imager (GE Healthcare) before Coomassie blue staining. NIH-3T3 fibroblasts and HeLa cells were cultured in complete Dulbecco's modified Eagles medium (DMEM) supplemented with 10 % heat inactivated fetal calf serum (FCS), 2 mM L-glutamine, 50 µg/mL penicillin and 50 µg/mL streptomycin at 37 °C with 5 % CO_2 + 95 % atmosphere.

5.2.2 CCMV bioconjugation protocol

As shown in Fig. 5.3 step (1), CCMV was first modified with amine by incubating 1 mg/mL CCMV (500 µL) with 5 mM propargyl-amine aided with EDC and N-hydroxysulfosuccinimide sodium salt (sulfo-NHS) in the assembly buffer for 24 h at 4 °C. The product CCMV-alkyne was isolated by cesium chloride gradient ultracentrifugation and resuspended in 80 % assembly buffer and 20 % DMSO.

After the optimization and setup of CuAAC reaction, the conjugation (step (2) in Fig. 5.3) of CCMV-alkyne with the grafted moieties was carried out by incubating 1 mg/mL CCMV-alkyne with 7-(diethylamino)coumarin-3-carbonyl azide, oligo-ethylene glycol bisazide, and azide-terminated RGD oligopeptide separately, in the presence of 1 mM copper sulfate, 2 mM tris(2-carboxyethyl)phosphine hydrochloride (TCEP), and 3 mM ligand bathocuproindisulfonic acid disodium salt (BCDS) for 24 h at 4 °C.

The corresponding products (cumarin-CCMV, OEG-CCMV, and RGD-CCMV) were purified by two successive series of cesium chloride gradient ultracentrifugation and resuspended in the assembly buffer. The reactions were analyzed by FPLC, SDS-PAGE, TEM, DLS, and fluorescence spectroscopy.

5.2.3 Immobilization of modified CCMV on APTES slides

The modified CCMV capsids (0.5 mg/mL) were adsorbed onto APTES slides separately. Wild type CCMV was used as a control. 500 µL virus solutions were dropped onto the substrates (10×10 mm^2) so that they fully covered the surface, and the samples were set at room temperature in a biosafe hood for 10 min. The samples were washed in pure water and dried at room temperature. The resultant systems were denoted as APTES-CCMV, APTES-OEG-CCMV, and APTES-RGD-CCMV, respectively. The adsorpted virus particles onto the APTES slides were prepared for further utilization.

5.2.4 Cell adhesion

HeLa cells were cultured in complete DMEM at 37 °C in a humidified 5 % CO_2 incubator. Monolayers of HeLa cells in their growth phase (ca. 80 % confluence) were routinely split 1:5 in 10 cm culture dishes and placed at 37°C for 5–10 minutes. The cells were washed twice in preheated PBS containing 0.25 % (w/v) trypsin-EDTA. After the cells were detached from the dishes, 1 mL preheated culture medium was added and the cells

transferred to a 50 mL falcon tube. Cells were spun down and plated in new dishes with fresh culture medium for subsequent cell adhesion studies.

APTES-CCMV, APTES-OEG-CCMV, and APTES-RGD-CCMV slides (10×10 mm^2) were put into 12 well plates; 2 mL of HeLa cell suspension in complete DMEM at a density of 2×10^4 cells/mL was added to each well of the 12-well plate, and incubated at 37 °C in a humidified 5 % CO_2 incubator. Empty APTES slides were used as control.

Cell adhesion, spreading, and proliferation on precoated substrates were examined at 24 h postseeding. Nonadherent cells on the slides were removed by washing with PBS, and adherent cells were fixed using formaldehyde and stained with Giemsa stain. Photomicrographs of the cytoplasmic-stained cells were obtained (100× total magnification using Nikon Eclipse TS100 microscope).

5.3 Results and discussion

5.3.1 Introduction of alkyne group on CCMV

From the space filling model of CCMV in Fig. 5.1, there are plenty of exposed carboxyl groups on the exterior surface of CCMV: 11 aspartic acid and glutamic acid residues for each CP subunit and total 1980 residues for each capsid. Many studies have shown that the carboxyl residues of various viral capsids are amenable to reaction with primary amines under activation [Schlick et al., 2005; Steinmetz et al., 2006]. Therefore, carboxylic groups were chosen for further derivatization with alkyne in this study. The reactivity of CCMV carboxyl groups was tested with fluorescein cadaverine under activation with EDC and sulfo-NHS, which revealed that 560 carboxylates modified in high yields [Gillitzer et al., 2002]. This was approximately 4.7–6.2 times more than that accessible in TYMV (90 to 120 carboxylic groups) [Zeng et al., 2011]. To explore the potential of introducing multifunctional group on the surface of CCMV, the viral capsids were labeled with

acetylene at surface-exposed carboxylic groups. More than 90 % of the coat protein was recovered by ultracentrifugation after the removal of small molecules. The high recovery yield encouraged the continuation of CuAAC reaction between CCMV-alkyne and azides.

5.3.2 CuAAC reaction on CCMV-alkyne capsids

The conditions of CuAAC reaction are crucial for the productivity and need to be optimized. $CuSO_4$-sodium ascorbate is the preferred reducing agent for most reactions, due to its convenience and effectiveness at generating the catalytically active Cu(I) oxidation state. However, the byproduct of ascorbate to dehydroascorbate can hydrolyze to form reactive aldehydes such as 2,3-diketogulonate and presumably glyoxal [Shangari et al., 2007]. These species can cross-link with arginine, cysteine, and lysine residues on the viral capsid, which subsequently lead to the aggregation-dependent decomposition. This was clearly observed in the case CCMV modification. Thus TCEP and BCDS were introduced to for CuAAC bioconjugations as Cu(I) source. However the reaction rate was slowed down in the presence of TCEP. So the reaction time was extended to 24 h at 4 °C.
After the setup of CuAAC reaction, the acetylene functional group on the CCMV-alkyne surface was further addressed by the CuAAC reaction to attach fluorogenic or peptide moiety *via* triazole connection.

The fluorochrome 7-(diethylamino)coumarin-3-carbonyl azide was first employed as the azido counterpart in the CuAAC reaction, which could be easily monitored by the increase of fluorescence at 475 nm upon formation of triazole ring. The purified and diluted cycloaddition product coumarin-CCMV produced a strong detectable fluorescent signal at 475 nm upon excitation at 340 nm. FPLC result showed that CCMV particles were stable throughout the click reaction conditions and remained in the assembled state, indicated by similar elution with wild type CCMV particles. The result showed a single intact peak at t = 38 min which was similar with wild type CCMV, indicating the integrity of the particles and

the successful attachment of the coumarin dye (Fig. 5.4). The coumarin-CCMV sample was also analyzed using SDS-PAGE with fluorescence visualization of the attached coumarin, followed by Coomassie staining; the result revealed one dye-labeled band corresponding to the same molecular weight of CCMV CP subunit because of the covalent attachment with coumarin (Fig. 5.5).TEM confirmed the integrity of the particle after two-step modification with the size of approximately 30 nm (Fig. 5.6).

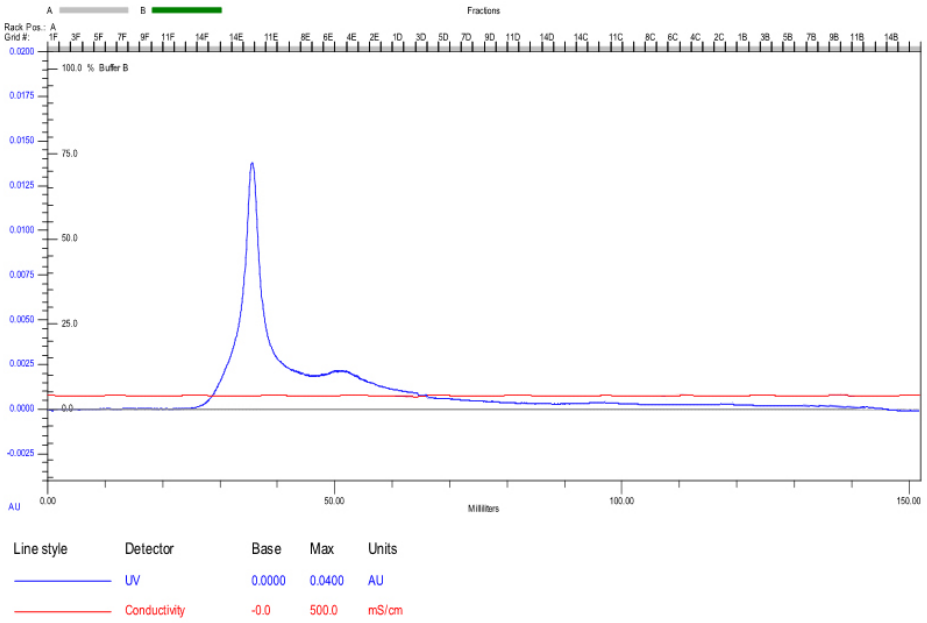

Fig. 5.4 Size-exclusion FPLC of coumarin-CCMV. The result showed a single intact peak at t = 38 min which was similar with wild type CCMV, indicating the integrity of the particles and the coumarin dye attachment.

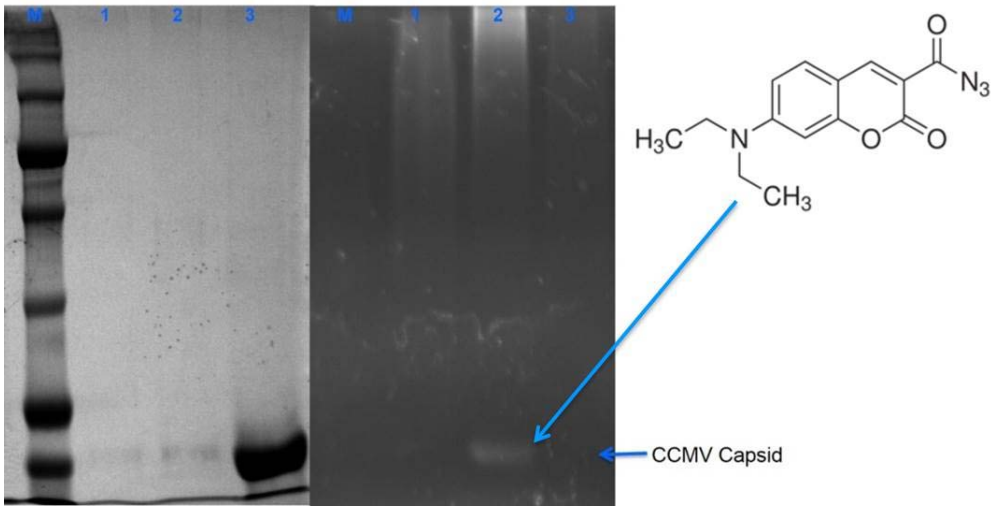

Fig. 5.5 SDS-PAGE of coumarin-CCMV visualized under UV irradiation and upon Coomassie blue staining. The left was taken under white light after Coomassie blue staining and the right was taken under UV irradiation. Lane 1, alkyne-CCMV; 2, coumarin-CCMV; 3, wild type CCMV; M, DokDo-MARKTM broad-range.

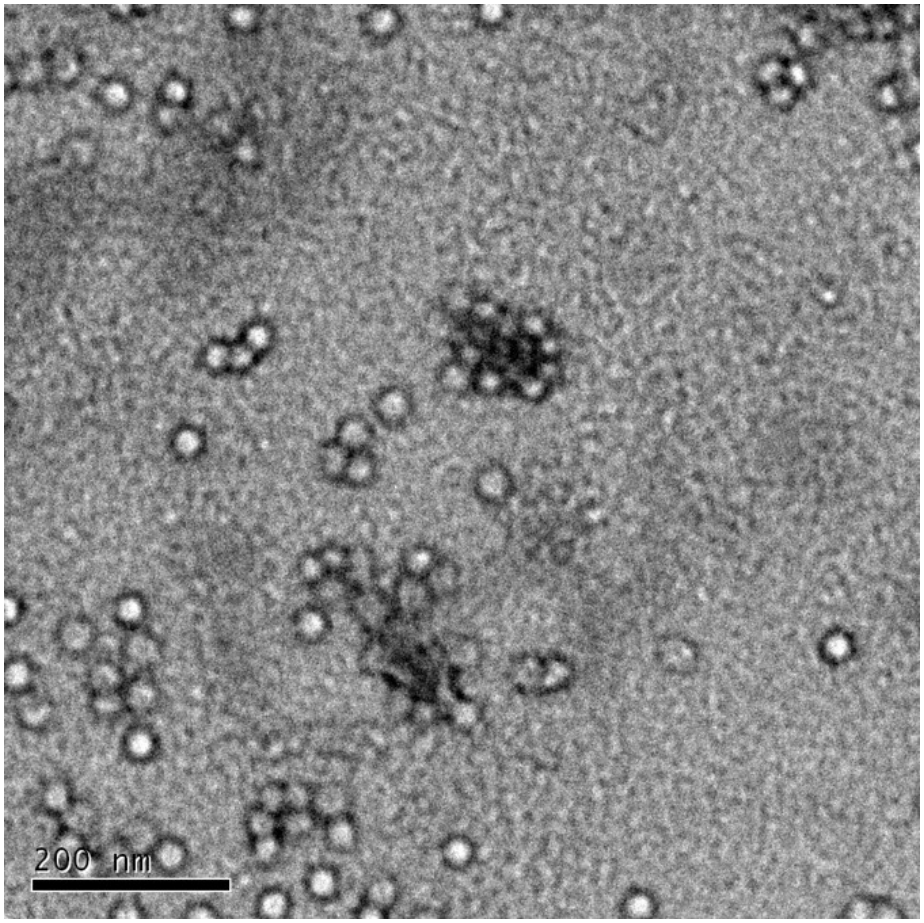

Fig. 5.6 TEM image of coumarin-CCMV particles. Size bar represents 200 nm.

Following the same procedure, oligo-ethylene glycol bisazide and azide-terminated RGD oligopeptide were also installed onto acetylene-functionalized CCMV. As expected with the high coupling efficiency of CuAAC reaction, the modified OEG-CCMV and RGD-CCMV were confirmed by FPLC analysis with similar elution time with wild type CCMV particles indicated by a single intact peak at t = 38 min verifying the integrity of the particles with OEG attachment. (Fig. 5.7). TEM image of OEG-CCMV showed a distinct phenomenon of connected bridges with the intact capsids cross-linked with each other (Fig. 5.8). As the obtained sticky solution distinguished with other samples, the reasonable explanation might stem from the possible double CuAAC reaction from the bisazide. The hydrodynamic diameters (measured by DLS) for OEG-CCMV were 30.7±1.5 nm (Fig. 5.9).

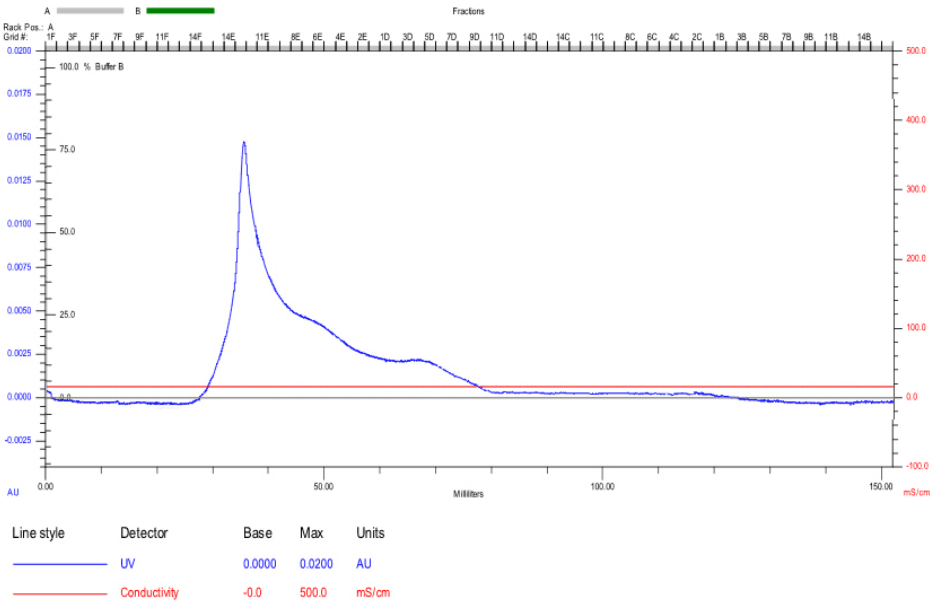

Fig. 5.7 Size-exclusion FPLC of OEG-CCMV. The result showed a single intact peak at t = 38 min which was similar with wild type CCMV, indicating the integrity of the particles with OEG attachment.

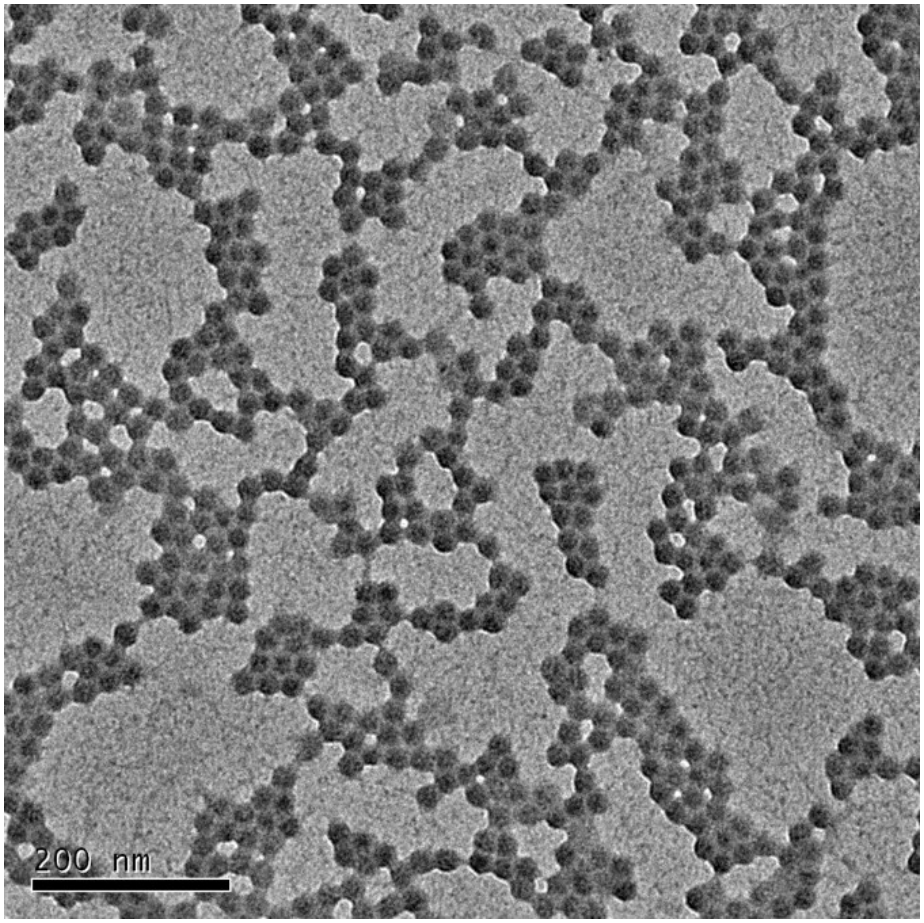

Fig. 5.8 TEM image of OEG-CCMV particles. Size bar represents 200 nm.

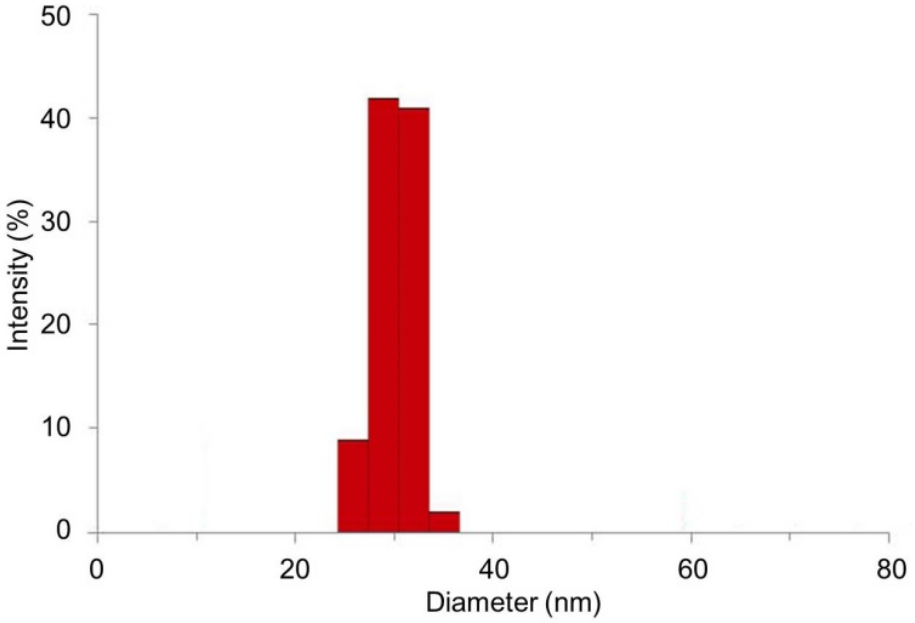

Fig. 5.9 DLS size distribution of OEG-CCMV particles.

5.3.3 Immobilization of on APTES slides

APTES slides were used to immobilize virus particles onto 2D surfaces prior to cell binding studies. APTES is positively charged which can hold negatively charged virus particles on the slides via electrostatic interactions at around neutral [Yamada et al., 2006; Rong et al., 2008]. CCMV and modified CCMV display negative surface charges at pH 5.2 (pI of CCMV is about 3.6). Therefore after drop coating and setting, the virus particles were anchored strongly on APTES slides as shown in Fig. 5.10. NIH-3T3 fibroblasts were first cultured on APTES slides to investigate the cell behavior and performance. As presented in in Fig. 5.11, the results showed elongated and stretched shape, and spread as time went on.

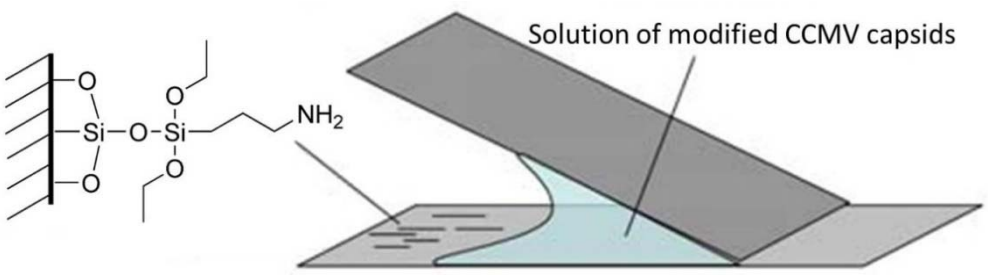

Fig. 5.10 Schematic representation of the system used to deposit aligned CCMV capsids.

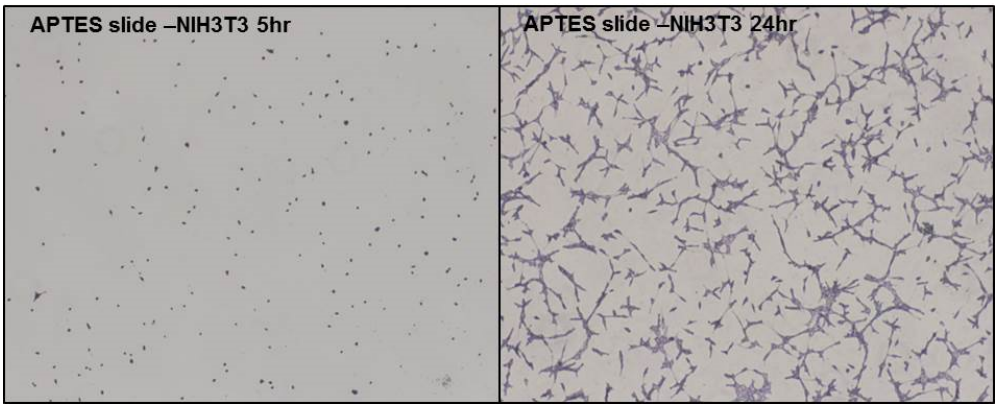

Fig. 5.11 Optical images of NIH-3T3 cells cultured on APTES slides (after 5 and 24 h).

Scale bar represents 100 μm.

5.3.4 Cell adhesion

HeLa cells were selected for the preliminary adhesion studies on virus-coated silane surface, as this kind of cell has already been widely used as a prototype cell to study cell-substrate interactions. RGD (Arg-Gly-Asp) tripeptide is the primary sequence with adhesive proteins of the extracellular matrix of $\alpha_v\beta_3$, which can bind to integrin receptors of all mammalian cells [Waldeck et al., 2008; Laitinen et al., 2009]. As the identification as a pervasive cell adhesive peptide, RGD has been extensively investigated to enhance the binding activity with mammalian cells. On the contrary, OEG presents inhibition to cell binding similar as PEG, a water-soluble polymer. Thus OEG and RGD were selected out to observe the opposite effects on the adhesion behavior of CCMV with HeLa cells.

After 5 and 24 h proliferation of HeLa cells with modified CCMV particles, the attachment was stained with Giemsa and verified by microscopy. As presented in Fig. 5.12, the cell proliferation was observed on all slides. At 5 h, the cell proliferation of APTES-OEG-CCMV slides showed slight inhibition compared to the control of APTES-coumarin-CCMV, while APTES-RGD-CCMV enhanced the binding in contrast. This was similar with former report that normally APTES-OEG-CCMV was nonadhesive to HeLa cells due to the lack of a biological recognition motif on OEG and its resistance to binding membrane proteins. However, as time went on to 24 h, the cell proliferation of APTES-OEG-CCMV slides showed more combination which might be caused by the cross-linked structure of OEG-CCMV (see Fig. 5.3 and 5.8). The explanation might lie on the structure of OEG polymer with diazide moieties at both terminuses caused the crosslinked structure of CCMV capsids bridged by triazole ligands with each other which could further affect the cell binding process. This unique structure of modified capsids generated a net-like sticky solution which then resulted in the higher adhesion with HeLa cells as times extended. Similar phenomena was reported by Kaur et al. using a dialkyne dye molecule for CuAAC reaction to modify

TYMV capsids which changed the hydrophobicity of the modified capsids at the interface of two liquids [Kaur et al. 2010].

As the results of APTES-RGD-CCMV were concerned, there was obvious enhancement of the binding compared with the control of APTES-coumarin-CCMV at 5 and 24 h. This indicated that the cell attachment occurred specifically in response to the RGD sequence. This suggested RGD ligand density and its spatial arrangement could play a vital role in the adhesion process. Also HeLa cell did not show similar elongated or stretched morphology as NIH3T3 fibroblast on APTES slides [Rong et al. 2008]. So the different property of two cell types made it difficult to observe the adhesion behavior with HeLa cell under microscopy.

The protein cage of CCMV would provide a more biomimetic soft and elastic atmosphere to the cells. Thus, the low-tension viral surface differs from the high-tension glass surface in terms of penetration, entanglement, and remodeling, and therefore provides a more cell-friendly environment with nanometer-scale surface features.

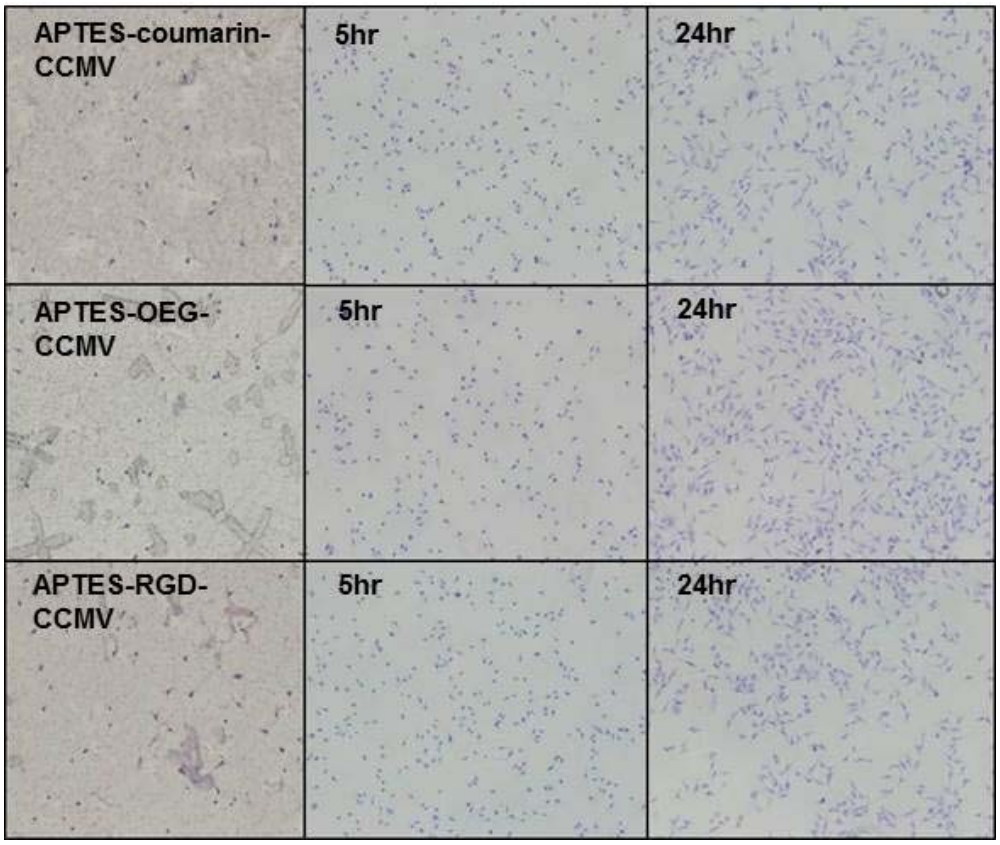

Fig. 5.12 Optical microscopy of cell adhesion results by different CCMV particles with HeLa cells. (A) APTES slides only of time 0, 5, and 24 h; (B) APTES-OEG-CCMV of time 0, 5, and 24 h; (C) APTES-RGD-CCMV of time 0, 5, and 24 h.

5.4 Summary

For the first time CCMV was grafted with different moieties from fluorogenic coumarin and OEG short chain to RGD peptide via CuAAC reaction. The carboxyl residues on the exterior surface were chosen to be addressed with alkyne and further modified with azide through triazole connection. The resulting viral capsids were confirmed intact by FPLC, SDS-PAGE, TEM, and fluorescence spectroscopy analysis. The cell adhesion and proliferation behavior of OEG and RGD decorated CCMV was studied to show the opposite effects.

Utilizing the spatially addressable surface chemistry of CuAAC reaction, CCMV-based material paves the way for the design of bionanoparticle-based nanosensor, drug delivery carrier, and tissue engineering materials. This approach represents a convenient, rapid, and versatile synthesis that can be employed in future.

Appendix I. Expression of HcRNAV and Co-expression with PMAP-23-D7 in *P. pastoris*

6.1 Introduction

Harmful algal blooms (HABs), also known as red tides, have had a negative impact on aquatic ecosystems and have increasingly become a threat to human and marine health [Anderson, 1997]. Rapid increases in an algal population can lead to water discoloration, shading of submerged vegetation, disruption of food-web dynamics and oxygen depletion in the water. HABs are known to have damaged the fishing industry, and to have affected shoreline quality and local economies [Friedman and Levin, 2005]. The potent neurotoxins can concentrate in filter-feeding shellfish and poison human consumers [Erdner et al., 2008]. Even non-toxic algae can be harmful when they amass in sufficient numbers. HABs occur in many regions around the world, including Scandinavia, the North Pacific, the Caribbean and the South Pacific [Kirkpatrick et al., 2004].

The toxic or harmful phytoplanktons that cause HABs are commonly dinoflagellates such as *Alexandrium* and *Karenia* [Garrett et al., 2010]. Most dinoflagellates have a unique structure that includes a nucleus known as the dinokaryon within which the chromosomes are attached to the nuclear membrane. Many efforts have been made to control harmful algal blooms with little success [Sengco and Anderson, 2004]. Today, the biological control of HABs is considered to be feasible [Solé et al., 2006]. Viruses that are abundant in marine systems replicate rapidly and tend to be host-specific, suggesting that single algal species could be targeted [Lawrence et al., 2001; Baudoux and Brussaard, 2005].

Heterocapsa circularisquama RNA virus (HcRNAV) is the first single-stranded RNA virus to be characterized that infects dinoflagellates [Tomaru et al., 2004]. *H. circularisquama*

Horiguchi, first observed in Uranouchi Bay, Japan, is a harmful bloom-causing dinoflagellate that specifically kills bivalves [Horiguchi, 1995]. HcRNAV particles are polyhedral with a diameter of approximately 30 nm, and encapsulate a single positive-stranded 4.4 kb RNA genome. The virus clones have been divided into types CY and UA (HcRNAV109 and HcRNAV34, respectively), based on their host strain specificity [Mizumoto et al., 2007]. The structure of HcRNAV109 was revealed by cryo-EM that 180 quasi-equivalent monomers arrange in a $T = 3$ symmetry and each monomer contributes to a 'bump' on the surface of the capsid as shown in Fig. 6.1 [Miller et al., 2011]. There are two open reading frames (ORF-1 and ORF-2) identified in the RNA genome, with ORF-2 coding for the viral coat protein [Nagasaki et al., 2005]. HcRNAV was found to target and accumulate in the dinoflagellate nucleus.

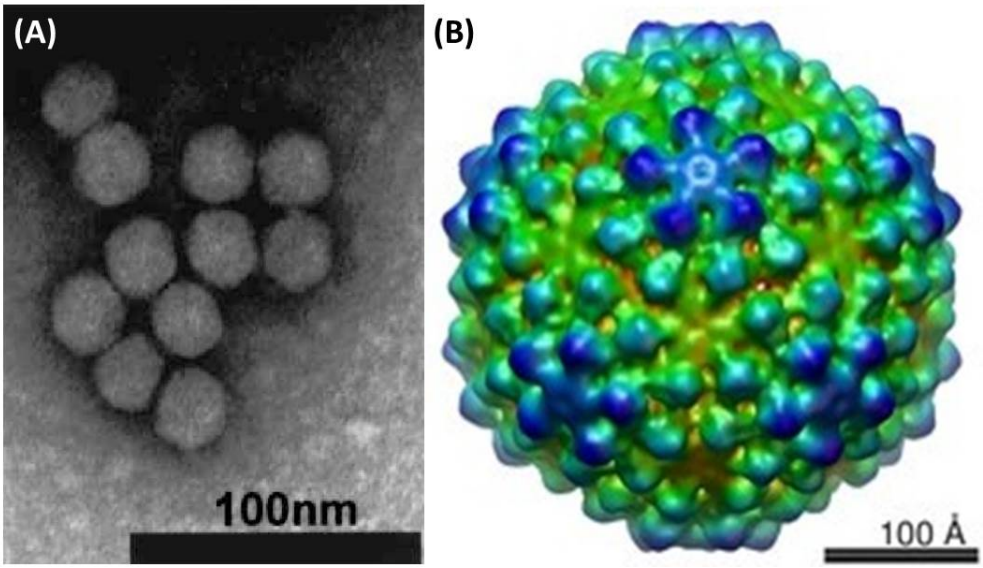

Fig. 6.1 TEM image and three-dimensional reconstruction of HcRNAV109 capsid. (A) TEM image of purified HcRNAV109 capsids; (B) Three-dimensional reconstruction of HcRNAV109 by cryo-EM.

Antimicrobial peptides are small molecular weight proteins with broad spectrum antimicrobial activity against bacteria, viruses, and fungi [Zasloff, 2002; Izadpanah and Gallo, 2005]. They are an evolutionarily conserved component of the innate immune response and are found among all classes of life. The mechanism of their antibacterial activity is mainly based on association to the pathogen plasma membranes and perturbation of their permeability [Bechinger and Lohner, 2006; Giuliani et al., 2008]. Peptide PMAP-23-D7 is an efficient algicidal peptide which is derived from antibacterial peptide PMAP-23 [Orioni et al., 2009]. It is composed of 23 amino acids: Asp Ile Ile Asp Leu Leu Trp Asp Val Asp Asp Pro Gln Asp Pro Asp Phe Val Thr Val Trp Val Asp (DIIDLLWDVDDPQDPDFVTVWVD), of which there are multiple substitutions of lysine and arginine by aspartic acids (Fig. 6.2).

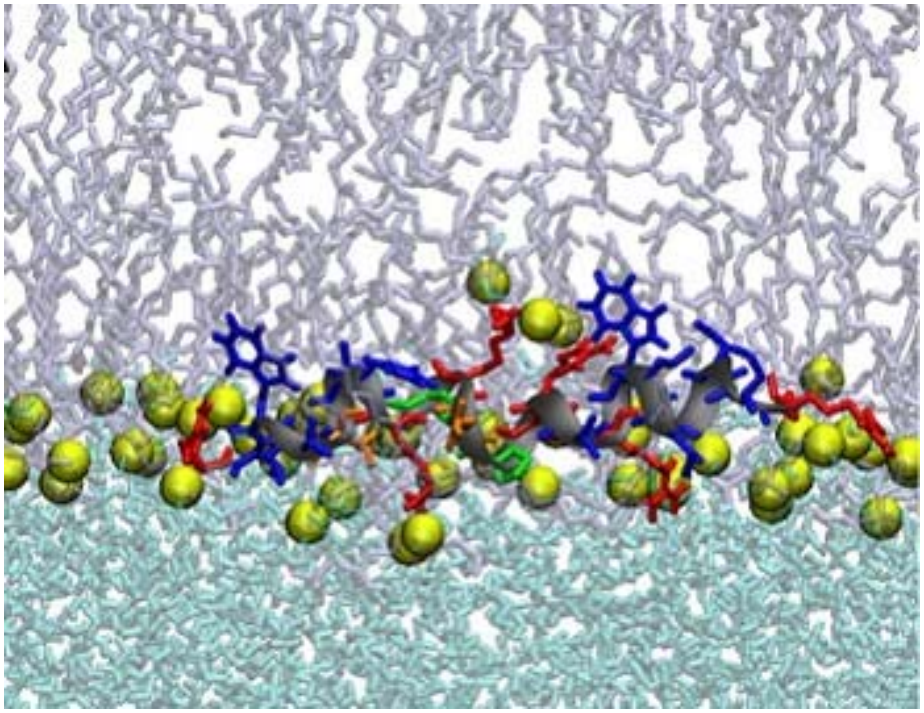

Fig. 6.2 Representative structure of peptide PMAP-23-D7 at the end of two molecular dynamics simulations. Water is represented in cyan, phospholipids in gray, and phospholipids' phosphorus atoms as yellow spheres. The peptide backbone is shown in grey, charged side chains in red, polar amino acids in orange, apolar residues in blue, and prolines in green.

In this chapter, we report on the heterologous synthesis of HcRNAV109 CP by *P. pastoris* and its co-expression with PMAP-23-D7. The successful large-scale fermentation and purification of the self-assembled HcRNAV VLPs suggest their potential application as nanocontainers. To our knowledge, this is the first paper to report the heterologous expression of HcRNAV [Wu et al., 2012].

6.2 Materials and methods

6.2.1 Synthesis of P. pastoris codon-optimized HcRNAV CPHsyns

Following the similar methodology in section 3.2, HcRNAV109 CP gene, GenBank accession no. AB218609 [Nagasaki et al., 2005], was redesigned to substitute amino acid codons that are seldom used in *P. pastoris* similar to section 3.2. Chemical synthesis of the new CP gene (CPHsyns) was accomplished with GenScript Co. Restriction sites for *EcoR*I and *Not*I were added upstream and downstream, respectively, of the CPHsyns gene. The plasmid pUC57-CPHsyns was transformed into *E.coli* Top10 for amplification and preservation.

6.2.2 Insertion of peptide PMAP-23-D7 at N-terminus of HcRNAV109 CPHsyns

Peptide PMAP-23-D7 and HcRNAV109 CPHsyns was spliced by Overlapping Extension PCR (SOE-PCR) [Warrens et al., 1997]. Four primers were designed to amplify PMAP-23-D7 (Primer F1 and R1) and HcRNAV109 CPHsyns (Primer F2 and R2) separately. The two fragments were then mixed and amplified using two outer primers (Primer P1 and P2) to introduce *EcoR*I and *Not*I restriction sites (Table 6.1). Because there were 20 nucleotides overlapped in PMAP-23-D7 and HcRNAV109 CPHsyns, the final PCR resulted in the production of fusion HcRNAV CPHsyns-PMAP.

Table 6.1 Primers used for HcRNAV CPHsyns-PMAP gene fusion

Primers No.	Oligonucleotide sequence (5' to 3')
F1	5'GACATTATCGATCTGCTGTGGGACGTTGACGATCCACAGGATCCTGACT3'
R1	5'GACGGGTCATGTCAACCCAGACAGTGACAAAGTCAGGATCCTGTGGATC3'
F2	5'CTGGGTTGACATGACCCGTCCCCTAGC3'
R2	5'TTAAGCAGCCATCAATGCTGGCATAGC3'
P1	5'CCGGAATTCATGGACATTATCGATCTGCTGT3' (*EcoR*I restriction site)
P2	5'ATAGTTTAGCGGCCGCTTAAGCAGCCATCAA3' (*Not*I restriction site)

6.2.3 Construction of the recombinant vector pPICZ A-CPHsyns

The 1.1 kb CPHsyns gene was retrieved from the pUC57 vector as an *EcoR*I/*Not*I fragment and cloned into the corresponding *EcoR*I and *Not*I sites of vector pPICZ A. The resultant vector pPICZ A-CPHsyns was then transformed into *E.coli* Top10 for its amplification. Recombinant pPICZ A-CPHsyns-PMAP was also constructed using 1.2 kb HcRNAV CPHsyns-PMAP gene and pPICZ A.

6.2.4 Transformation of P. pastoris and cultivation of HCRNAV CPHsyns

The transformation and expression of the CPHsyns and CPHsyns-PMAP gene in *P. pastoris* was performed using established procedures in section 3.2 [Sambrook and Russell, 2001].

Verified t transformants of CPHsyns and CPHsyns-PMAP were grown in a BMGY at 30 °C for 16–20 h. The yeast cells were harvested using centrifugation and resuspended in BMMY. Incubation was continued for an additional 96 h at 30 °C with 1 % methanol induction every 24 h. To determine the optimal harvest time after induction, one mL of the expression medium was withdrawn every 12 h and the protein expression levels were determined using SDS-PAGE.

6.2.5 Purification of HcRNAV and HcRNAV-PMAP VLPs

A modified virus capsid purification procedure based on PEG precipitation and density gradient centrifugation was employed to purify the soluble assembled HcRNAV and HcRNAV-PMAP VLPs [Ali and Roossinck, 2007]. The *Pichia* cells gathered by centrifugation at 4000× *g* for 30 min were resuspended in five times (w/w) lysis buffer and disrupted by sonication. Cell debris and insoluble material were removed by centrifugation at 10,000× *g* for 30 min, and PEG 8000 was added to the supernatant to a final concentration of 10 %. After overnight incubation at 4 °C, the solution was centrifuged at 10,000× *g* for 30 min and the resulting pellet was resuspended in phosphate buffer (10 mM Na_2HPO_4, 10 mM

KH_2PO_4, 1 mM EDTA, 5 mM DTT, 0.5 mM PMSF, pH 7.2). The resuspended PEG pellet was loaded onto a 10–40 % cesium chloride gradient and centrifuged at 35,000× *g* for 2 h. The pellet was dissolved in the same phosphate buffer for further analysis.

6.2.6 Analysis of purified HcRNAV and HcRNAV-PMAP VLPs

The purified HcRNAV and HcRNAV-PMAP VLPs were analyzed by UV spectrometry and TEM. The A_{260}:A_{280} ratio was calculated. TEM images of VLPs negatively-stained with 2 % (w/v) uranyl acetate were obtained with a CM30 electron microscope.

6.2.7 Encapsulation of fluorescence dye-labeled myoglobin

Purified HcRNAV VLPs in PBS, obtained from section 6.2.5, were dialyzed against three changes of disassembly buffer (0.05 M phosphate buffer, 0.15 M NaCl, 2 mM DTT, pH 8.0). Myoglobin was labeled with a fluorescent dye, Alexa Fluor 594, according to the Alexa Fluor® 594 Protein Labeling Kit (A10239, Invitrogen, USA). The disassembled HcRNAV VLPs and fluorescent myoglobin were mixed at the ratio of 5:1 and the resulting mixture was incubated at room temperature for 1.5 h. The incubated solution was then dialyzed against three changes of reassembly buffer (0.05 M phosphate buffer, 0.5 M NaCl, pH 7.2) and concentrated by freeze-drying. Free myoglobin was removed using Vivaspin 6 ultrafiltration spin column (Sartorius, Germany). The VLPs containing encapsulated myoglobin were further analyzed and purified by size exclusion FPLC as described in section 5.2. The purified myoglobin-containing HcRNAV capsids were used to perform fluorescence spectroscopy (Confocal Laser Scanning Biological Microscope FV1000, Olympus, Japan) [Comellas-Aragonès et al., 2007].

6.3 Results and discussion

6.3.1 Construction of expression vector pPICZ A-CPHsyns

To enhance the efficiency of gene expression in *P. pastoris*, the HcRNAV CPHsyns gene was optimized to the codon usage of *P. pastoris* (Fig. 6.3). The synthesized 1080 bp sequence showed 95.6 % nucleotide identity (1033/1080) and 100 % deduced amino acid identity with the native CP gene. In total, 47 changes were introduced into the synthesized gene. The resulting HcRNAV CPHsyns was then inserted into the pPICZ A plasmid. The digestion of the recombinant vector by *Eco*RI and *Not*I showed two bands of 3.3 kb (pPICZ A) and 1.1 kb (CPHsyns), which indicated that the expression vector pPICZ A-CPHsyns was successfully constructed (Fig. 6.4).

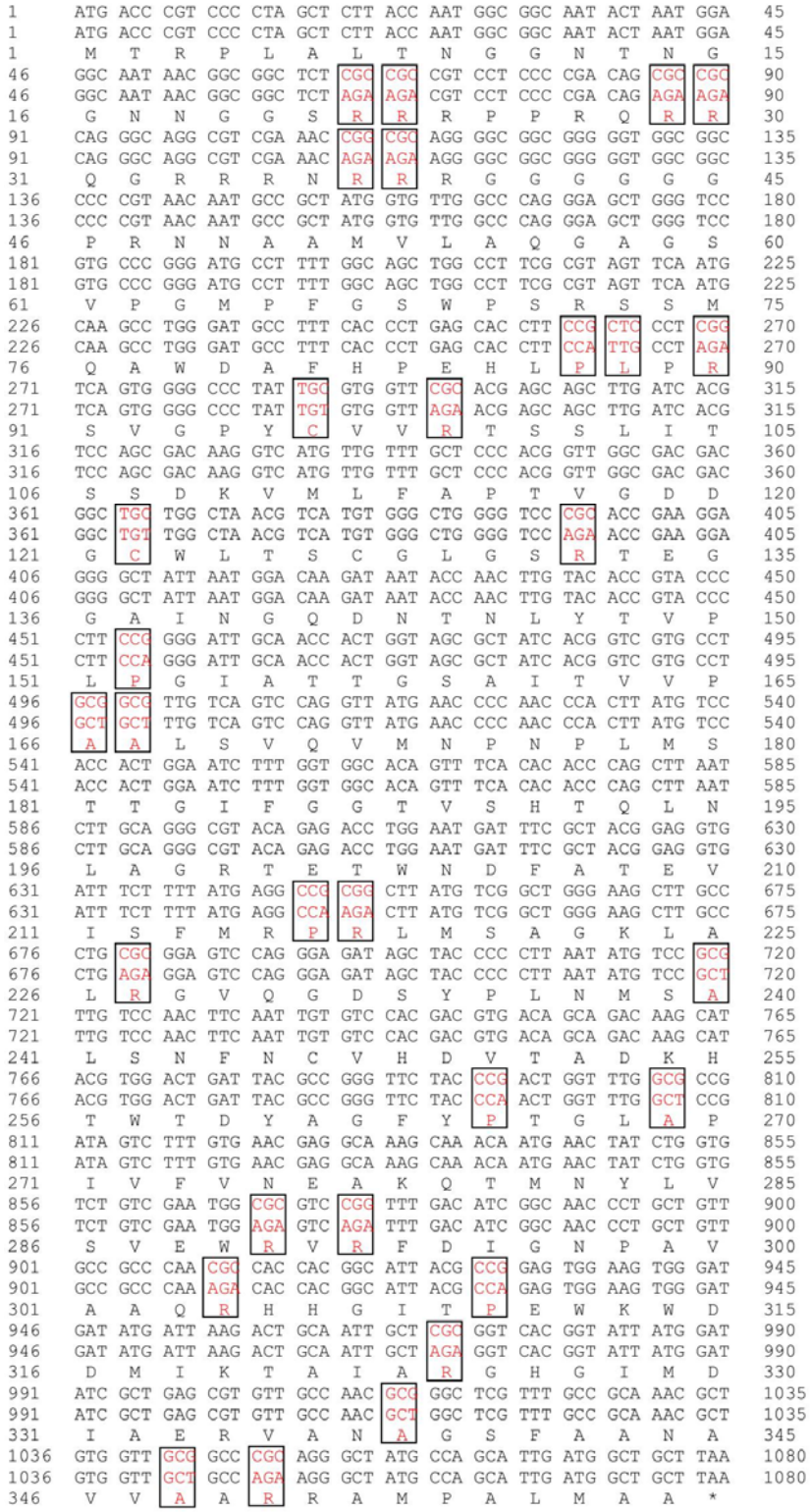

Fig. 6.3 Nucleotide and deduced amino acid sequence of HcRNAV109 CP gene and HcRNAV CPHsyns gene. The alterations in nucleotide sequence are boxed in red.

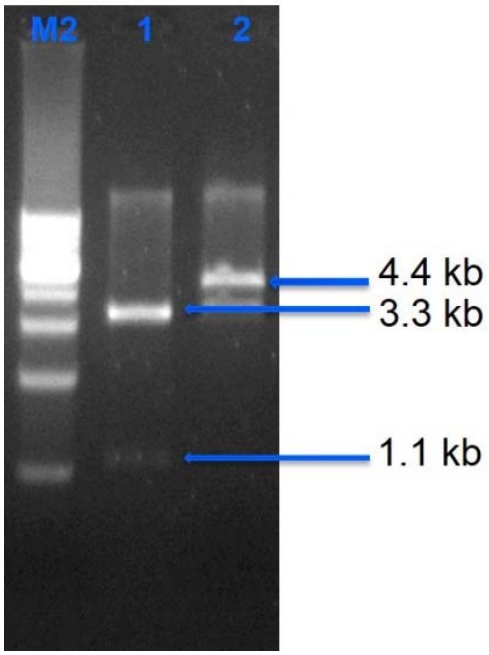

Fig. 6.4 Digestion results of pPICZ A-CPHsyns with *EcoR*I and *Not*I. Lane 1, digestion of pPICZ A-CPHsyns with *EcoR*I; 2, double-digestion of pPICZ A-CPHsyns with *EcoR*I and *Not*I; M, Takara 1 kb DNA ladder.

6.3.2 Insertion of peptide PMAP-23-D7 at N-terminus of HcRNAV109 CPHsys

SOE-PCR was employed for the construction of peptide PMAP-23-D7 and HcRNAV109 CPHsys fusion. After 2 rounds of PCR, PMAP-23-D7 was successfully inserted at N-terminus of HcRNAV109 CPHsys (Fig. 6.5). The 1.2 kb HcRNAV CPHsys-PMAP gene was sequenced by Genotech Co and deduced amino acid sequence showed 100 % identity with peptide PMAP-23-D7 and HcRNAV109 CPHsys gene.

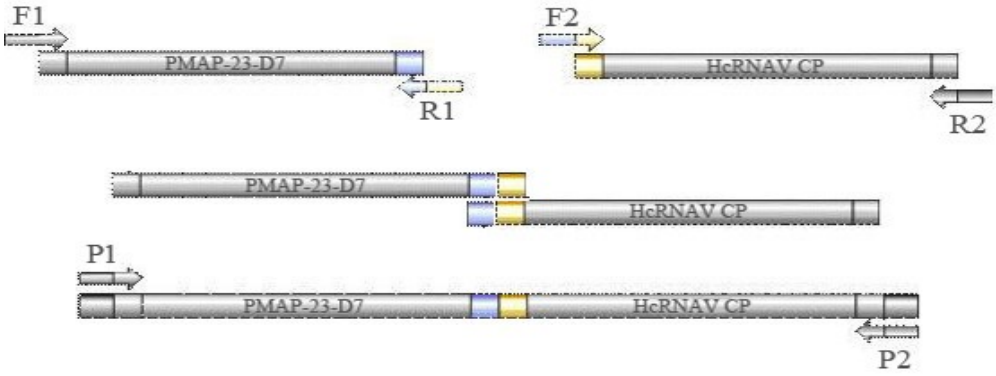

Fig. 6.5 Scheme of SOE-PCR for peptide PMAP-23-D7 and HcRNAV109 CPHsys fusion.

6.3.3 Expression of the HcRNAV CPHsyns gene in P. pastoris

After screening on zeocin-YPD plates, over 10 *P. pastoris* transformants were induced with methanol and examined for HcRNAV CPHsyns production. The supernatant samples were diluted ten times after cell lysis and five μL of each sample were subjected to SDS-PAGE (Fig. 6.6). All of the transformants showed a band at approximately 40 kDa, which was the theoretical molecular weight of the HcRNAV coat protein monomer. Transformant GS115-24 was selected for further fermentation.

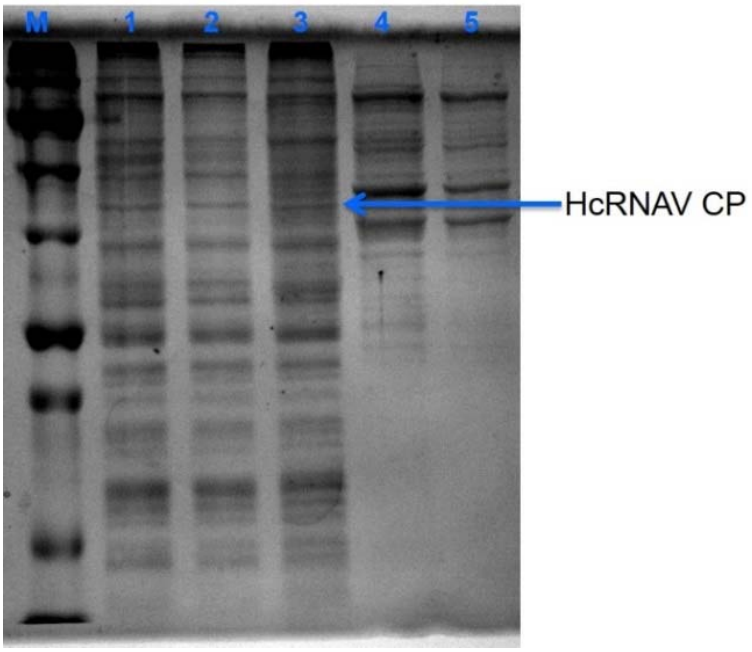

Fig. 6.6 SDS-PAGE results of *P. pastoris* transformants. Lane 1-3, Soluble fractions of pPICZ A-CPHsyns transformants after sonication; 4, Control of pPICZ A/GS115; 5, Control of GS115; M, DokDo-MARK^{TM} broad-range.

6.3.4 Purification of HcRNAV and HcRNAV-PMAP VLPs

Transformant GS115-24 cells were lysed by ultrasonic disruption and the HcRNAV CP purified by PEG precipitation and density gradient centrifugation. PEG treatment of the supernatant preferentially precipitated HcRNAV CP with almost no precipitation of other proteins. Ultracentrifugation in CsCl further purified HcRNAV CP to a single band of 40 kDa, which showed that the coat protein was able to assemble into high molecular weight structures (HcRNAV VLPs) (Fig. 6.7). HcRNAV-PMAP VLPs were also purified in the same way.

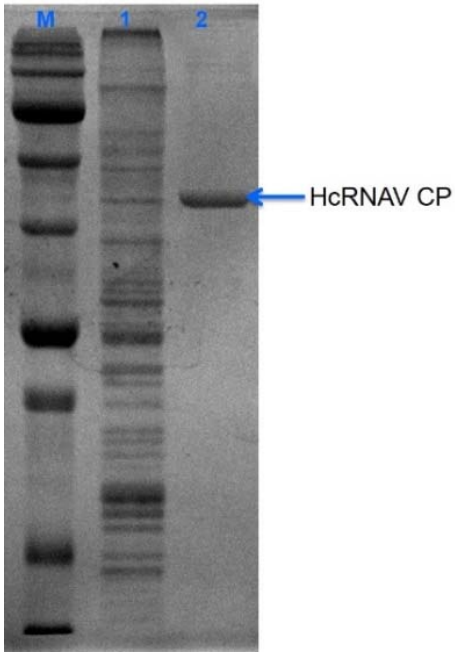

Fig. 6.7 Purification results of HcRNAV CP. Lane 1, Soluble fractions of GS115-24 after sonication; 2, HcRNAV CP purified by ultracentrifugation in CsCl; M, DokDo-MARK™ Broad-range.

6.3.5 Characterization of purified HcRNAV and HcRNAV-PMAP VLPs

The VLPs were analyzed by UV spectrophotometry and showed an A_{260}:A_{280} ratio of 1.51, which was similar to the ratio of 1.56 observed with other VLPs. TEM examination of the VLPs showed spherical particles of ca. 30 nm in diameter (Fig. 6.8). This similarity to native HcRNAV particles indicated that the synthesized coat protein was successfully expressed and self-assembled into VLPs *in vitro* [Tomaru et al., 2004]. Also shown in Fig. 6.8, HcRNAV particles obtained from *P. pastoris* were more regular in shape and size compared with VLPs from *E.coli*.

As for the expressed HcRNAV-PMAP VLPs, the sample showed rod-like particles with the cylinder diameter of ca. 30 nm and the length over several hundreds nanometers. This was significantly different with native HcRNAV VLPs (Fig. 6.9). The phenomenon suggested that the insertion of PMAP-23-D7 at N-terminus of HcRNAV CPHsys changed the virus capsid phenotype. This was also observed by Gross et al. in the N-terminal extension of HIV capsid protein [Gross et al., 1998]. The insertion of foreign peptide at N-terminus of HcRNAV CPHsys might alter the interactions between virus capsid protein monomers thus disrupt virus particle formation ultimately [Mukherjee et al., 2006]. This could help us to understand the assembly process of HcRNAV.

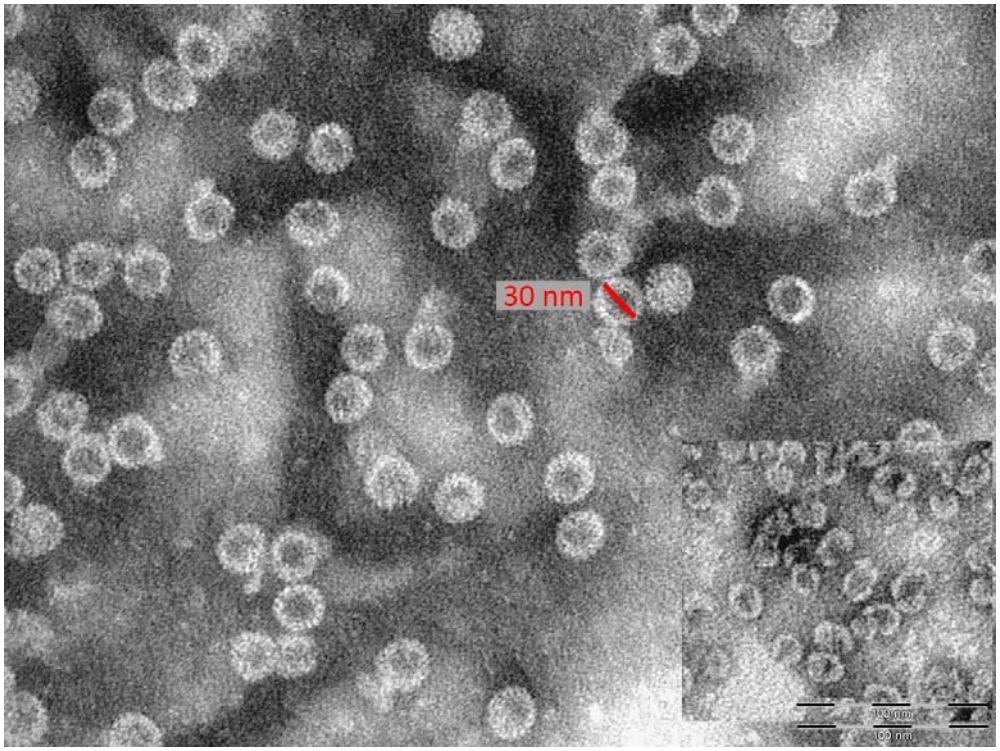

Fig. 6.8 TEM image of HcRNAV VLPs expressed in *P. pastoris*. The diameter of the capsids was about 30 nm. Insert was TEM image of HcRNAV VLPs expressed in *E.coli*. Size bar represents 100 nm.

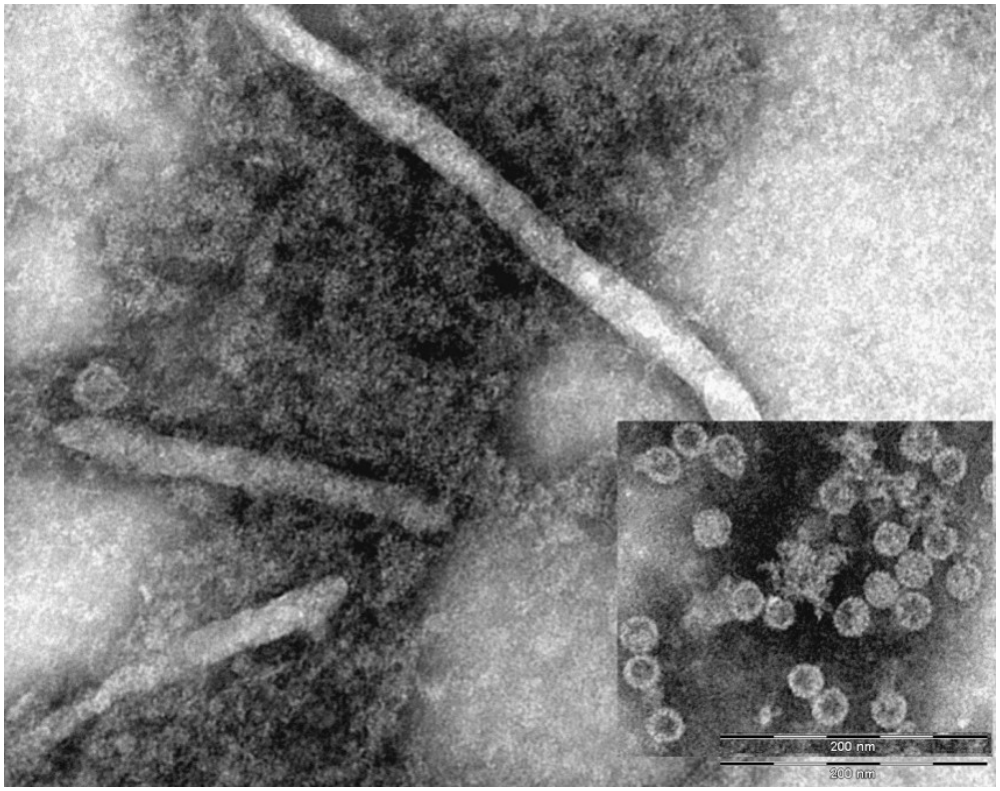

Fig. 6.9 TEM image of HcRNAV-PMAP VLPs expressed in *P. pastoris*. The capsids were rod-like with length over several hundreds nanometers; Inserted was TEM image of native HcRNAV VLPs. Size bar represents 200 nm.

6.3.6 Encapsulation of fluorescence dye-labeled myoglobin

The co-elution of HcRNAV VLPs and guest myoglobin (t = 36 min) was observed in the FPLC traces (Fig. 6.10), showing the same elution time as the original capsids. These pointed to the successful reassembly of the viral cage after the encapsulation process.

The correct reassembly of HcRNAV capsids with fluorescent myoglobin was further proven by fluorescence spectroscopy. The capsids containing this guest protein displayed significant emission at λ = 590 nm (Fig. 6.11), indicating that inclusion of myoglobin had occurred successfully. When HcRNAV VLPs were used as control, no emission under the same condition was observed.

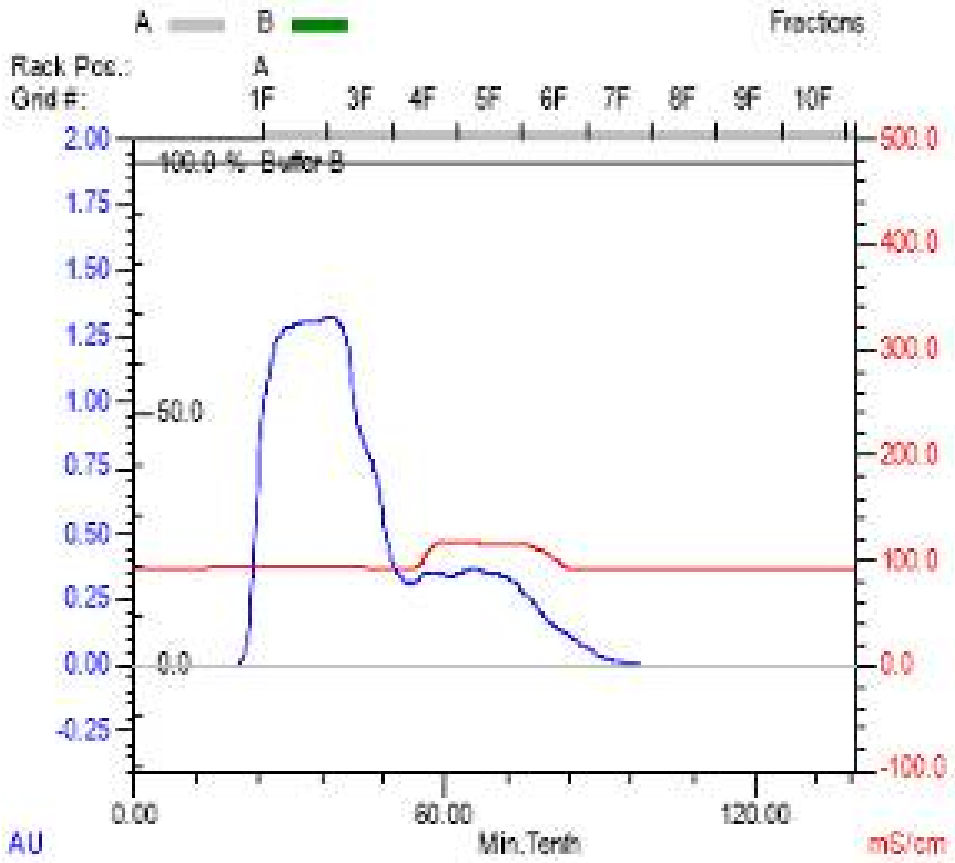

Fig. 6.10 Size-exclusion FPLC of myoglobin-containing HcRNAV VLPs at 280 nm. The peak at elution time of 36 min corresponded to the intact virus capsids.

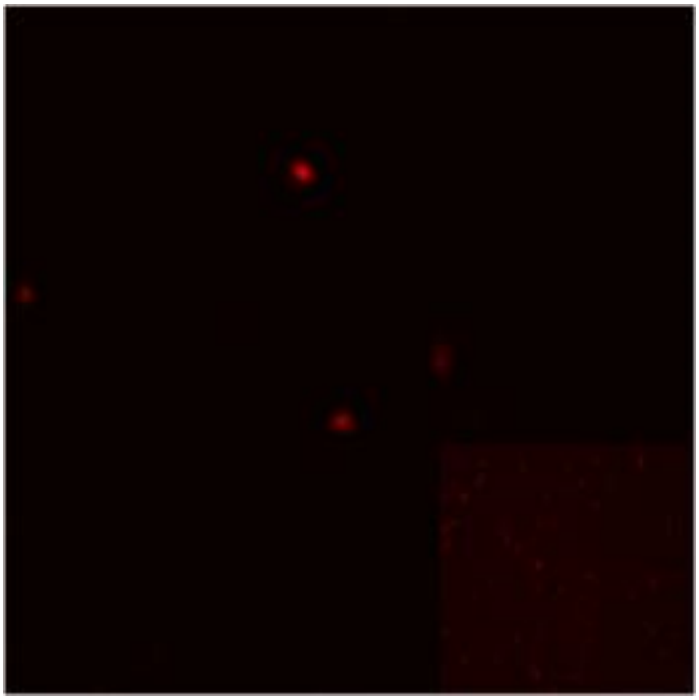

Fig. 6.11 Fluorescence spectroscopy of myoglobin-containing HcRNAV VLPs. A typical confocal fluorescence image (1.68×1.68 μm) showed the formation of a fluorescent protein encapsulated inside a capsid. Inset: AFM image (to scale) at the same sample location, showing that only a small fraction of the capsids contained myoglobin molecules.

6.4 Summary

HcRNAV109 coat protein was expressed in *P. pastoris* and successfully self-assembled into polyhedral virus-like particles. To our knowledge, this is the first report on the efficient expression and assembly in *P. pastoris* of the capsid of a virus infecting a harmful alga. The successful expression and purification of HcRNAV VLPs makes their abundant and rapid production now possible. Also we have shown that the fusion expression of peptide PMAP-23-D7 and HcRNAV109 capsid protein in *P. pastoris* and self-assembled HcRNAV-PMAP VLPs *in vitro*. The virus phenotype conversion from spherical to rod-like ones was first observed. This method also represents a promising tool for the preparation of large amounts of VLPs for use in gene therapy, vaccine development, and other applications such as the control of harmful algal blooms.

The encapsulation of myoglobin as a model protein inside HcRNAV VLPs revealed that these virus capsids derived from *P. pastoris* were suitable nanocontainers for drug delivery and imaging reagent carriers. The specific targeting by HcRNAV of *H. circularisquama* would be extremely useful in controlling harmful algal blooms. The encapsulation of algicidal compounds inside the capsids to improve the efficiency is another useful approach for future investigation. HcRNAV could become a model virus capsid that might be used as a nanoplatform in materials science and medicine.

Appendix II. Improved Cell Disruption of *P. pastoris* Utilizing Aminopropyl Magnesium Phyllosilicate (AMP) Clay

7.1 Introduction

Pichia pastoris has become an efficient expression system for producing recombinant proteins of intracellular and extracellular origin from different sources [Cereghino and Cregg, 2000]. However, intracellular products expressed in *P. pastoris* require an additional step to disrupt the mechanically rigid cell wall, which is composed of multiple layers of cross-linked β-1,3-glucan, chitin and glycosylated mannoproteins [Kollar et al., 1997; Smits et al., 2001]. Common protocols of cell wall disruption include breaking the cell wall either mechanically or enzymatically, which were usually tedious and time-consuming [Geciova et al., 2002; Stowers and Boczko, 2007]. The improvement of disruption methods is essential to acquire higher protein yields with low cost and good reproducibility.

In this chapter, we developed a simple method to disrupt *Pichia* cells utilizing glass beads mill combined with organic clay. Aminopropyl magnesium phyllosilicate (AMP) clay is a sandwiched organo-functionality with layered lamella sheets ranging from 20 to 200 nm that resemble talc parent structure $Si_8Mg_6O_{20}(OH)_4$ as shown in Fig. 7.1 [Ferreira et al., 2008; Lee et al., 2010]. It has been reported that AMP clay at high concentration displays antimicrobial activities against *E. coli*, *Staphylococcus aureus* and *Candida albicans* by permeating the bacterial membrane and causing cell lysis [Chandrasekaran et al., 2011]. Therefore, the applicability of AMP clay to enhance cell disruption was investigated to assess its efficiency on cell lysis. The demonstration system involves CCMV CP expressed in *P. pastoris* GS115 and spontaneously assembled into icosahedral virus-like particles (VLPs) [Wenger et al., 2007; Kim et al., 2013].

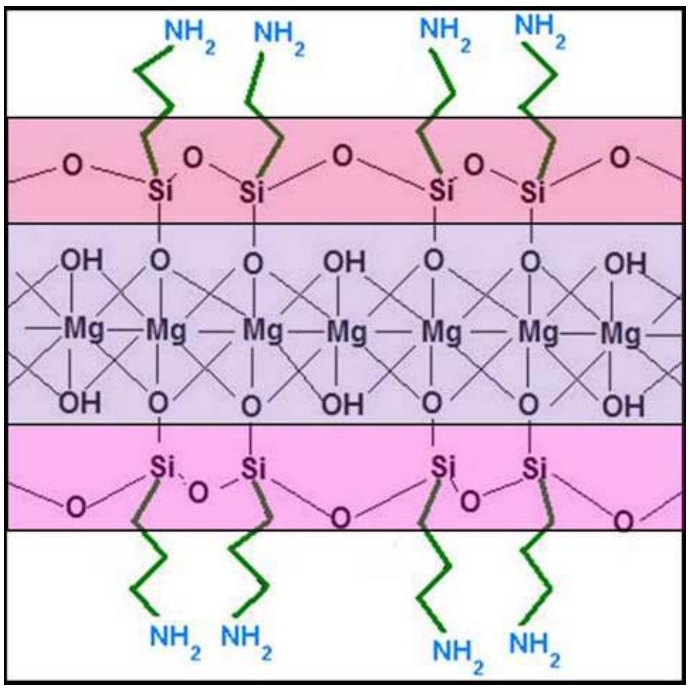

Fig. 7.1 Representative structure of AMP clay $Si_8Mg_6O_{20}(OH)_4$.

7.2 Materials and methods

7.2.1 Culture of P. pastoris transformant of CCMV CP

The recombinant strain G48 carrying CCMV CP was inoculated in 25 mL buffered glycerol-complex medium (BMGY) at 30 °C with shaking at 240 rpm for 16-18 h and then transferred into 100 mL BMMY for 72 h induction. *Pichia* cells were centrifuged at 4000× g for 10 min for disruption.

7.2.2 Disruption of P. pastoris cells

The pellets were washed with distilled water and resuspended in breaking buffer. An equal volume of acid-washed glass beads (0.5 mm, Sigma) and 0.2 % (w/v) AMP clay; glass beads only; or 0.2 % AMP clay only were added to the cell suspensions. In a primary experiment the concentration of 0.2 % was chosen from a serial of 0.2, 0.5 and 1 % as the most suitable amount of AMP clay added. The mixture was agitated as follows: a 30 sec vortex followed by an interval of 30 sec on ice and sample collection after every 2 min. The samples were centrifuged at 4000× *g* for 10 min at 4 °C, and protein concentration of the supernatant was measured by Bradford assay. The experiments were repeated 5 times and each figure was measured 3 times for average.

7.2.3 Analysis of disrupted P. pastoris cells

The supernatant of the lysed samples were diluted ten times and checked by SDS-PAGE with 15 % polyacrylamide gel at 120 V for 2.5 h.

To check the influence of AMP clay on the lysis process, oil-immersion light microscopy was introduced to assess cell breakage and debris size using Nikon Eclipse TS100 microscope (Nikon, Japan). Samples were diluted to the equivalent of a 1 % cell slurry solution and examined at 400× magnification.

7.2.4 Evaluation of effect on CCMV CP by added AMP-clay

Subsequently, a modified viral capsid purification procedure based on PEG precipitation and density gradient centrifugation was used to purify CCMV VLPs [Ali and Roossinck, 2007]. The purified CCMV VLPs were reassembled in sodium acetate buffer and analyzed by transmission electron microscopy (TEM) with high-resolution transmission electron microscope JEOL JEM 3010 (Electron Microscopy Laboratory, KAIST, Korea).

7.3 Results and discussion

7.3.1 Disruption of P. pastoris cells

As shown in table 1, the starting concentrations of all samples (from 0 to 2 min) were too low to show any difference; as time went on, the results of AMP clay-assisted glass beads and glass beads mill only method displayed statistically significant difference ($p = 0.038$). In the combined method, the protein concentration increased and reached the highest level at 4.24 mg/mL after 4 min. With the beads mill only method, the highest protein concentration obtained was 3.81 mg/mL at 8 min. The disruption time assisted with AMP clay was half shorten, while the protein concentration extracted increased by 11.2 %. As expected, the methods using the negative control or AMP clay only did not yield proteins at a detectable level. Similar results were also observed when AMP clay was combined with sonication.

Table 7.1 Total protein concentration of *P. pastoris* G48 by different cell disruption methods

Time (min)	Total protein concentration by AMP clay+glass beads (mg/mL)	Total protein concentration by glass beads only (mg/mL)	Total protein concentration by AMP clay only (mg/mL)
0	0.07±0.02	0.07±0.03	0.08±0.02
2	0.32±0.06	0.39±0.03	0.09±0.04
4	4.24±0.04 *	3.57±0.05 *	0.09±0.03
6	4.04±0.05 *	3.59±0.03 *	0.11±0.05
8	3.85±0.03 *	3.81±0.04 *	0.11±0.04
10	3.74±0.03 *	3.58±0.02 *	0.12±0.03

* The difference in the mean values of the two groups is greater than would be expected by chance; there is a statistically significant difference between the input groups ($p = 0.038$).

7.3.2 Analysis of disrupted P. pastoris cells

The diluted supernatant samples were checked by SDS-PAGE. As presented in Fig. 1, there was a significant increase in protein extraction from 0 to 2 mg/mL at 4 min using both the AMP clay-assisted beads mill and the beads mill only; however, all the bands from the method using AMP clay only were obscure. It's interesting to find that the amount of CCMV CP (approximate 20 kDa, boxed bands in Fig. 7.2) obtained from the combined method was much higher than that from the method using glass beads only: 0.82 mg/mL compared to 0.73 mg/mL (calculated by software BandScan v5.0). This indicated that AMP clay could preserve coat protein from degradation during disruption.

The oil-immersion light microscopy was introduced to assess cell breakage and debris size. From Fig. 7.3, the lysate from the AMP clay-assisted method showed a change from the initial aggregation to small cellular debris with large and irregular in shape. This change may be attributed to the binding of *Pichia* cells to AMP clay in the solution via electrostatic interactions. In contrast, the lysate from the glass beads only method revealed extensive fragmentation of cells with almost no large particles of aggregated cellular debris visible after the disruption.

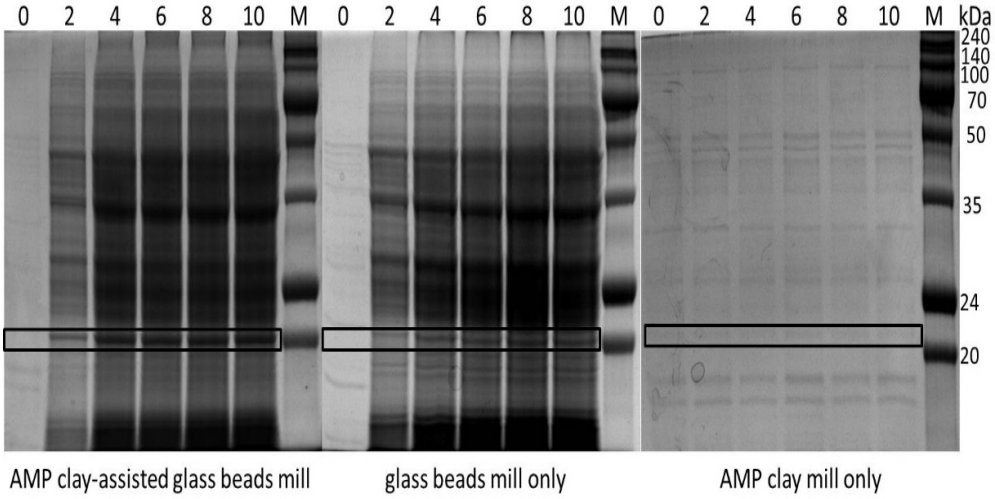

Fig. 7.2 Comparison of SDS-PAGE results by different cell disruption methods. Time 0, 2, 4, 6, 8, 10 min; the boxed band region was recombinant CCMV capsid protein; M, DokDo-MARK^{TM} Broad-range.

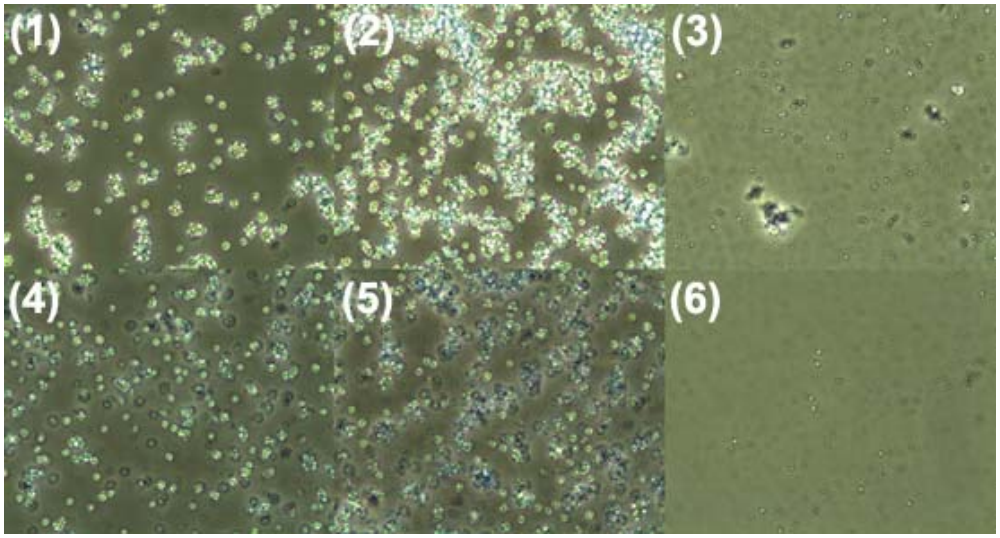

Fig. 7.3 Optical microscopy of *Pichia* cell disruption by different methods. (1), (2), (3) were from AMP clay-assisted glass beads mill as time of 0, 4, and 10 minutes; (4), (5), (6) were from glass beads mill only as time of 0, 4, and 10 minutes as control.

7.3.3 Evaluation of effect on CCMV CP by added AMP-clay

The concentration of purified CCMV CP by AMP clay assisted method was 0.28 mg/mL, which was a little higher compared to 0.23 mg/mL obtained by glass beads mill only. The recovery efficiency of target product by the combined method was 6.6 % of total protein (4.24 mg/mL) while it was 6.1 % of total protein (3.81 mg/mL) in the unmodified method. The reassembled CCMV VLPs were evaluated by TEM. CCMV CP reassembled into spherical VLPs with an average diameter of 28 nm as observed in Fig. 7.4 This result was identical to that of the control disrupted by the beads mill, implying that the assembly of viral capsids was not affected by AMP clay. Another recombinant GS115/pPICZ/lacZ (Mut^+) carried a fused lacZ gene was also disrupted by both methods to check whether AMP clay would affect the functionality of recombinant proteins in *P. pastoris*. Similar enzyme activity of crude β-galactosidase was observed in both methods. This suggested that AMP clay caused no denaturation or side effect on enzyme activity of recombinant proteins in *P. pastoris*.

As demonstrated by Lee et al. [Lee et al., 2010], AMP clay was an organoclay-modified derivative in the form of nanocomposite $Si_8Mg_6O_{20}(OH)_4$. It was easy and inexpensive to synthesize and the amount added here was quite little which would not cause the increase of material cost. From the parent structure, AMP clay possesses hydrophilic and protonated groups ($R\text{-}NH_2$) which create a number of binding sites for ion exchange within the interlayer spaces and serve as surface groups on the lamella [Holmström et al., 2007]. The interaction between AMP clay and the negatively charged layer of glucan, chitin and mannoproteins destroyed the rigidity of cell wall, encouraged cell wall leakage and increased permeability, which ultimately lead to cell lysis. Under the high shear stress resulting from the collision between cells and glass beads in vigorous agitation, the addition of AMP clay may enhance the lysis process significantly. Considering the higher yield of

CCMV CP and well-assembled VLPs, the spaces between the clay sheets may shelter the proteins extracted from the cytoplasm in the buffer and preserve them from degradation caused by glass beads.

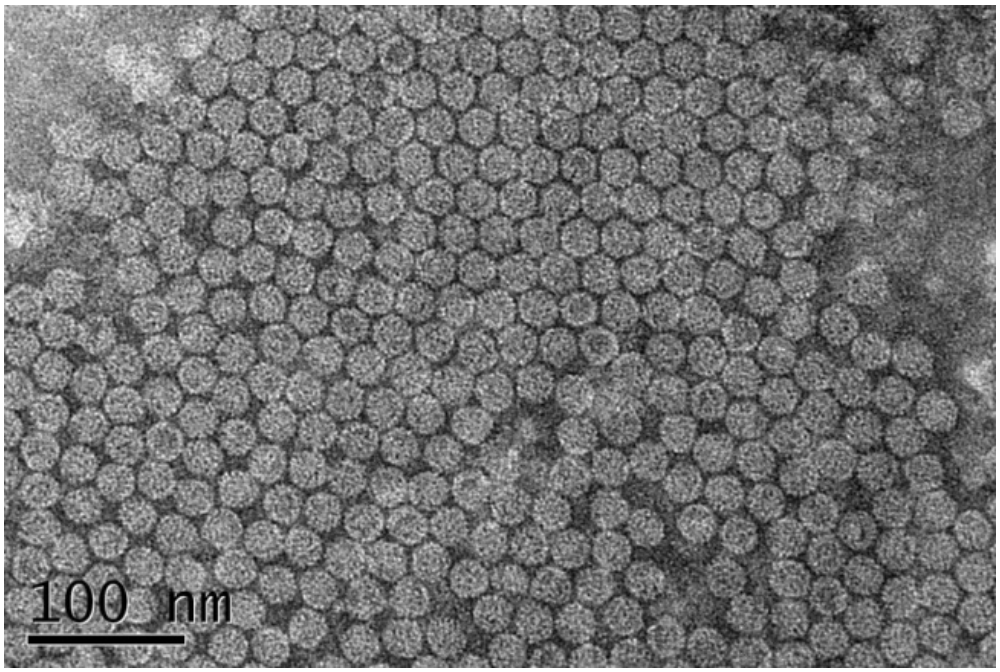

Fig. 7.4 TEM image of CCMV VLPs by AMP clay combined glass beads mill. The spherical particles showed an average diameter of 28 nm. Size bar represents 100 nm.

7.4 Summary

In conclusion, a modified AMP clay-assisted glass beads mill was provided for *Pichia* cell disruption at the laboratory scale without cost increase. The treatment time was shortened by half, while the yield of extracted proteins was 11.2 % higher. The stability of CCMV VLPs demonstrated this method to be a simple and reliable method for yeast cell lysis.

Overall Conclusions and Future Aspects

CCMV and HcRNAV CP were expressed in *Pichia pastoris* and assembled into appropriate VLPs, indicating *P. pastoris* as a promising expression system for mass production of virus capsids. A unique pigment, Prussian blue, was encapsulated and synthesized inside the cavity of CCMV capsids. CuAAC reaction was employed to decorate the exterior surface of CCMV for the first time. The resulting modified capsids presented different adhesion behavior with HeLa cells. The co-expression of HcRNAV CP and algicidal peptide PMAP-23-D7 showed potential in controlling harmful algae blooms (HABs).

In the future, the combination of encapsulation and surface modification of virus capsids should be investigated. The drug molecules are first loaded inside virus capsids to be protected from surrounding environments. Then specific target moieties are attached on the outer surface for efficient targeting, release, and injection with minimum side effects. This could be the destination for their application in naonomaterial and pharmaceutics.

References

Abello, N., Kerstjens, H.A., Postma, D.S., Bischoff, R., 2007. Selective acylation of primary amines in peptides and proteins. *J Proteome Res*. 6(12):4770-4776.

Ali, A., Roossinck, M.J., 2007. Rapid and efficient purification of cowpea chlorotic mottle virus by sucrose cushion ultracentrifugation. *J Virol Methods*. 141(1):84-86.

Aljabali, A.A., Barclay, J.E., Lomonossoff, G.P., Evans, D.J., 2010. Virus templated metallic nanoparticles. *Nanoscale.* 2(12):2596-2600.

Allison, R.F., Janda, M., Ahlquist, P., 1988. Infectious in vitro transcripts from cowpea chlorotic mottle virus cDNA clones and exchange of individual RNA components with brome mosaic virus. *J Virol*. 62(10):3581-3588.

Amblard, F., Cho, J.H., Schinazi, R.F., 2009. Cu(I)-catalyzed Huisgen azide-alkyne 1,3-dipolar cycloaddition reaction in nucleoside, nucleotide, and oligonucleotide chemistry. *Chem Rev*. 109(9):4207-4220.

Anderson, D.M., 1997. Turning back the harmful red tide. *Nature*. 388(6634):513-514.

Aniagyei, S.E., Dufort, C., Kao, C.C., Dragnea, B., 2008. Self-assembly approaches to nanomaterial encapsulation in viral protein cages. *J Mater Chem*. 18(32):3763-3774.

Annamalai, P., Apte, S., Wilkens, S., Rao, A.L., 2005. Deletion of highly conserved arginine-rich RNA binding motif in cowpea chlorotic mottle virus capsid protein results in virion structural alterations and RNA packaging constraints. *J Virol.* 79(6):3277-3288.

Bancroft, J.B., Hiebert, E., 1967. Formation of an infectious nucleoprotein from protein and nucleic acid isolated from a small spherical virus. *Virology*. 32(2):354-356.

Bancroft, J.B., Hiebert, E., Bracker, C.E., 1969. The effects of various polyanions on shell formation of some spherical viruses.*Virology*. 39(4):924-930.

Bancroft, J.B., Hills, G.J., Markham, R., 1967. A study of the self-assembly process in a small spherical virus. Formation of organized structures from protein subunits in vitro. *Virology*. 31(2):354-379.

Baudoux, A.C., Brussaard, C.P., 2005. Characterization of different viruses infecting the marine harmful algal bloom species *Phaeocystis globosa*. *Virology*. 341(1):80-90.

Bazan, S.B., de Alencar Muniz Chaves, A., Aires, K.A., Cianciarullo, A.M., Garcea, R.L., Ho, P.L., 2009. Expression and characterization of HPV-16 L1 capsid protein in *Pichia pastoris*. *Arch Virol*. 154(10):1609-1617.

Bechinger, B., Lohner, K., 2006. Detergent-like actions of amphipathic cationic antimicrobial peptides. *Biochim Biophys Acta*. 1758(9):1529-1539.

Belyi, V.A., Muthukumar, M., 2006. Electrostatic origin of the genome packing in viruses. *Proc Natl Acad Sci*. 103(46):17174-17178.

Brasch, M., Cornelissen, J.J., 2012. Relative size selection of a conjugated polyelectrolyte in virus-like protein structures. *Chem Commun*. 48(10):1446-1448.

Brasch, M., de la Escosura, A., Ma, Y., Uetrecht, C., Heck, A.J., Torres, T., Cornelissen, J.J., 2011. Encapsulation of phthalocyanine supramolecular stacks into virus-like particles. *J Am Chem Soc*. 133(18):6878-6881.

Breitbart, M., Rohwer, F., 2005. Here a virus, there a virus, everywhere the same virus? *Trends Microbiol*. 13(6):278-284.

Bronstein, L.M., 2011.Virus-based nanoparticles with inorganic cargo: what does the future hold? *Small*. 7(12):1609-1618.

Bruckman, M.A., Kaur, G., Lee, L.A., Xie, F., Sepulveda, J., Breitenkamp, R., Zhang, X., Joralemon, M., Russell, T.P., Emrick, T., Wang, Q., 2008. Surface modification of tobacco mosaic virus with “Click” chemistry. *ChemBioChem*. 9(4):519-523.

Brumfield, S., Willits, D., Tang, L., Johnson, J.E., Douglas, T., Young, M., 2004. Heterologous expression of the modified coat protein of cowpea chlorotic mottle bromovirus results in the assembly of protein cages with altered architectures and function. *J Gen Virol*. 85(Pt 4):1049-1053.

Brunel, F.M., Lewis, J.D., Destito, G., Steinmetz, N.F., Manchester, M., Stuhlmann, H., Dawson, P.E., 2010. Hydrazone ligation strategy to assemble multifunctional viral nanoparticles for cell imaging and tumor targeting. *Nano Lett*. 10(3):1093-1097.

Bruton, J., Bouwer, G.T., Ward, V.K., 2005. Metal nanoshell assembly on a virus bioscaffold. *Nano Lett*. 5(6):1187-1191.

Cadena-Nava, R.D., Hu, Y., Garmann, R.F., Ng, B., Zelikin, A.N., Knobler, C. M., Gelbart, W.M., 2011. Exploiting fluorescent polymers to probe the self-assembly of virus-like particles. *J Phys Chem B*. 115(10):2386-2391.

Cardinale, D., Carette, N., Michon, T., 2012. Virus scaffolds as enzyme nano-carriers. *Trends Biotechnol*. 30(7):369-376.

Caspar, D.L., Klug, A., 1962. Physical principles in the construction of regular viruses. *Cold Spring Harb Symp Quant Biol*. 27:1-24.

Cereghino, G.P., Cereghino, J.L., Ilgen, C., Cregg, J.M., 2002. Production of recombinant proteins in fermenter cultures of the yeast *Pichia pastoris*. *Curr Opin Biotechnol*. 13(4):329-332.

Cereghino, J.L., Cregg, J.M., 2000. Heterologous protein expression in the methylotrophic yeast *Pichia pastoris*. *FEMS Microbiol Rev*. 24(1):45-66.

Chandrasekaran, G., Han, H.K., Kim, G.J., Shin, H.J., 2011. Antimicrobial activity of delaminated aminopropyl functionalized magnesium phyllosilicates. *Appl Clay Sci*. 53:729-736.

Chen, Z., Stauffacher, C., Johnson, J.E., 1990. Capsid structure and RNA packaging in comovirus. *Semin Virol*. 1:453-466.

Cheung, C.L., Chung, S.W., Chatterji, A., Lin, T., Johnson, J.E., Hok, S., Perkins, J., De Yoreo, J.J., 2006. Physical controls on directed virus assembly at nanoscale chemical templates. *J Am Chem Soc*. 128(33):10801-10807.

Comellas-Aragonès, M., de la Escosura, A., Dirks, A.T., van der Ham, A., Fusté-Cuñé, A., Cornelissen, J.J., Nolte, R.J., 2009. Controlled integration of polymers into viral capsids. *Biomacromolecules*. 10(11):3141-3147.

Comellas-Aragonès, M., Engelkamp, H., Claessen, V.I., Sommerdijk, N.A., Rowan, A.E., Christianen, P.C., Maan, J.C., Verduin, B.J., Cornelissen, J.J., Nolte, R.J., 2007. A virus-based single-enzyme nanoreactor. *Nat Nanotechnol*. 2(10):635-639.

Culp, J.T., Park, J.-H., Frye, F., Huh, Y.-D., Meisel, M.W., Talham, D. R., 2005. Magnetism of metal cyanide networks assembled at interfaces. *Coord Chem Rev*. 249:2642-2648.

Daniel, M. C., Tsvetkova, I. B., Quinkert, Z. T., Murali, A., De, M., Rotello, V. M., Kao, C. C., Dragnea, B., 2010. Role of surface charge density in nanoparticle-templated assembly of bromovirus protein cages. *ACS Nano*. 4(7):3853-3860.

De la Escosura, A., Verwegen, M., Sikkema, F.D., Comellas-Aragonès, M., Kirilyuk, A., Rasing, T., Nolte, R.J., Cornelissen, J.J., 2008. Viral capsids as templates for the production of monodisperse Prussian blue nanoparticles. *Chem Commun*. 13:1542-1544.

De Tacconi, N.R., Rajeshwar, K., Lezna, R.O., 2003. Metal hexacyanoferrates: electrosynthesis, in situ characterization, and applications. *Chem Mater*. 15:3046-3062.

Dei, A., 2005. Photomagnetic effects in polycyanometallate compounds: an intriguing future chemically based technology? *Angew Chem Int Ed*. 44(8):1160-1163.

DeLongchamp, D. M., Hammond, P. T., 2004. High-contrast electrochromism and controllable dissolution of assembled Prussian blue/polymer nanocomposites. *Adv Funct Mater*. 14(3):224-232.

Destito, G., Yeh, R., Rae, C.S., Finn, M.G., Manchester, M., 2007. Folic acid-mediated targeting of cowpea mosaic virus particles to tumor cells. *Chem Biol*. 14(10):1152-1162.

Dietzsch, C., Spadiut, O., Herwig, C., 2011. A dynamic method based on the specific substrate uptake rate to set up a feeding strategy for *Pichia pastoris*. *Microb Cell Fact*. 10:14.

Dimmock, N., Easton, A., Leppard, K., 2009. *Introduction to Modern Virology*. 6th edition. John Wiley & Sons, New York.

Dirksen, A., Dawson, P.E., 2008. Rapid oxime and hydrazone ligations with aromatic aldehydes for biomolecular labeling. *Bioconjug Chem*. 19:2543-2548.

Domingo, G.J., Orru', S., Perham, R.N., 2001. Multiple display of peptides and proteins on a macromolecular scaffold derived from a multienzyme complex. *J Mol Biol*. 305(2):259-267.

Domínguez-Vera, J.M., Colacio, E., 2003. Nanoparticles of Prussian blue ferritin: a new route for obtaining nanomaterials. *Inorg Chem*. 42(22):6983-6985.

Douglas, T., Strable, E., Willits, D., Aitouchen, A., Libera, M., Young, M., 2002. Protein engineering of a viral cage for constrained nanomaterials synthesis. *Adv Mater*., 14:415-418.

Douglas, T., Young, M., 1998. Host–guest encapsulation of materials by assembled virus protein cages. *Nature*. 393(6681):152-155.

Douglas, T., Young, M., 2006. Viruses: making friends with old foes. *Science*. 312(5775):873-875.

Edwards, R.A., Rohwer, F., 2005. Viral metagenomics. *Nat Rev Microbiol*. 3(6):504-510.

Endo, M., Fujitsuka, M., Majima, T., 2007. Porphyrin light-harvesting arrays constructed in the recombinant tobacco mosaic virus scaffold. *Chemistry*. 13(31):8660-8666.

Erdner, D.L., Dyble, J., Parsons, M.L., Stevens, R.C., Hubbard, K.A., Wrabel, M.L., Moore, S.K., Lefebvre, K.A., Anderson, D.M., Bienfang, P., Bidigare, R.R., Parker, M.S., Moeller, P., Brand, L.E., Trainer, V.L., 2008. Centers for oceans and human health: a unified approach to the challenge of harmful algal blooms. *Environ Health*. 7:1-17.

Ferlay, S., Mallah, T., Quahe´s, R., Veillet, P., Verdaguer, M., 1995. A room-temperature organometallic magnet based on Prussian blue. *Nature*. 378(6558):701-703.

Ferreira, R.B., da Silva, C.R., Pastore, H.O., 2008. Aminopropyl-modified magnesium phyllosilicates: layered solids with tailored interlayer access and reactivity. *Langmuir*. 24 (24):14215-14221.

Fischlechner, M., Donath, E., 2007. Viruses as building blocks for materials and devices. *Angew Chem Int Ed*. 46(18):3184-3193.

Fox, J.M., Zhao, X., Speir, J.A., Young, M.J., 1996. Analysis of a salt stable mutant of cowpea chlorotic mottle virus. *Virology*. 222(1):115-122.

Francis, M.B., Carrico, I.S., 2010. New frontiers in protein bioconjugation. *Curr Opin Chem Biol*. 14(6):771-773.

Freivalds, J., Dislers, A., Ose, V., Pumpens, P., Tars, K., Kazaks, A., 2011. Highly efficient production of phosphorylated hepatitis B core particles in yeast *Pichia pastoris*. *Protein Expr Purif*. 75(2):218-224.

Freivalds, J., Dislers, A., Ose, V., Skrastina, D., Cielens, I., Pumpens, P., Sasnauskas, K., Kazaks, A., 2006. Assembly of bacteriophage Qbeta virus-like particles in yeast *Saccharomyces cerevisiae* and *Pichia pastoris*. *J Biotechnol*. 123(3):297-303.

Friedman, M.A., Levin, B.E., 2005. Neurobehavioral effects of harmful algal bloom (HAB) toxins: a critical review. *J Int Neuropsychol Soc*. 11:331-338.

Garrett, M., Wolny, J., Truby, E., Heil, C., Kovach, C., 2010. Harmful algal bloom species and phosphate-processing effluent: field and laboratory studies. *Mar Pollut Bull*. 61(3):621-626.

Gazit, E., 2007. Use of biomolecular templates for the fabrication of metal nanowires. *FEBS J*. 274(2):317-322.

Geciova, J., Bury, D., Jelen, P., 2002. Methods for disruption of microbial cells for potential use in the dairy industry–a review. *Int Dairy J*. 12:541-553.

Gillitzer, E., Willits, D., Young, M., Douglas, T., 2002. Chemical modification of a viral cage for multivalent presentation. *Chem Commun*. 20:2390-2391.

Giuliani, A., Pirri, G., Bozzi, A., Di Giulio, A., Aschi, M., Rinaldi, A.C., 2008. Antimicrobial peptides: natural templates for synthetic membrane-active compounds. *Cell Mol Life Sci*. 65:2450-2460.

Glasgow, J.E., Capehart, S.L., Francis, M.B., Tullman-Ercek, D., 2012. Osmolyte-mediated encapsulation of proteins inside MS2 viral capsids. *ACS Nano*. 6(10):8658-8664.

Gross, I., Hohenberg, H., Huckhagel, C., Kräusslich, H.G., 1998. N-Terminal extension of human immunodeficiency virus capsid protein converts the *in vitro* assembly phenotype from tubular to spherical particles. *J Virol*. 72(6):4798-4810.

Gubser, C., Hué, S., Kellam, P., Smith, G.L., 2004. Poxvirus genomes: a phylogenetic analysis. *J Gen Virol*. 85(Pt 1):105-117.

Gupta, S.S., Kuzelka, J., Singh, P., Lewis, W.G., Manchester, M., Finn, M.G., 2005. Accelerated bioorthogonal cojugation: A practical method for ligation of diverse functional molecules to a polyvalent virus scaffold. *Bioconj Chem*. 16:1572-1579.

Gupta, S.S., Raja, K.S., Kaltgrad, E., Strable, E., Finn, M.G., 2005. Virus-glycopolymer conjugates by copper (i) catalysis of atom transfer radical polymerization and azide-alkyne cycloaddition. *Chem Commun*. 34:4315-4317.

Hemminga, M.A., Vos, W.L., Nazarov, P.V., Koehorst, R.B., Wolfs, C.J., Spruijt, R.B., Stopar, D., 2010. Viruses: incredible nanomachines. New advances with filamentous phages. *Eur Biophys J*. 39(4):541-550.

Higgins, D.R., Cregg, J.M., 1998. *Pichia protocols*. Humana Press, Totowa, N.J.

Hohenblum, H., Gasser, B., Maurer, M., Borth, N., Mattanovich, D., 2004. Effects of gene dosage, promoters, and substrates on unfolded protein stress of recombinant *Pichia pastoris*. *Biotechnol Bioeng*. 85(4):367-375.

Holmes, E.C., 2007. Viral evolution in the genomic age. *PLoS Biol*. 5(10):e278.

Holmström, S.C., Patil, A.J., Butler, M., Mann, S., 2007. Influence of polymer co-intercalation on guest release from aminopropyl-functionalized magnesium phyllosilicate mesolamellar nanocomposites. *J Mater Chem*. 17:3894-3900.

Hong, V., Presolski, S.I., Ma, C., Finn, M.G., 2009. Analysis and optimization of copper-catalyzed azide-alkyne cycloaddition for bioconjugation. *Angew Chem Int Ed.* 48(52):9879-9883.

Horiguchi, T., 1995. *Heterocapsa circularisquama* sp. nov. (Peridiniales, Dinophyceae): a new marine dinoflagellate causing mass mortality of bivalves in Japan. *Psychol Res*. 43:129-136.

Hu, Y., Zandi, R., Anavitarte, A., Knobler, C.M., Gelbart, W.M., 2008. Packaging of a polymer by a viral capsid: the interplay between polymer length and capsid size. *Biophys J*. 94(4):1428-1436.

Huang, Y., Chiang, C., Lee, S.K., Gao, Y., Hu, E.L., De, Yoreo, J., Belcher, A.M., 2005. Programmable assembly of nanoarchitectures using genetically engineered viruses. *Nano Lett*. 5(7):1429-1434.

Hung, C.W., 2008. RNA packaging and gene delivery using tobacco mosaic virus pseudo virions. ***Ph.D. Thesis***. University of Maryland, US.

Izadpanah, A., Gallo, R.L., 2005. Antimicrobial peptides. *J Am Acad Dermatol*. 52:381-390.

Jermutus, L., Ryabova, L.A., Plückthun, A., 1998. Recent advances in producing and selecting functional proteins by using cell-free translation. *Curr Opin Biotechnol*. 9(5):534-548.

Johnson, J.E., Speir, J.A., 1997. Quasi-equivalent viruses: a paradigm for protein assemblies. *J Mol Biol*. 269(5):665-675.

Jung, B., Rao, A.L., Anvari, B., 2011. Optical nano-constructs composed of genome-depleted brome mosaic virus doped with a near infrared chromophore for potential biomedical applications. *ACS Nano*. 5(2):1243-1252.

Kaiser, C.R., Flenniken, M.L., Gillitzer, E., Harmsen, A.L., Harmsen, A.G., Jutila, M.A., Douglas, T., Young, M.J., 2007. Biodistribution studies of protein cage nanoparticles demonstrate broad tissue distribution and rapid clearance in vivo. *Int J Nanomedicine*. 2(4):715-733.

Kaur, G., Zhan, W., Wang, C., Barnhill, H., Tian, H., Wang, Q., 2010. Crosslinking of viral nanoparticles with “clickable” fluorescent crosslinkers at the interface. *Sci China Chem.* 53(6):1287-1293.

Kay, L.E., 1986. W. M. Stanley's crystallization of the tobacco mosaic virus, 1930-1940. *Isis*. 77(288):450-472.

Kim, K.K., Kim, R., Kim, S.H., 1998. Crystal structure of a small heat-shock protein. *Nature*. 394(6693):595-599.

Kim, S.I., Wu, Y., Kim, K.L., Kim, G.J., Shin, H.J., 2013. Improved cell disruption of *Pichia pastoris* utilizing aminopropyl magnesium phyllosilicate (AMP) clay. *World J Microbiol Biotechnol*. 29(6):1129-1132.

Kirkpatrick, B., Fleming, L.E., Squicciarini, D., Backer, L.C., Clark, R., Abraham, W., Benson, J., Cheng, Y.S., Johnson, D., Pierce, R., Zaias, J., Bossart, G.D., Baden, D.G., 2004. Literature review of Florida red tide: implications for human health effects. *Harmful Algae*. 3(2):99-115.

Klem, M.T., Young, M., Douglas, T., 2008. Biomimetic synthesis of beta-TiO_2 inside a viral capsid. *J Mater Chem*. 18(32):3821-3823.

Klug, A., 1999. The tobacco mosaic virus particle: structure and assembly. *Philos Trans R Soc Lond B Biol Sci*. 354(1383):531-535.

Knipe, D.M., Howley, P.M., Griffin, D.E., Lamb, R.A., Martin, M.A., Roizman, B., Straus, S.E., 2007. *Fields Virology*, 5th edition. Lippincott Williams & Wilkins (LWW), Philadelphia.

Kolb, H.C., Finn, M.G., Sharpless, K.B., 2001. Click chemistry: diverse chemical function from a few good reactions. *Angew Chem Int Ed*. 40(11):2004-2021.

Kollar, R., Reinhold, B.B., Petrakova, E., Yeh, H.J., Ashwell, G., Drgonova, J., Kapteyn, J.C., Klis, F.M., Cabib, E., 1997. Architecture of the yeast cell wall. β(1-6)-glucan interconnects mannoprotein, β(1-3)-glucan and chitin. *J Biol Chem*. 272(28):17762-17775.

Kost, T.A., Condreay, J.P., Jarvis, D.L., 2005. Baculovirus as versatile vectors for protein expression in insect and mammalian cells. *Nat Biotechnol*. 23(5):567-575.

Koudelka, K.J., Manchester, M., 2010. Chemically modified viruses: principles and applications. *Curr Opin Chem Biol*. 14(6):810-817.

Laitinen, I., Saraste, A., Weidl, E., Poethko, T., Weber, A.W., Nekolla, S.G., Leppänen, P., Ylä-Herttuala, S., Hölzlwimmer, G., Walch, A., Esposito, I., Wester, H.J., Knuuti, J., Schwaiger, M., 2009. Evaluation of alphavbeta3 integrin-targeted positron emission tomography tracer 18F-galacto-RGD or imaging of vascular inflammation in atherosclerotic mice. *Circ Cardiovasc Imaging*. 2(4):331-338.

Lavelle, L., Michel, J.P., Gingery, M., 2007. The disassembly, reassembly and stability of CCMV protein capsids. *J Virol Methods*. 146(1-2):311-316.

Lawrence, J.E., Chan, A.M., Suttle, C.A., 2001. A novel virus (HaNIV) causes lysis of the toxic bloom-forming alga *Heterosigma akashiwo* (Raphidophycea). *J Phycol*. 37:216-222.

Lee, L.A., Niu, Z., Wang, Q., 2009. Viruses and virus-like protein assemblies–chemically programmable nanoscale building blocks. *Nano Res*. 2(5):349-364.

Lee, S.Y., Lim, J.S., Harris, M.T., 2012. Synthesis and application of virus-based hybrid nanomaterials. *Biotechnol Bioeng*. 109(1):16-30.

Lee, Y.C., Lee, T.H., Han, H.K., Go, W.J., Yang, J.W., Shin, H.J., 2010. Optical properties of fluorescein-labeled organoclay. *Photochem Photobiol*. 86(3):520-527.

Li, P., Anumanthan, A., Gao, X.G., Ilangovan, K., Suzara, V.V., Düzgüneş, N., Renugopalakrishnan, V., 2007. Expression of recombinant proteins in *Pichia pastoris*. *Appl Biochem Biotechnol*. 142(2):105-124.

Lin, H.K., van der Schoot, P., Zandi, R., 2012. Impact of charge variation on the encapsulation of nanoparticles by virus coat proteins. *Phys Biol*. 9(6):066004.

Liu, W.L., Alim, K., Balandin, A.A., Mathews, D.M., Dodds, J.A., 2005. Assembly and characterization of hybrid virus-inorganic nanotubes. *Appl Phys Lett*. 86(25):253108.

Lin, T., Chen, Z., Usha, R., Stauffacher, C., Dai, J., Schmidt, T., Johnson, J.E., 1999. The refined crystal structure of cowpea mosaic virus at 2.8 Å resolution. *Virology*. 265(1):20-34.

Liu, Z., Qiao, J., Niu, Z., Wang, Q., 2012. Natural supramolecular building blocks: from virus coat proteins to viral nanoparticles. *Chem Soc Rev*. 41(18):6178-6194.

Loo, L., Guenther, R.H., Lommel, S.A., Franzen, S., 2008. Infusion of dye molecules into red clover necrotic mosaic virus. *Chem Commun*. 1:88-90.

Ma, Y., Nolte, R.J., Cornelissen, J.J., 2012. Virus-based nanocarriers for drug delivery. *Adv Drug Deliv Rev*. 64:811-825.

Macauley-Patrick, S., Fazenda, M.L., McNeil, B., Harvey, L.M., 2005. Heterologous protein production using the *Pichia pastoris* expression system. *Yeast*. 22(4):249-270.

Manchester, M., Singh, P., 2006. Virus-based nanoparticles (VNPs): Platform technologies for diagnostic imaging. *Adv Drug Deliv Rev*. 58(14):1505-1522.

Mateu, M.G., 2011. Virus engineering: functionalization and stabilization. *Protein Eng Des Sel*. 24:53-63.

Meldrum, F.C., Wade, V.J., Nimmo, D.L., Heywood, B.R., Mann, S., 1991. Synthesis of inorganic nanophase materials in supramolecular protein cages. *Nature*. 349(6311):684-687.

Miller, J.L., Woodward, J., Chen, S., Jaffer, M., Weber, B., Nagasaki, K., Tomaru, Y., Wepf, R., Roseman, A., Varsani, A., Sewell, T., 2011. Three-dimensional reconstruction of *Heterocapsa circularisquama* RNA virus by electron cryo-microscopy. *J Gen Virol*. 92(Pt 8):1960-1970.

Miller, R.A., Presley, A.D., Francis, M.B., 2007. Self-assembling light-harvesting systems from synthetically modified tobacco mosaic virus coat proteins. *J Am Chem Soc*. 129(11):3104-3109.

Minten, I.J., Claessen, V.I., Blank, K., Rowan, A.E., Nolte, R.J., Cornelissen, J.J., 2011. Catalytic capsids: the art of confinement. *Chem Sci*. 2(2):358-362.

Minten, I.J., Hendriks, L.J., Nolte, R.J., Cornelissen, J.J., 2009. Controlled encapsulation of multiple proteins in virus capsids. *J Am Chem Soc*. 131(49):17771-17773.

Minten, I.J., Ma, Y., Hempenius, M.A., Vancso, G.J., Nolte, R.J., Cornelissen, J.J., 2009. CCMV capsid formation induced by a functional negatively charged polymer. *Org Biomol Chem*. 7(22):4685-4688.

Minten, I.J., Nolte, R.J., Cornelissen, J.J., 2010. Complex assembly behavior during the encapsulation of green fluorescent protein analogs in virus derived protein capsules. *Macromol Biosci*. 10(5):539-545.

Mizumoto, H., Tomaru, Y., Takao, Y., Shirai, Y., Nagasaki, K., 2007. Intraspecies host specificity of a single-stranded RNA virus infecting a marine photosynthetic protist is determined at the early steps of infection. *J Virol*. 81(3):1372-1378.

Mukherjee, S., Pfeifer, C.M., Johnson, J.M., Liu, J., Zlotnick, A., 2006. Redirecting the coat protein of a spherical virus to assemble into tubular nanostructures. *J Am Chem Soc*. 128(8):2538-2539.

Nagasaki, K., Shirai, Y., Takao, Y., Mizumoto, H., Nishida, K., Tomaru, Y., 2005. Comparison of genome sequences of single-stranded RNA viruses infecting the bivalve-killing dinoflagellate *Heterocapsa circularisquama*. *Appl Environ Microbiol*. 71(12):8888-8894.

Ng, B.C., 2010. Encapsulation of synthetic materials in biological self-assembled systems. *Ph.D. Thesis*. University of California, Los Angeles, US.

Nguyen, T.T., Bruinsma, R.F., Gelbart, W.M., 2005. Elasticity theory and shape transitions of viral shells. *Phys Rev E Stat Nonlin Soft Matter Phys*. 72(5 Pt 1):051923.

Ohtake, N., Niikura, K., Suzuki, T., Nagakawa, K., Mikuni, S., Matsuo, Y., Kinjo, M., Sawa, H., Ijiro, K., 2010. Low pH-triggered model drug molecule release from virus-like particles. *Chembiochem*. 11(7):959-962.

Orioni, B., Bocchinfuso, G., Kim, J.Y., Palleschi, A., Grande, G., Bobone, S., Park, Y., Kim, J.I., Hahm, K.S., Stella, L., 2009. Membrane perturbation by the antimicrobial peptide PMAP-23: a fluorescence and molecular dynamics study. *Biochim Biophys Acta*. 1788(7):1523-1533.

Parrish, B., Breitenkamp, R.B., Emrick, T., 2005. PEG-and peptide-grafted aliphatic polyesters by click chemistry. *J Am Chem Soc*. 127(20):7404-7410.

Phelps, J.P., Dao, P., Jin, H., Rasochova, L., 2007. Expression and self-assembly of cowpea chlorotic mottle virus-like particles in *Pseudomonas fluorescens*. *J Biotechnol*. 128(2):290-296.

Porta, C., Spall, V.E., Findlay, K.C., Gergerich, R.C., Farrance, C.E., Lomonossoff, G., 2003. Cowpea mosaic virus-based chimeras. Effects of inserted peptides on the phenotype, host range, and transmissibility of the modified viruses. *Virology*. 310(1):50-63.

Reddy, V.S., Natarajan, P., Okerberg, B., Li, K., Damodaran, K.V., Morton, R.T., Brooks, C.L. 3rd, Johnson, J.E., 2001. Virus Particle Explorer (VIPER), a website for virus capsid structures and their computational analyses. *J Virol*. 75(24):11943-11947.

Rodríguez-Limas, W.A., Sekar, K., Tyo, K.E., 2013. Virus-like particles: the future of microbial factories and cell-free systems as platforms for vaccine development. *Curr Opin Biotechnol*. S0958-1669(13)00022-0.

Rong, J., Lee, L.A., Li, K., Harp, B., Mello, C.M., Niu, Z., Wang, Q., 2008. Oriented cell growth on self-assembled bacteriophage M13 thin films. *Chem Commun*. 41:5185-5187.

Rostovtsev, V.V., Green, L.G., Fokin, V.V., Sharpless, K.B., 2002. A stepwise huisgen cycloaddition process: copper(I)-catalyzed regioselective "ligation" of azides and terminal alkynes. *Angew Chem Int Ed*. 41(14):2596-2599.

Roy, P., Noad, R., 2009. Virus-like particles as a vaccine delivery system: myths and facts. *Pharm Biotechnol*. 655:145-158.

Sambrook, J., Russell, D.W., 2001. *Molecular Cloning: A Laboratory Manual*, 3rd edition. Cold Spring Harbor Laboratory Press, Cold Spring Harbor, NY, US.

Sato, O., Iyoda, T., Fujishima, A., Hashimoto, K., 1996. Photoinduced magnetization of a cobalt-iron cyanide. *Science*. 272(5262):704-705.

Schlick, T.L., Ding, Z., Kovacs, E.W., Francis, M.B., 2005. Dual-surface modification of the tobacco mosaic virus. *J Am Chem Soc*. 127(11):3718-3723.

Schneemann, A., Young, M.J., 2003. Viral assembly using heterologous expression systems and cell extracts. *Adv Protein Chem*. 64:1-36.

Scholthof, K.B., Adkins, S., Czosnek, H., Palukaitis, P., Jacquot, E., Hohn, T., Hohn, B., Saunders, K., Candresse, T., Ahlquist, P., Hemenway, C., Foster, G.D., 2011. Top 10 plant viruses in molecular plant pathology. *Mol Plant Pathol*. 12(9):938-954.

Sengco, M.R., Anderson, D.M., 2004. Controlling harmful algal blooms through clay flocculation. *J Eukaryot Microbiol*. 51:169-172.

Shangari, N., Chan, T.S., Chan, K., Huai, Wu S., O'Brien, P.J., 2007. Copper-catalyzed ascorbate oxidation results in glyoxal/AGE formation and cytotoxicity. *Mol Nutr Food Res*. 51(4):445-455.

Sheehan, D., O'Sullivan, S., 2003. Fast Protein Liquid Chromatography. *Protein Purification Protocols*. 244.

Shen, L., Bao, N., Zhou, Z., Prevelige, P.E., Gupta, A., 2011. Materials design using genetically engineered proteins. *J Mater Chem*. 21:18868-18876.

Siber, A., Božič, A.L., Podgornik, R., 2012. Energies and pressures in viruses: contribution of nonspecific electrostatic interactions. *Phys Chem Chem Phys*. 14 (11):3746-3765.

Singh, P., Gonzalez, M.J., Manchester, M., 2006. Viruses and their uses in nanotechnology. *Drug Dev Res*. 67(1):23-41.

Smith, M.T., Hawes, A.K., Bundy, B.C., 2013. Reengineering viruses and virus-like particles through chemical functionalization strategies. *Curr Opin Biotechnol*. S0958-1669(13)00014-1.

Smits, G.J., van den Ende, H., Klis, F.M., 2001. Differential regulation of cell wall biogenesis during growth and development in yeast. *Microbiology*. 147(Pt 4):781-794.

Solé, J., Estradaa, M., Garcia-Ladona, E., 2006. Biological control of harmful algal blooms: a modelling study. *J Marine Syst*. 61:165-179.

Sotiropoulou, S., Sierra-Sastre, Y., Mark, S.S., Batt, C.A., 2008. Biotemplated nanostructured materials. *Chem Mater*. 20: 821-834.

Soto, C.M., Ratna, B.R., 2010. Virus hybrids as nanomaterials for biotechnology. *Curr Opin Biotechnol*. 21(4):426-438.

Speir, J.A., 1994. The 3.2 Angstrom resolution structure of the polymorphic cowpea chlorotic mottle virus ribonucleoprotein particle. *Ph.D. Thesis*. Purdue University, US.

Speir, J.A., Munshi, S., Baker, T.S., Johnson, J.E., 1993. Preliminary X-ray data analysis of crystalline cowpea chlorotic mottle virus. *Virology*. 193(1):234-241.

Speir, J.A., Munshi, S., Wang, G., Baker, T.S., Johnson, J.E., 1995. Structures of the native and swollen forms of cowpea chlorotic mottle virus determined by X-ray crystallography and cryo-electron microscopy. *Structure*. 3(1):63-78.

Sreekrishna, K., Brankamp, R.G., Kropp, K.E., Blankenship, D.T., Tsay, J.T., Smith, P.L., Wierschke, J.D., Subramaniam, A., Birkenberger, L.A., 1997. Strategies for optimal synthesis and secretion of heterologous proteins in the methylotrophic yeast *Pichia pastoris*. *Gene*. 190(1):55-62.

Steinmetz, N.F., 2010. Viral nanoparticles as platforms for next-generation therapeutics and imaging devices. *Nanomedicine*. 6(5):634-641.

Steinmetz, N.F., Evans, D.J., 2007. Utilisation of plant viruses in bionanotechnology. *Org Biomol Chem*. 5:2891-2902.

Steinmetz, N.F., Lomonossoff, G.P., Evans, D.J., 2006. Cowpea mosaic virus for material fabrication: addressable carboxylate groups on a programmable nanoscaffold. *Langmuir*. 22(8):3488-3490.

Stowers, C.C., Boczko, E.M., 2007. Reliable cell disruption in yeast. *Yeast*. 24(6):533-541.

Strable, E., Finn, M.G., 2009. Chemical modification of viruses and virus-like particles. *Curr Top Microbiol Immunol*. 327:1-21.

Su, Z., Wang, Q., 2010. A hierarchical assembly process to engineer a hydrophobic core for virus-like particles. *Angew Chem Int Ed*. 49(52):10048-10050.

Suttle, C.A., 2005. Viruses in the sea. *Nature*. 437(7057):356-361.

Taguchi, M., Yamada, K., Suzuki, K., Sato, O., Einaga, Y., 2005. Photoswitchable magnetic nanoparticles of Prussian blue with amphiphilic azobenzene. *Chem Mater*. 17:4554-4559.

Tama, F., Brooks, C.L. 3rd, 2002. The mechanism and pathway of pH induced swelling in cowpea chlorotic mottle virus. *J Mol Biol*. 318(3):733-747.

Tomaru, Y., Katanozaka, N., Nishida, K., Shirai, Y., Tarutani, K., Yamaguchi, M., Nagasaki, K., 2004. Isolation and characterization of two distinct types of HcRNAV, a single-stranded RNA virus infecting the bivalve-killing microalga *Heterocapsa circularisquama*. *Aquat Microb Ecol*. 34:207-218.

Tong, G.J., Hsiao, S.C., Carrico, Z.M., Francis, M.B., 2009.Viral capsid DNA aptamer conjugates as multivalent cell-targeting vehicles. *J Am Chem Soc*. 131(31):11174-11178.

Tornøe, C.W., Christensen, C., Meldal, M., 2002. Peptidotriazoles on solid phase: [1,2,3]-triazoles by regiospecific copper(i)-catalyzed 1,3-dipolar cycloadditions of terminal alkynes to azides. *J Org Chem*. 67(9):3057-3064.

Tu, R.S., Tirrell, M., 2004. Bottom-up design of biomimetic assemblies. *Adv Drug Deliv Rev*. 56(11):1537-1563.

Uchida, M., Klem, M.T., Allen, M., Suci, P., Flenniken, M., Gillitzer, E., Varpness, Z., Liepold, L.O., Young, M., Douglas, T., 2007. Biological containers: protein cages as multifunctional nanoplatforms. *Adv Mater*. 19:1025-1042.

Van der Graaf, M., van Mierlo, C.P., Hemminga, M.A., 1991. Solution conformation of a peptide fragment representing a proposed RNA-binding site of a viral coat protein studied by two-dimensional NMR. *Biochemistry.* 30(23):5722-5727.

Van Kammen, A., 1967. Purification and properties of the components of cowpea mosaic virus. *Virology*. 31(4):633-642.

Vriezema, D.M., Comellas-Aragones, M., Elemans, J.A., Cornelissen, J.J., Rowan, A.E., Nolte, R.J., 2005. Self-assembled nanoreactors. *Chem Rev*. 105(4):1445-1489.

Waldeck, J., Häger, F., Höltke, C., Lanckohr, C., von Wallbrunn, A., Torsello, G., Heindel, W., Theilmeier, G., Schäfers, M., Bremer, C., 2008. Fluorescence reflectance imaging of macrophage-rich atherosclerotic plaques using an alphav-beta3 integrin-targeted fluorochrome. *J Nucl Med*. 49(11):1845-1851.

Wang, Q., Chan, T.R., Hilgraf, R., Fokin, V.V., Sharpless, K.B., Finn, M.G., 2003. Bioconjugation by copper(I)-catalyzed azide-alkyne [3 + 2] cycloaddition. *J Am Chem Soc*. 125(11):3192-3193.

Wang, Q., Kaltgrad, E., Lin, T., Johnson, J.E., Finn, M.G., 2002. Natural supramolecular building blocks. Wild-type cowpea mosaic virus. *Chem Biol*. 9(7):805-811.

Wang, Q., Lin, T., Johnson, J.E., Finn, M.G., 2002. Natural supramolecular building blocks. Cysteine-added mutants of cowpea mosaic virus. *Chem Biol*. 9(7):813-819.

Warrens, A.N., Jones, M.D., Lechler, R.I., 1997. Splicing by overlap extension by PCR using asymmetric amplification: an improved technique for the generation of hybrid proteins of immunological interest. *Gene*. 186(1):29-35.

Wenger, M.D., DePhillips, P., Price, C.E., Bracewell, D.G., 2007. An automated microscale chromatographic purification of virus-like particles as a strategy for process development. *Biotechnol Appl Biochem*. 47(Pt 2):131-139.

Wimmer, E., Mueller, S., Tumpey, T.M., Taubenberger, J.K., 2009. Synthetic viruses: a new opportunity to understand and prevent viral disease. *Nat Biotechnol*. 27(12):1163-1172.

Wu, Y., Kim, W., Kim, S.W., Eom, C.Y., Yang, H., Shin, H.J., 2012. Expression and self-assembly of *Heterocapsa circularisquama* RNA virus-like particles synthesized in *Pichia pastoris*. *Chin Sci Bull*. 57(25):3288-3293.

Wu, Y., Yang, H., Shin, H.J., 2011. Expression and self assembly of cowpea chlorotic mottle virus capsid proteins in *Pichia pastoris* and encapsulation of fluorescent myoglobin. *MRS Proceedings*. 1317 (2011) mrsf10-1317-rr03-05, doi: 10.1557/opl.2011.138.

Wu, Y., Yang, H., Shin, H.J., 2013. Viruses as self-assembled nanocontainers for encapsulation of functional cargoes. *Korean J Chem Eng.* 30(7):1359-1367.

Yamada, K., Yoshii, S., Kumagai, S., Fujiwara, I., Nishio, K., Okuda, M., Matsukawa, N., Yamashita, I., 2006. High-density and highly surface selective adsorption of protein-nanoparticle complexes by controlling electrostatic interaction. *Jpn J Appl Phys*. 45:4259-4264.

Yi, H., Nisar, S., Lee, S.Y., Powers, M.A., Bentley, W.E., Payne, G.F., Ghodssi, R., Rubloff, G.W., Harris, M.T., Culver, J.N., 2005. Patterned assembly of genetically modified viral nanotemplates via nucleic acid hybridization. *Nano Lett*. 5(10):1931-1936.

Yokoyama, S., 2003. Protein expression systems for structural genomics and proteomics. *Curr Opin Chem Biol*. 7(1):39-43.

Yoshimura, H., 2006. Protein-assisted nanoparticle synthesis. *Colloids Surf A*. 282-283:464-470.

Zasloff, M., 2002. Antimicrobial peptides of multicellular organisms. *Nature*. 415(6870):389-395.

Zeng, Q., Saha, S., Lee, L.A., Barnhill, H., Oxsher, J., Dreher, T., Wang, Q., 2011. Chemoselective modification of turnip yellow mosaic virus by Cu(I) catalyzed azide–

alkyne 1,3-dipolar cycloaddition reaction and its application in cell binding. *Bioconjugate Chem*. 22:58-66.

Zhao, Q., Chen, W., Chen, Y., Zhang, L., Zhang, J., Zhang, Z., 2011. Self-assembled virus-like particles from rotavirus structural protein VP6 for targeted drug delivery. *Bioconjug Chem*. 22(3):346-352.

Zhao, X., Fox, J.M., Olson, N.H., Baker, T.S., Young, M.J., 1995. In vitro assembly of cowpea chlorotic mottle virus from coat protein expressed in *Escherichia coli* and in vitro-transcribed viral cDNA. *Virology*. 207(2):486-494.

Zlotnick, A., Stray, S.J., 2003. How does your virus grow? Understanding and interfering with virus assembly. *Trends Biotechnol*. 21(12):536-542.

초 록

Pichia 효모를 이용한 CCMV 바이러스 캡시드의 발현과 나노공학분야의 응용

오원정

지도교수: 신현재

화학공학과

조선대학교 대학원

바이러스와 감염성이 없는 바이러스 유사 입자는 높은 대칭성과 많은 표면개질 가능성, 균일한 입자크기 등 나노기술분야의 이상적인 재료의 특징을 많이 지니고 있다. 콩에 감염되는 CCMV 바이러스는 20 면체로 이루어졌고 지름이 28 nm 의 크기로서 지난 40 여년간 모델 시스템으로 많이 연구되었다. 최근에는 이 CCMV 바이러스가 재료과학과 의학분야에서 사용될 수 있는 나노재료로서 다시 각광을 받고 있다. CCMV 바이러스 단량체는 자기조직화하여 바이러스 유사입자로 형성되어 다양한 물질을 봉입할 수 있고 표면을 개질하여 다양한 기능을 부여할 수 있다. 본 박사학위 논문을 구성을 살펴보면 다음과 같다.

1 장: 바이러스와 바이러스 캡시드의 일반적인 내용 설명과 이 입자들의 나노기술 분야의 응용에 대하여 서술하였다.

2 장: 본 논문의 독창성과 관련된 연구목적과 연구의 배경을 다루었다.

3 장: CCMV 바이러스의 외피유전자(CP)를 *Pichia pastoris* GS115 에서 발현시키기 위하여 코돈을 변경하여 최적화하였다. 합성된 CP 유전자는 AOX1 유전자를 프로모터로 가진 pPICZ 셔틀벡터에 옮겨졌으며, 이렇게 재조합된 pPICZ A-CPsyns 유전자는 전기천공법으로 주입하였다. 유전자가 주입된 콜로니는 PCR 로 스크리닝 하였으며 SDS-PAGE 를 이용하여 발현단백질을 확인하였다. 재조합된 GS115-27-6 균주를 대상으로하여 5 리터 발효조 배양을 실시하였으며 최종 CCMV CP 의 생산 농도는 4.8 mg/mL 였다. 생산된 외비단백질은 PEG 를 첨가하고 염화세슘 농도구배를 이용하여 초고속원심분리기로 정제하였다. 생산된 재조합 단백질이 자기조직화하여 구형의 캡시드 단백질을 이루는 것은 UV 분광법과 투과전자현미경으로 확인하였다. 이 결과는 효모인 *P. pastoris* 를 이용하여 CCMV 의 외피유전자를 성공적으로 발현하는데 성공하였고, 이렇게 발현된 단백질을 대량생산하기 위하여 발효조를 이용하여 스케일업하였으며, 이렇게 생산된 단백질이 고유한 구형의 모양으로 자기조직화할 수 있음을 보여주었다. 이렇게 생산된 단백질 입자는 의학분야와 나노기술분야로 다양하게 적용이 가능할 것이다.

4 장: CCMV 캡시드에 정전기적 결합을 이용하여 Prussian blue (PB)를 봉입하였다. PB 에 존재하는 음이온화된 금속염은 캡시드의 pH 를 7.5 에서 5.2 로 변경함에 따라 해체와 재결합을 통 성공적으로 봉입되었다. 이렇게 PB 가 봉입된 캡시드는 나노반응기로서의 역할을 할 수 있었는데, 외부에 존재하는 또 다른 금속이온인

철 2 가 이온과 반응하여 PB 의 색이 변하는 것을 확인할 수 있었다. 성공적으로 봉입된 것은 FPLC 를 이용하여 크기의 차이를 확인하였으며, 성공적인 반응은 UV 분광법으로 710 nm 에서 측정함으로 알 우 있었다. 투과전자현미경 분석을 통하여 봉입된 입자는 균일한 구형암을 확인할 수 있었다. 입자의 크기는 나노입자분석기(DLS)로 분석하여 T 가 3 인경우는 29.2±1.7 nm 임을, T 가 2 인 경우는 17.5±1.2 nm 임을 확인하였다. 이 결과를 통하여 CCMV 입자내부로 PB 를 봉입할 수 있음을 확인하였고 봉입된 물질과 외부물질과 반응할 수 있는 나노반응기로의 가능성을 확인할 수 있었다. 이 방법을 통하여 빠르고 효율적인 자기조직화와 균일/불균일 이중금속나노입자의 제조가 가능하였다.

5 장: CCMV 캡시드 단백질의 외피를 변형 혹은 수식하기 위하여 CuAAC 반응을 처음으로 시도하였다. 캡시드 단백질의 표면에 나와있는 카르복시기를 alkyne 으로 처리하고 다시 azide 로 처리한 후 황산구리, TCEP, BCDS 존재하에서 triazole 연결을 만들었다. 이 방법으로 CCMV 의 표면에 형광을 띄는 coumarin 을 부착시켰으며 부착된 형광 coumarin 은 FPLC 와 자외선을 조사한 SDS-PAGE 방법으로 확인하였다. 짧은 길이의 OEG 와 RGD 펩타이드도 CuAAC 반응을 이용하여 CCMV 캡시드의 표면에 부착시켰다. FPLC, TEM, DLS 분석을 통하여 표면이 성공적으로 개질되었음을 확인하였다. 흥미롭게도 OEG-CCMV 는 캡시드 상호간에 결합으로 인하여 입자가 붙어있는 현상이 발견되었다. 최초상태의 CCMV, OEG-CCMV, RGD-CCMV 를 APTES 슬라이드에 처리하고 HeLa 세포의 부착정도를 확인하였다. OEG-CCMV 는 부착을 저해하는 반응이, RGD-CCMV 는

부착을 촉진하는 것을 알 수 있었다. 이번에 사용된 반응은 다른 click chemistry 의 대표적인 예로서 바이오나노입자의 설계에 중요한 역할을 할 수 있을 것으로 판단되며, 약물전달, 바이오센서, 조직공학용 재료 제조에 큰 역할을 할 것으로 판단된다.

본 연구와 직접 관련은 없으나 간접적으로 관련이 있는 연구 또한 다양하게 수행하였고 그 내용을 부록에 수록하였다.

부록 1: *Heterocapsa circularisquama* RNA 바이러스 (HcRNAV)의 109 CP 유전자를 위에서 언급한 방법과 동일하게 발현시켰으며, 형광단백질인 myoglobin 을 봉입시켰다. 이렇게 만들어진 바이러스는 유해한 조류의 조절에 사용될 수 있는 가능성을 가진다. 조류를 죽이는 살조능을 가진 펩타이인 PMAP-23-D7 과 공발현을 시도하였으며 이때는 구형이 아닌 막대기 모양의 다면체 구조가 형성됨을 알 수 있었다. 이러한 구조적 차이는 HcRNAV CP 의 N-말단에 PMAP-23-D7 연결되어서 나타난 효과로 예측된다.

부록 2: 효모인 *Pichia* 는 세포내 단백질 회수를 위한 세포파쇄가 어렵다. 본 연구에서는 아미노프로필기가 붙어 있는 마그네슘 유기클레이(aminopropyl magnesium phyllosilicate, AMP clay)를 글래스비드와 같이 사용하여 분쇄효율을 증가시켰다. AMP clay 는 활석과 유사한 구조로서 다양한 관능기를 붙여 기능성을 부여할 수 있다. 글래스비드와 0.2 % AMP clay 를 결합하여 4 분간 분쇄한 결과 4.24 mg/mL 의 단백질을 얻을 수 있었으며 이 수치는 글래스비드를

단독으로 사용했을 때보다 11.2 % 높은 수치이다. 분쇄시간은 반으로 줄어들었다. 이렇게 분리된 CCMV VLPs 의 안정성도 높아, 이 분쇄방법은 다양한 효모세포를 처리하는데 사용할 수 있을 것으로 판단된다.

결론으로서 효모인 *Pichia pastoris* 를 이용한 바이어스 캡시드의 발현은 성공적으로 이루어졌으며, 캡시드를 이용한 봉입과 캡시드의 표면개질도 성공적으로 수행되었다. 이러한 기술을 활용하면 제약과 나노기술 분야의 다양한 응용이 가능할 것으로 판단된다.

List of Publications

1. **Yuanzheng Wu**, Young-Jin Jeon, Min-Young Lee, Hetong Yang, Hyun-Jae Shin, Surface modification of cowpea chlorotic mottle virus capsids via copper(I)-catalyzed azide-alkyne cycloaddition (CuAAC) reaction and their adhesion behavior with HeLa cells, to be submitted.

2. **Yuanzheng Wu**, Soo-Kyung Choi, Hetong Yang, Hyun-Jae Shin, Encapsulation and crystallization of Prussian blue nanoparticles by cowpea chlorotic mottle virus capsids, to be submitted.

3. **Yuanzheng Wu**, Hetong Yang, Hyun-Jae Shin, Viruses as self-assembled nanocontainers for encapsulation of functional cargoes, *Korean Journal of Chemical Engineering*, 2013, 30(7):1359-1367.

4. Sun-Il Kim, **Yuanzheng Wu**, Ka-Lyun Kim, Geun-Joong Kim, Hyun-Jae Shin, Improved cell disruption of *Pichia pastoris* utilizing aminopropyl magnesium phyllosilicate (AMP) clay, *World Journal of Microbiology and Biotechnology*, 2013, 29(6):1129-1132.

5. **Yuanzheng Wu**, Wonduck Kim, Si-Wouk Kim, Chi-Yong Eom, Hetong Yang, Hyun-Jae Shin, Expression and self-assembly of Heterocapsa circularisquama RNA virus-like particles synthesized in *Pichia pastoris*, *Chinese Science Bulletin*, 2012, 57(25):3288-3293.

6. **Yuanzheng Wu**, Hetong Yang, Hyun-Jae Shin, Expression and self assembly of cowpea chlorotic mottle virus capsid proteins in *Pichia pastoris* and encapsulation of fluorescent myoglobin, *MRS Online Proceedings Library*, 2011, mrsf10-1317-rr03-05, doi: 10.1557/opl.2011.138.

Scientific Activities

Oral presentations

1. **Yuanzheng Wu**, Hyun-Jae Shin, Optimization of recombinant HcRNAV 109 capsid protein in *Pichia pastoris* and their self assembly into virus-like particles, BIT's 3rd Symposium on Enzymes and Biocatalysis (SEB2012), April 25-28, 2012, Xi'an, China.

2. **Yuanzheng Wu**, Hyun-Jae Shin, Optimization of recombinant HcRNAV 109 capsid protein in *Pichia pastoris* and their self assembly into virus-like particles, 2011 KSBB Fall Meeting and International Symposium, October 5-8, 2011, Incheon, Korea.

Poster presentations

1. **Yuanzheng Wu**, Ka-Lyun Kim, Hyo-Kyung Hang, Geun-Joong Kim, Hyun-Jae Shin, Improvement of cell disruption of *Pichia pastoris* using organoclay-assisted glass bead, 15th International Biotechnology Symposium and Exhibition (IBS2012), September 16-21, 2012, Daegu, Korea.

2. **Yuanzheng Wu**, Gayathri Chandrasekaran, Eun-Mi Ryu, Hyun-Jae Shin. Co-expression of Heterocapsa circularisquama RNA virus coat protein with antialgal peptide PMAP-23-D7 in *Pichia pastoris* and their self-assembly of virus-like particles and anti-dinoflagellate properties, Asian Congress on Biotechnology 2011 (ACB-2011), May 11-15, 2011, Shanghai, China.

3. **Yuanzheng Wu**, Hetong Yang, Hyun-Jae Shin, Expression and large scale production of cowpea chlorotic mottle virus-like particles in *Pichia pastoris*, 9th International Marine Biotechnology Conference (IMBC2010), October 8-12, 2010, Qingdao, China.

Curriculum Vitae

Name: Wu Yuanzheng

Gender: Male

Date of birth: October 7, 1979

Address:

Department of Chemical and Biochemical Engineering, Chosun University, #375 Seosuk-dong, Dong-gu, Gwangju, 501-759, Republic of Korea

Biotechnology Center of Shandong Academy of Sciences, No 19, Keyuan Road, Lixia District, Jinan, Shandong Province, 250014, P.R. China

Tel: +82-62-230-7865, +86-531-88728276

Email: yuanzehng.wu@hotmail.com

Educational and research experience

1997-2001: B.SC in Microbiology, Department of Microbiology, Shandong University, Jinan, Shandong Province, China

2001-2004: M. SC in Microbiology, Department of Microbiology, Shandong University, Jinan, Shandong Province, China

2004-Present: Biotechnology Center of Shandong Academy of Sciences, Jinan, Shandong Province, China

2010-2013: Ph.D, Department of Chemical and Biochemical Engineering, Chosun University, Gwangju, Korea

Acknowledgements

I would like to take this opportunity to thank all people who helped to make this dissertation possible.

First of all, I wish to thank my supervisor, **Professor Hyun-Jae Shin** for offering me the great chance to study under his kind guidance and constant support. Through these years, his extraordinary passion and excellent scientific mentor has been and will always be remembered by me. “Life is full of up’s and down’s, we shall live in the moment.” As you said, I thank you for selecting the most exciting topic, providing the state of art facilities, and helping to develop my presentation and writing skills throughout my Ph. D. studies.

I also thank **Dr. Hetong Yang**, director of Biotechnology Center of Shandong Academy of Sciences for the encouragement and support for my studies. It would not be possible for me to study in Korea without you.

It is an honour for me to thank **Prof. Jung-Gyu Kim**, **Prof. Jung-Heon Lee**, **Prof. Jae-Wook Lee**, **Prof. Byung-Wook Jo**, **Prof. Sun-Il Kim**, and **Prof. Wol-Suk Cha** at Department of Chemical and Biochemical Engineering in Chosun University for their guidance, lectures and supports during my studies.

I wish to thank **Prof. Young-Jin Jeon** and **Dr. Min-Young Lee** at Department of Pharmacology in Chosun University for the scientific discussion and experimental support in the cell culture and binding parts.

I would like to thank **Prof. Geun-Joong Kim** at Department of Biological Sciences in Chonnam National University for the kind support in various ways.

I am grateful to **Dr. Soo-Kyung Choi** for her scientific discussion and invaluable support.

I want to acknowledge **Dr. Young-Chul Lee** in KAIST and **Dr. Chi-Young Eom** in Korea Basic Science Institute for the kind discussion and support.

I would like to thank **Dr. Kechun Liu**, **Dr. Jianguo Shi**, **Dr. Jianing Wang, Mr. Jishun Li**, **Mr. Jindong Hu**, **Dr. Xinjian Zhang**, **Dr. Liwen Han**, **Dr. Weibing Peng, Mrs. Yanli Wei**, **Mrs. Kai Chen**, and all my colleagues in SAS for their supports and helps.

Thanks to my previous and present lab members who have made my time in Korea warmly remembered: **Dr. Gayathri Chandrasekaran**, **Dr. Hwan-Seok Choi**, **Dr. Mizhang Xiao**, **Mrs. Eun-Mi Ryu**, **Mrs. Moon-Hee Choi**, **Mrs. Myoung-Ja Min**, **Ms. Dream Gong**, **Mr. Yun-Soo Kim**, **Mr. Jin-Young Kim**, **Mr. Yong-Jo Lee**, **Ms. Eun-Sil Choi**, **Ms. Ga-Eun Lim**, **Ms. Ka-Lyun Kim**, and **Ms. Mi-Hwa Lee**. I shall always cherish the sheer agony and ecstasy of research that I have experienced in the lab working with you guys.

I am especially indebted to my family for unconditional love, encouragement and great support during my abroad study. Thanks to my mother for her support and help in my family.

Finally, I would like to express my very special gratitude to my dear wife **Mrs. Huijie Hao**, I owe you the most. And to my dear daughter **You Wu**, you are the source of my happiness.

I convey my thanks to all my friends whom I cannot name individually for their support directly and indirectly. None of what has been described in the next few pages.

Thanks to all of you!

저작물 이용 허락서

학과	화학공학과	학번	20107722	과정	박사
성명	한글 : 오원정 한문 : 20107722 영문 : Yuanzheng Wu				
주소	광주광역시 동구 필문대로 263번지				
연락처	e-mail : yuanzheng.wu@hotmail.com				
논문제목	한글 : *Pichia* 효모를 이용한 CCMV 바이러스 캡시드의 발현과 나노공학분야의 응용				
	영문 : Expression of Cowpea Chlorotic Mottle Virus Capsids in *Pichia pastoris* and their Application in Nanotechnology				

본인이 저작한 위의 저작물에 대하여 다음과 같은 조건 아래 조선대학교가 저작물을 이용할 수 있도록 허락하고 동의합니다.

- 다 음 -

저작물의 DB 구축 및 인터넷을 포함한 정보통신망에의 공개를 위한 저작물의 복제, 기억장치의 저장, 전송 등을 허락함.

위의 목적을 위하여 필요한 범위 내에서의 편집과 형식상의 변경을 허락함. 다만, 저작물의 내용변경을 금지함.

배포.전송된 저작물의 영리적 목적을 위한 복제, 저장, 전송 등은 금지함.

저작물에 대한 이용기간은 5년으로 하고, 기간종료 3개월 이내에 별도의 의사 표시가 없을 경우에는 저작물의 이용기간을 계속 연장함.

해당 저작물의 저작권을 타인에게 양도하거나 출판을 허락을 하였을 경우에는 1개월 이내에 대학에 이를 통보함.

조선대학교는 저작물 이용의 허락 이후 해당 저작물로 인하여 발생하는 타인에 의한 권리 침해에 대하여 일체의 법적 책임을 지지 않음.

소속 대학의 협정기관에 저작물의 제공 및 인터넷 등 정보통신망을 이용한 저작물의 전송.출력을 허락함.

동의여부 : 동의(0) 반대( )

2013년 8월

저작자 : Yuanzheng Wu (인)

조선대학교 총장 귀하

Article

Chinese Science Bulletin

SPECIAL TOPIC
Omics in Marine Biotechnology

September 2012 Vol.57 No.25: 3288–3293
doi: 10.1007/s11434-012-5125-z

Expression and self-assembly of *Heterocapsa circularisquama* RNA virus-like particles synthesized in *Pichia pastoris*

WU YuanZheng[1,4], KIM Wonduck[2], KIM Si-Wouk[2], EOM Chi-Yong[3], YANG HeTong[4] & SHIN Hyun-Jae[1*]

[1] *Department of Chemical and Biochemical Engineering, Chosun University, Gwangju 501-759, Republic of Korea;*
[2] *Department of Environmental Engineering, Chosun University, Gwangju 501-759, Republic of Korea;*
[3] *Seoul Center, Korea Basic Science Institute, Seoul 136-713, Republic of Korea;*
[4] *Biotechnology Center of Shandong Academy of Sciences, Jinan 250014, China*

Received November 3, 2011; accepted March 8, 2012; published online April 10, 2012

Heterocapsa circularisquama RNA virus (HcRNAV) is the first single-stranded RNA virus to be characterized that infects dinoflagellates. The ability of HcRNAV coat protein (HcRNAV CP) to self-assemble into virus-like particles (VLPs) *in vitro* suggested that heterologous expression was possible, and that the VLPs might be ideal nanocontainers for the targeted delivery of genes and chemicals. In this paper, we report the expression of a codon-optimized *HcRNAV 109 CP* gene in *Pichia pastoris* and the production of self-assembled HcRNAV VLPs using large-scale fermentation. The *HcRNAV 109 CP* gene was synthesized according to the codon preference of *P. pastoris* and cloned into a pPICZA vector. The recombinant plasmid pPICZA-CPsyns was transformed into *P. pastoris* by electroporation. The resulting yeast colonies were screened by PCR and analyzed for protein expression by SDS polyacrylamide gel electrophoresis. After large-scale fermentation, the yield of HcRNAV CPsyns reached approximately 2.5 g L^{-1} within 4 d. The HcRNAV VLPs were purified using PEG precipitation followed by cesium chloride density gradient ultracentrifugation, and were subsequently analyzed using UV spectrophotometry and transmission electron microscopy. Fluorescence dye-labeled myoglobin was loaded into the cages of the HcRNAV VLPs and the encapsulation was confirmed by fluorescence spectroscopy. The results point to the possible utilization in pharmacology or nanotechnology of HcRNAV VLPs produced by *P. pastoris* fermentation.

Heterocapsa circularisquama* RNA virus (HcRNAV), virus-like particles (VLPs), expression, self-assembly, *Pichia pastoris

Citation: Wu Y Z, Kim W, Kim S W, et al. Expression and self-assembly of *Heterocapsa circularisquama* RNA virus-like particles synthesized in *Pichia pastoris*. Chin Sci Bull, 2012, 57: 3288–3293, doi: 10.1007/s11434-012-5125-z

Harmful algal blooms (HABs), also known as red tides, have had a negative impact on aquatic ecosystems and have increasingly become a threat to human and marine health [1,2]. Rapid increases in an algal population can lead to water discoloration, shading of submerged vegetation, disruption of food-web dynamics and oxygen depletion in the water. HABs are known to have damaged the fishing industry, and to have affected shoreline quality and local economies. The potent neurotoxins can concentrate in filter-feeding shellfish and poison human consumers [3–5]. Even non-toxic algae can be harmful when they amass in sufficient numbers. HABs occur in many regions around the world, including Scandinavia, the North Pacific, the Caribbean and the South Pacific [6,7].

The toxic or harmful phytoplanktons that cause HABs are commonly dinoflagellates, such as *Alexandrium* and *Karenia* [8]. Most dinoflagellates have a unique structure that includes a nucleus known as the dinokaryon within which the chromosomes are attached to the nuclear membrane. Many efforts have been made to control harmful algal blooms with little success [9]. Today, the biological control of HABs is considered to be feasible [10]. Viruses that are abundant in marine systems replicate rapidly and tend to be host-specific, suggesting that single algal species

*Corresponding author (email: shinhj@chosun.ac.kr)

could be targeted [11,12]. Parasites also have the potential to control algal bloom species, but their specific role in this regard is largely unknown [13].

Heterocapsa circularisquama RNA virus (HcRNAV) is the first single-stranded RNA virus to be characterized that infects dinoflagellates [14]. *H. circularisquama* Horiguchi, first observed in Uranouchi Bay, Japan, is a harmful bloom-causing dinoflagellate that specifically kills bivalves [15]. HcRNAV particles are polyhedral with a diameter of approximately 30 nm, and encapsulate a single positive-stranded 4.4 kb RNA genome. Two open reading frames (ORF-1 and ORF-2) were identified in the genome, ORF-2 coding for the viral coat protein [16]. HcRNAV targets and accumulates in the dinoflagellate nucleus. The virus clones have been divided into types CY and UA (HcRNAV109 and HcRNAV34, respectively), based on their host strain specificity [17].

The methylotropic yeast, *Pichia pastoris*, has been shown to be a suitable system for the heterologous expression of virus coat protein, which could then self assemble into virus-like particles (VLPs) *in vitro*. The successful examples include cowpea chlorotic mottle virus (CCMV), hepatitis B virus (HBV), and bacteriophage Qbeta [18–20]. Besides its ability to express foreign proteins at a high level, *P. pastoris* has been shown to have several advantages over other expression systems. The fermentation period was usually 4–5 d, compared to the plant hosts in which production took weeks [21]. The synthesized VLPs were soluble and able to self-assemble, while production in prokaryote hosts, such as *E. coli*, often results in insoluble inclusions [22].

In this paper, we report on the heterologous synthesis of HcRNAV 109 coat protein by *P. pastoris.* The successful large-scale fermentation and purification of the self-assembled HcRNAV VLPs suggest their potential application as nanocontainers. To our knowledge, this is the first paper to report the heterologous expression of HcRNAV.

1 Materials and methods

1.1 Synthesis of *P. pastoris* codon-optimized HcRNAV 109 CPsyns

The sequence of the *HcRNAV 109 CP* gene, GenBank accession [AB218609] [23], was redesigned to substitute amino acid codons that are seldom used in *P. pastoris* with those more frequently used [24]. Chemical synthesis of the new *CP* gene (*CPsyns*) was accomplished with GenScript, USA. Restriction sites for *Eco*R I (GAATTC) and *Not* I (GCGGCCGC) were added upstream and downstream, respectively, of the *CPsyns* gene. The plasmid pUC57-CPsyns was transformed into *E. coli* Top10 for amplification and preservation.

1.2 Construction of the recombinant vector pPICZA-CPsyns

The *P. pastoris* host strain GS115 (*his4*, histidine-requiring auxotroph) and the intracellular expression vector pPICZA were purchased from Invitrogen, USA. For the *in vivo* expression in *P. pastoris*, the 1.1-kb *CPsyns* gene was retrieved from the pUC57 vector as an *Eco*R I/*Not* I fragment and cloned into the corresponding *Eco*R I and *Not* I sites of the *Pichia* integrative vector, pPICZA. The resultant vector pPICZA-CPsyns was then transformed into *E. coli* Top10 for its amplification.

1.3 Transformation of *P. pastoris* and cultivation of HCRNAV 109 CPsyns

The transformation and expression of the *CPsyns* gene in *P. pastoris* was performed using established procedures [25]. The recombinant plasmid pPICZA-CPsyns was linearized with *Sac* I and subsequently used to transform *P. pastoris* GS115 by electroporation (Multiporator, Eppendorf, Germany). The transformed yeast cells were incubated in YPD agar containing Zeocin at 30°C for 2–3 d. Because the *CPsyns* gene was integrated into the 5′ alcohol oxidase promoter (AOX1) locus on the *Pichia* chromosome, all transformants would be His^+ Mut^+. The *CPsyns* gene in the transformed yeast cells was amplified with PCR using the CPsyns and AOX1 primers (data not shown).

Verified transformants were grown in a buffered glycerol-complex medium (BMGY) at 30°C for 16–20 h. The yeast cells were harvested using centrifugation and resuspended in buffered methanol-complex medium (BMMY) at an optical density of 1.0 at 600 nm (about 5×10^7 cells mL^{-1}). Incubation was continued for an additional 96 h at 30°C with 1% methanol induction every 24 h. To determine the optimal harvest time after induction, 1 mL of the expression medium was withdrawn every 12 h and the protein expression levels were determined using SDS polyacrylamide gel electrophoresis (SDS-PAGE). Non-transformed *P. pastoris* GS115 and cells transformed with the expression vector pPICZA/GS115 were included as controls for the same induction process.

1.4 Large scale fermentation of HcRNAV 109 CPsyns

A positive transformant GS115-24, reliably expressing the *HcRNAV CPsyns* gene, was selected to scale-up CPsyns production in a 5-liter fermenter (Fermentec XP 50, Korea) using established protocols (Pichia Fermentation Process Guidelines, Invitrogen, USA). A total of 10% of the initial fermentation volume of GS115-24 in BMGY was inoculated into BMGY in the fermenter. One mL of the fermentation medium was withdrawn every 12 h to monitor cell growth using absorbance at 600 nm. Coat protein expression levels were determined using SDS-PAGE. After the glycerol fed-batch phase and the methanol fed-batch phase, the culture was centrifuged to separate the cells from the supernatant. The harvested *P. pastoris* cells were placed on ice for further lysis, while protein concentration was analyzed using

the Bradford protein assay.

1.5 Purification of HcRNAV 109 VLPs

A modified virus capsid purification procedure based on PEG precipitation and density gradient centrifugation was employed to purify the soluble assembled HcRNAV VLPs [26]. The *Pichia* cells gathered by centrifugation at 4000×*g* for 30 min were resuspended in five times (w/w) lysis buffer (50 mmol L^{-1} sodium phosphate, pH 7.4, 1 mmol L^{-1} PMSF, 1 mmol L^{-1} EDTA, and 5% glycerol) and disrupted by sonication (30 s on, 30 s off, 15 cycles, Vibra-cell VCX-750, Sonics, USA). Cell debris and insoluble material were removed by centrifugation at 10000×*g* for 30 min, and PEG 6000 was added to the supernatant to a final concentration of 10%. After overnight incubation at 4°C, the solution was centrifuged at 10000×*g* for 30 min and the resulting pellet was resuspended in phosphate buffer (10 mmol L^{-1} Na_2HPO_4, 10 mmol L^{-1} KH_2PO_4, pH 7.2). The resuspended PEG pellet was loaded onto a 10%–40% cesium chloride gradient and centrifuged at 35000×*g* for 2 h. The pellet was dissolved in the same phosphate buffer for further analysis.

1.6 Analysis of purified HcRNAV 109 VLPs

The purified HcRNAV VLPs were analyzed by UV spectrometry and transmission electron microscopy (TEM). Absorption at 260 nm and 280 nm was measured on a Scinco S-3100 UV spectrophotometer (Seoul, Korea), and the A_{260}∶A_{280} ratio was calculated. TEM images of VLPs negatively-stained with 2%(wt:vol) uranyl acetate were obtained with a CM30 electron microscope (FEI/Philips) operated at 200 kV (Korea Basic Science Institute, Chunchon Center, Korea) [26].

1.7 Encapsulation of fluorescence dye-labeled myoglobin

Purified HcRNAV VLPs in PBS, obtained from Section 2.5, were dialyzed against three changes of disassembly buffer (0.05 mol L^{-1} phosphate buffer, 0.15 mol L^{-1} NaCl, 2 mmol L^{-1} DTT, pH 8.0). Myoglobin was labeled with a fluorescent dye, Alexa Fluor 594, according to the Alexa Fluor® 594 Protein Labeling Kit (A10239, Invitrogen, USA). The disassembled HcRNAV VLPs and fluorescent myoglobin were mixed at the ratio of 5∶1 and the resulting mixture was incubated at room temperature for 1.5 h. The incubated solution was then dialyzed against three changes of reassembly buffer (0.05 mol L^{-1} phosphate buffer, 0.5 mol L^{-1} NaCl, pH 7.2) and concentrated by freeze-drying. Free myoglobin was removed using Vivaspin 6 ultrafiltration spin column (Sartorius, Germany). The VLPs containing encapsulated myoglobin were further analyzed and purified by size exclusion fast performance liquid chromatography (FPLC) on Biologic DuoFlow™ Chromatography System (Bio-Rad, USA) equipped with a Superose 6 PC 3.2/30 column (flow rate 40 μL min^{-1}, GE Healthcare, USA). The purified myoglobin-containing HcRNAV capsids were used to perform fluorescence spectroscopy (Confocal Laser Scanning Biological Microscope FV1000, Olympus, Japan) [27].

2 Results and discussion

2.1 Construction of expression vector pPICZA-CPsyns

The *P. pastoris* expression system was chosen due to its relatively simple fermentation protocol and high final cell density. To enhance the efficiency of gene expression, the HcRNAV CPsyns gene was optimized to the codon usage of *P. pastoris* (Figure 1). The synthesized 1080 bp sequence showed 95.6% nucleotide identity (1033/1080) and 100% deduced amino acid identity with the native *HcRNAV 109 CP* gene. The inclusion of seldom-used codons in *P. pastoris*, such as CGG (arginine) and GCG (alanine), can lead to low efficiency of gene translation via early termination. These codon alterations (CGG→AGA, GCG→GGT) were expected significantly to improve the expression level of foreign proteins. In total, 47 changes were introduced into the synthesized gene. The resulting HcRNAV CPsyns was then inserted into the pPICZA plasmid. The digestion of the recombinant vector by *Eco*R I and *Not* I showed two bands of 3.3 kb (pPICZA) and 1.1 kb (CPsyns), which indicated that the expression vector pPICZA-CPsyns was constructed successfully (Figure 2).

2.2 Expression of the HcRNAV 109 *CPsyns* gene in *P. pastoris*

After screening on Zeocin-YPD plates, over 10 *P. pastoris* transformants were induced with methanol and examined for HcRNAV CPsyns production. Each supernatant (5 μL) after cell lysis was subjected to SDS-PAGE (Figure 3). All of the transformants showed a band at approximately 40 kD, which was the theoretical molecular weight of the HcRNAV coat protein monomer. Transformant GS115-24 was selected for further fermentation.

The *P. pastoris* transformant GS115-24 grew exponentially for more than 40 h in the glycerol fed-batch phase in the 5-liter fermenter. Then, a methanol-fed induction was commenced over 72 h with the methanol concentration beginning at 3.6 mL h^{-1} L^{-1} and reaching 10.9 mL h^{-1} L^{-1}. The maximum wet cell weight reached was 400 g L^{-1} (A_{600} of approximately 160). The concentration of crude HcRNAV coat protein approached 2.5 g L^{-1} as determined by the Bradford protein assay, which was more than 12-fold the yield of HcRNAV CP in the shaking flasks. This is one of the highest productions of viral coat protein reported to date.

2.3 Purification of HcRNAV 109 VLPs

Recombinant GS115-24 cells were lysed by ultrasonic

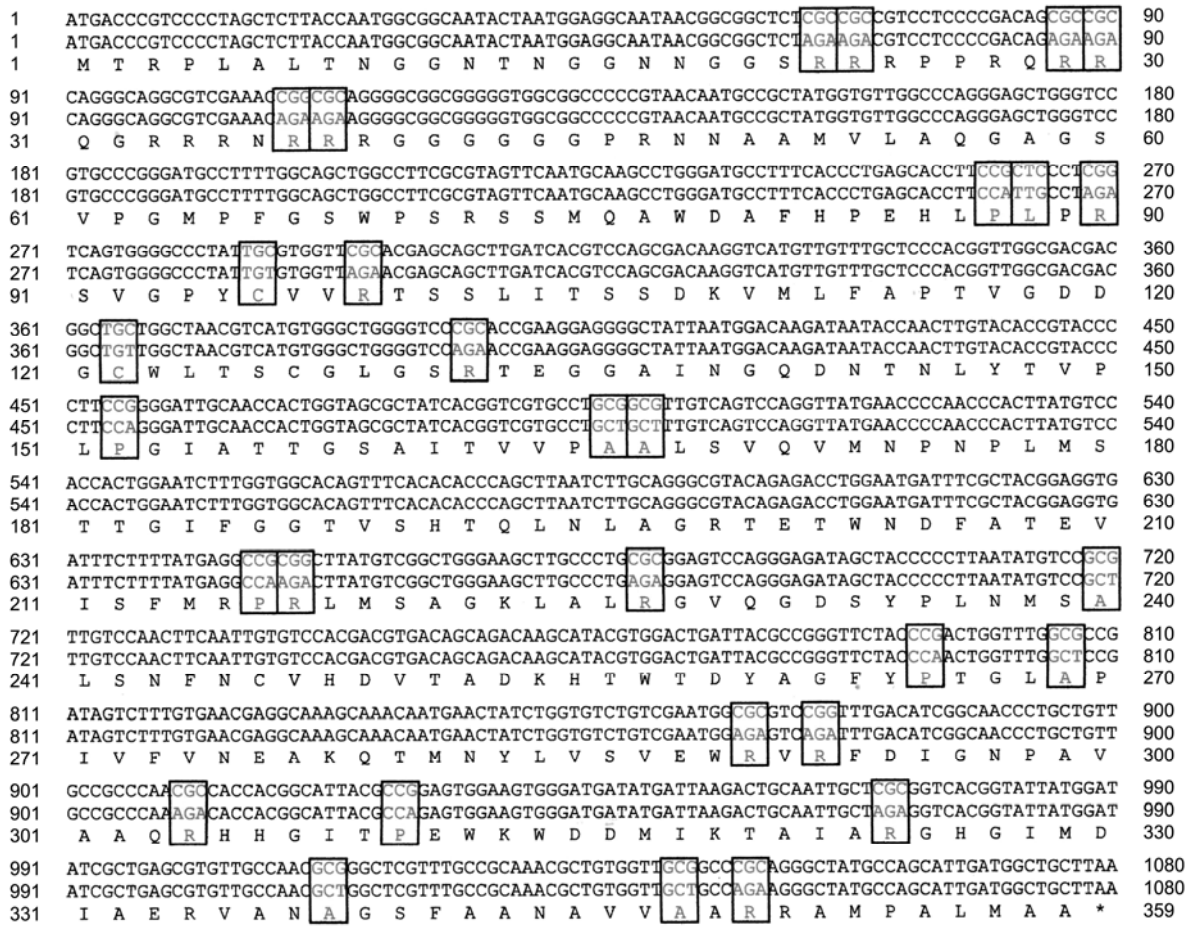

Figure 1 Nucleotide sequences and deduced amino acid sequence of *HcRNAV 109 CP* gene (top line) and HcRNAV *CPsyns* gene (bottom line). The alterations in nucleotide sequence are boxed in gray.

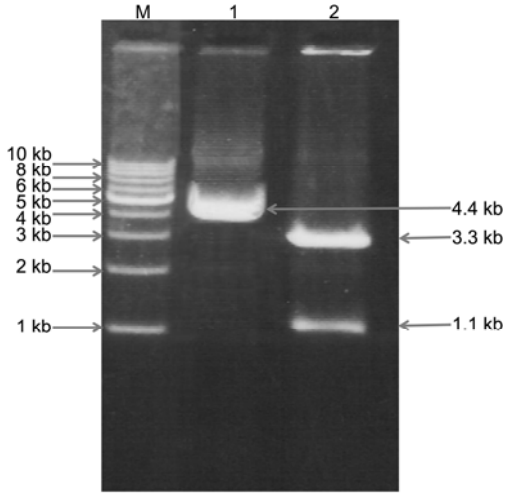

Figure 2 Digestion of pPICZA-CPsyns with *Eco*R I and *Not* I. Lane 1, digestion of pPICZA-CPsyns with *Eco*R I; 2, double-digestion of pPICZA-CPsyns with *Eco*R I and *Not* I; M, Takara 1 kb DNA ladder.

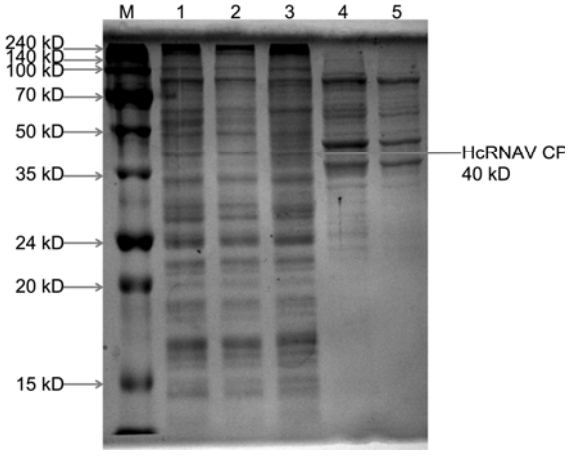

Figure 3 SDS-PAGE of *P. pastoris* transformants. Lanes 1–3, soluble fractions of pPICZA-CPsyns transformants after sonication; 4, control of pPICZA/GS115; 5, control of GS115; M, DokDo-MARK^{TM} broad-range.

disruption and the HcRNAV CP purified by PEG precipitation and density gradient centrifugation. PEG treatment of the supernatant preferentially precipitated HcRNAV CP with almost no precipitation of other proteins. Ultracentrifugation in CsCl further purified HcRNAV CP to a single band of 40 kD, which showed that the coat protein was able to assemble into high molecular weight structures (HcR-

NAV VLPs) (Figure 4).

2.4 Characterization of purified HcRNAV 109 VLPs

The VLPs were analyzed by UV spectrophotometry and showed an A_{260}:A_{280} ratio of 1.51, which was similar to the ratio of 1.56 observed with other VLPs.

TEM examination of the VLPs showed spherical particles of ca. 30 nm diameter (Figure 5). This similarity to native HcRNAV particles indicated that the synthesized coat protein was successfully expressed and self-assembled into VLPs *in vitro* [14].

2.5 Encapsulation of fluorescence dye-labeled myoglobin

The co-elution of HcRNAV VLPs and guest myoglobin (t = 36 min) was observed in the FPLC traces (Figure 6), showing the same elution time as the original capsids. These pointed to the successful reassembly of the viral cage after the encapsulation process.

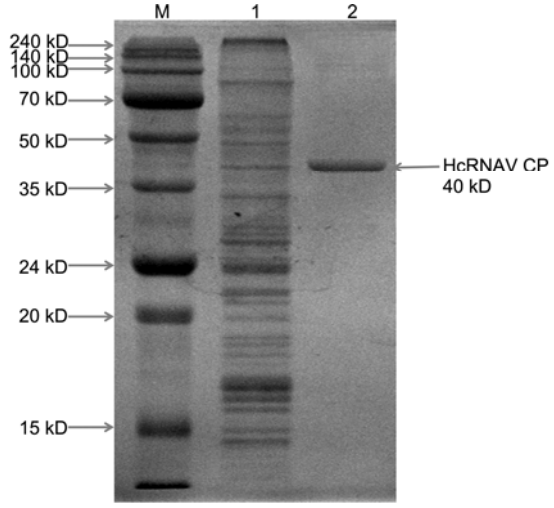

Figure 4 Purification of HcRNAV coat protein. Lane 1, soluble fractions of GS115-24 after sonication; 2, HcRNAV CP purified by ultracentrifugation in CsCl; M, DokDo-MARK^{TM} broad-range.

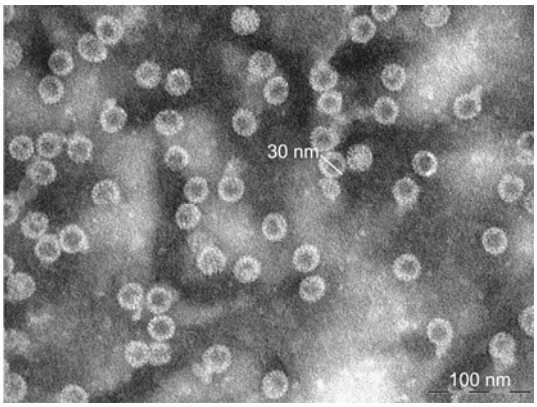

Figure 5 TEM image of HcRNAV VLPs. The diameter of the capsids was about 30 nm. Size bar represents 100 nm.

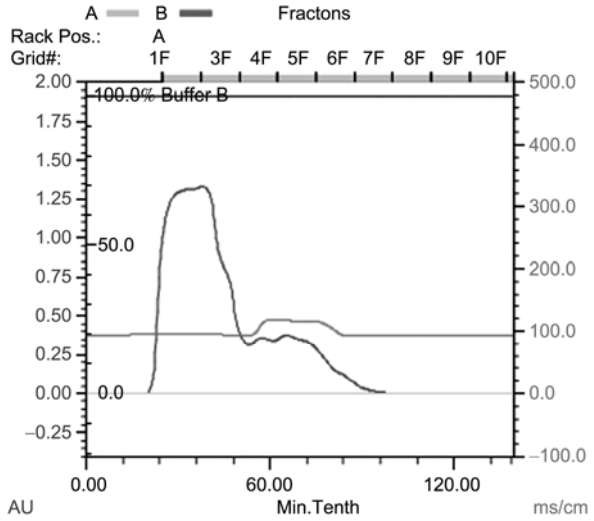

Figure 6 Size-exclusion FPLC of myoglobin-containing HcRNAV VLPs at 280 nm. The peak at elution time of 36 min corresponded to the intact virus capsids.

The correct reassembly of HcRNAV capsids with fluorescent myoglobin was further proven by fluorescence spectroscopy. The capsids containing this guest protein displayed significant emission at $\lambda = 590$ nm (Figure 7), indicating that inclusion of myoglobin had occurred successfully. When HcRNAV VLPs were used as control, no emission under the same condition was observed.

3 Conclusion

HcRNAV 109 coat protein was expressed in *Pichia pastoris*

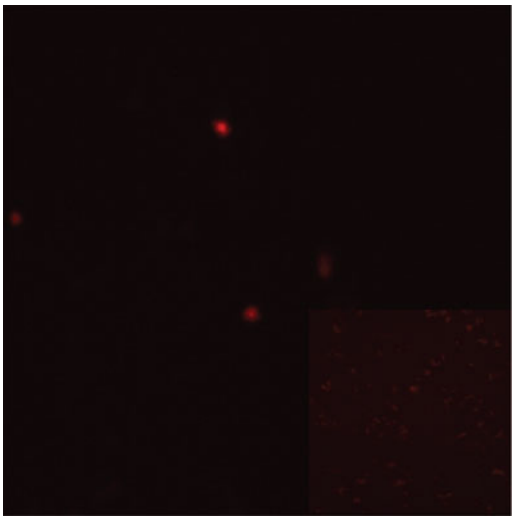

Figure 7 Fluorescence spectroscopy of myoglobin-containing HcRNAV VLPs. A typical confocal fluorescence image (1.68 μm×1.68 μm) showed the formation of a fluorescent protein encapsulated inside a capsid. Inset: AFM image (to scale) at the same sample location, showing that only a small fraction of the capsids contained myoglobin molecules.

and successfully self-assembled into polyhedral virus-like particles. To our knowledge, this is the first report on the efficient expression and assembly in *P. pastoris* of the capsid of a virus infecting a harmful alga. Optimization of codons to those preferred by *P. pastoris* was necessary for the high expression of the foreign gene in the *P. pastoris* system [28]. The successful expression and purification of HcRNAV VLPs makes their abundant and rapid production now possible. This method also represents a promising tool for the preparation of large amounts of VLPs for use in gene therapy, vaccine development, and other applications such as the control of harmful algal blooms.

The encapsulation of myoglobin as a model protein inside HcRNAV VLPs revealed that these virus capsids derived from *P. pastoris* were suitable nanocontainers for drug delivery and imaging reagent carriers. The specific targeting by HcRNAV of *H. circularisquama* would be extremely useful in controlling harmful algal blooms. The encapsulation of algicidal compounds inside the capsids to improve the efficiency is another useful approach for future investigation. HcRNAV could become a model virus capsid that might be used as a nanoplatform in materials science and medicine. Further analysis to compare the properties of the recombinant HcRNAV capsids with those of the native types is ongoing. The modification of HcRNAV CP by altering certain functional amino acids could also be useful in revealing the detailed structure, currently unknown, of the HcRNAV capsid.

This work was supported by the Pioneer Research Center Program through the National Research Program of Korea funded by the Ministry of Education, Science and Technology, Korea (*Grant M1071118001-08M1118-00110*) (*2010*). *We thank Dr. Song Her (KBSI) for providing the TEM pictures.*

1 Anderson D M. Turning back the harmful red tide. Nature, 1997, 388: 513–514
2 Hallegraeff G M. A review of harmful algal blooms and their apparent global increase. Phycologia, 1993, 32: 79–99
3 Van Dolah F M, Roelke D, Greene R M. Health and ecological impacts of harmful algal blooms: Risk assessment needs. Hum Ecol Risk Assess, 2001, 7: 1329–1345
4 Friedman M A, Levin B E. Neurobehavioral effects of harmful algal bloom (HAB) toxins: A critical review. J Int Neuropsychol Soc, 2005, 11: 331–338
5 Erdner D L, Dyble J, Parsons M L, et al. Centers for oceans and human health: A unified approach to the challenge of harmful algal blooms. Environ Health, 2008, 7(Suppl 2): 1–17
6 Corrales R A, Maclean J L. Impacts of harmful algae on seafarming in the Asia-Pacific areas. J Appl Phycol, 1995, 7: 151–162
7 Kirkpatrick B, Fleming L E, Squicciarini D, et al. Literature review of Florida red tide: Implications for human health effects. Harmful Algae, 2004, 3: 99–115
8 Garrett M, Wolny J, Truby E, et al. Harmful algal bloom species and phosphate-processing effluent: Field and laboratory studies. Mar Pollut Bull, 2010, 61: 621–626
9 Sengco M R, Anderson D M. Controlling harmful algal blooms through clay flocculation. J Eukaryot Microbiol, 2004, 51: 169–172
10 Solé J, Estradaa M, Garcia-Ladona E. Biological control of harmful algal blooms: A modelling study. J Marine Syst, 2006, 61: 165–179
11 Lawrence J E, Chan A M, Suttle C A. A novel virus (HaNIV) causes lysis of the toxic bloom-forming alga *Heterosigma akashiwo* (Raphidophycea). J Phycol, 2001, 37: 216–222
12 Baudoux A C, Brussaard C P. Characterization of different viruses infecting the marine harmful algal bloom species *Phaeocystis globosa*. Virology, 2005, 341: 80–90
13 Chambouvet A, Morin P, Marie D, et al. Control of toxic marine dinoflagellate blooms by serial parasitic killers. Science, 2008, 322: 1254–1257
14 Tomaru Y, Katanozaka N, Nishida K, et al. Isolation and characterization of two distinct types of HcRNAV, a single-stranded RNA virus infecting the bivalve-killing microalga *Heterocapsa circularisquama*. Aquat Microb Ecol, 2004, 34: 207–218
15 Horiguchi T. *Heterocapsa circularisquama* sp. nov. (Peridiniales, Dinophyceae): A new marine dinoflagellate causing mass mortality of bivalves in Japan. Psychol Res, 1995, 43: 129–136
16 Nagasaki K, Shirai Y, Takao Y, et al. Comparison of genome sequences of single-stranded RNA viruses infecting the bivalve-killing dinoflagellate *Heterocapsa circularisquama*. Appl Environ Microbiol, 2005, 71: 8888–8894
17 Mizumoto H, Tomaru Y, Takao Y, et al. Intraspecies host specificity of a single-stranded RNA virus infecting a marine photosynthetic protist is determined at the early steps of infection. J Virol, 2007, 81: 1372–1378
18 Brumfield S, Willits D, Tang L, et al. Heterologous expression of the modified coat protein of cowpea chlorotic mottle bromovirus results in the assembly of protein cages with altered architectures and function. J Gen Virol, 2004, 85: 1049–1053
19 Hu B, Liang M J, Hong G Q. Expression of hepatitis B virus S gene in *Pichia pastoris* and application of the product for detection of anti-HBs antibody. J Biochem Mol Biol, 2005, 38: 683–689
20 Freivalds J, Dislers A, Ose V, et al. Assembly of bacteriophage Qbeta virus-like particles in yeast *Saccharomyces cerevisiae* and *Pichia pastoris*. J Biotechnol, 2006, 123: 297–303
21 Yokoyama S. Protein expression systems for structural genomics and proteomics. Curr Opin Chem Biol, 2003, 7: 39–43
22 Zhao X, Fox J M, Olson N H, et al. *In vitro* assembly of cowpea chlorotic mottle virus from coat protein expressed in *Escherichia coli* and *in vitro*-transcribed viral cDNA. Virology, 1995, 207: 486–494
23 Nagasaki K. Dinoflagellates, diatoms and their viruses. J Microbiol, 2008, 46: 235–243
24 Sreekrishna K, Brankamp R G, Kropp K E, et al. Strategies for optimal synthesis and secretion of heterologous proteins in the methylotrophic yeast *Pichia pastoris*. Gene, 1997, 190: 55–62
25 Sambrook J, Russell D W. Molecular Cloning: A Laboratory Manual, 3rd ed. Cold Spring Harbor: Cold Spring Harbor Laboratory Press, 2001
26 Ali A, Roossinck M J. Rapid and efficient purification of cowpea chlorotic mottle virus by sucrose cushion ultracentrifugation. J Virol Methods, 2007, 141: 84–86
27 Comellas-Aragonès M, Engelkamp H, Claessen V I, et al. A virus-based single-enzyme nanoreactor. Nat Nanotechnol, 2007, 10: 635–639
28 Macauley-Patrick S, Fazenda M L, McNeil B, et al. Heterologous protein production using the *Pichia pastoris* expression system. Yeast, 2005, 22: 249–270

World J Microbiol Biotechnol (2013) 29:1129–1132
DOI 10.1007/s11274-013-1262-z

SHORT COMMUNICATION

Improved cell disruption of *Pichia pastoris* utilizing aminopropyl magnesium phyllosilicate (AMP) clay

Sun-Il Kim · Yuanzheng Wu · Ka-Lyun Kim · Geun-Joong Kim · Hyun-Jae Shin

Received: 24 October 2012 / Accepted: 14 January 2013 / Published online: 30 January 2013

Abstract An efficient method for *Pichia* cell disruption that employs an aminopropyl magnesium phyllosilicate (AMP) clay-assisted glass beads mill is presented. AMP clay is functionalized nanocomposite resembling the talc parent structure $Si_8Mg_6O_{20}(OH)_4$ that has been proven to permeate the bacterial membrane and cause cell lysis. The recombinant capsid protein of cowpea chlorotic mottle virus (CCMV) expressed in *Pichia pastoris* GS115 was used as demonstration system for their ability of self-assembly into icosahedral virus-like particles (VLPs). The total protein concentration reached 4.24 mg/ml after 4 min treatment by glass beads mill combined with 0.2 % AMP clay, which was 11.2 % higher compared to glass beads mill only and the time was half shortened. The stability of purified CCMV VLPs illustrated AMP clay had no influence on virus assembly process. Considering the tiny amount added and simple approach of AMP clay, it could be a reliable method for yeast cell disruption.

Keywords AMP clay · Cell disruption · *Pichia pastoris* · Virus-like particles

Pichia pastoris has become an efficient expression system for producing recombinant proteins of intracellular and extracellular origin from different sources at high yields (Cereghino and Cregg 2000). However, intracellular products expressed in *P. pastoris* require an additional step to disrupt the mechanically rigid cell wall, which is composed of multiple layers of cross-linked β-1,3-glucan, chitin and glycosylated mannoproteins (Kollár et al. 1997; Smits et al. 2001). Common protocols of cell wall disruption include breaking the cell wall either mechanically or enzymatically, which are usually tedious and time-consuming (Geciova et al. 2002; Stowers and Boczko 2007). The improvement of disruption methods is essential to acquire higher protein yields with low cost and good reproducibility.

In this work, we developed a simple method to disrupt *Pichia* cells utilizing glass beads mill combined with organic clay. Aminopropyl magnesium phyllosilicate (AMP) clay is a sandwiched organo-functionality with layered lamella sheets ranging from 20 to 200 nm that resemble talc parent structure $Si_8Mg_6O_{20}(OH)_4$ (Ferreira et al. 2008; Lee et al. 2010). It has been reported that AMP clay at high concentration displays antimicrobial activities against *Escherichia coli*, *Staphylococcus aureus* and *Candida albicans* by permeating the bacterial membrane and causing cell lysis (Chandrasekaran et al. 2011). Therefore, the applicability of AMP clay to enhance cell disruption was investigated to assess its efficiency on cell lysis. The demonstration system involves the recombinant capsid protein (CP) of cowpea chlorotic mottle virus (CCMV) which was expressed in *P. pastoris* GS115 and spontaneously assembled into icosahedral virus-like particles (VLPs) (Wenger et al. 2007; Wu et al. 2011).

The recombinant strain G48 was constructed by inserting CCMV CP into *Pichia* integrative vector pPICZ A under the highly-inducible AOX1 promoter (Wu et al. 2011). As described in EasySelect *Pichia* Expression Kit

S.-I. Kim · Y. Wu · K.-L. Kim · H.-J. Shin (✉)
Department of Chemical and Biochemical Engineering, Chosun University, #375 Seosuk-dong, Dong-gu, Gwangju 501-759, Republic of Korea
e-mail: shinhj@chosun.ac.kr

G.-J. Kim
Department of Biological Sciences, College of Natural Sciences, Chonnam National University, #300 Yongbong-dong, Buk-gu, Gwangju 500-757, Republic of Korea

Table 1 Total protein concentration of *P. pastoris* G48 by different cell disruption methods

Time (min)	Total protein concentration by AMP clay-assisted glass beads (mg/ml)	Total protein concentration by glass beads only (mg/ml)	Total protein concentration by AMP clay only (mg/ml)
0	0.07 ± 0.02	0.07 ± 0.03	0.08 ± 0.02
2	0.32 ± 0.06	0.39 ± 0.03	0.09 ± 0.04
4	4.24 ± 0.04 *	3.57 ± 0.05 *	0.09 ± 0.03
6	4.04 ± 0.05 *	3.59 ± 0.03 *	0.11 ± 0.05
8	3.85 ± 0.03 *	3.81 ± 0.04 *	0.11 ± 0.04
10	3.74 ± 0.03 *	3.58 ± 0.02 *	0.12 ± 0.03

* The difference in the mean values of the two groups is greater than would be expected by chance; there is a statistically significant difference between the input groups ($p = 0.038$)

(Invitrogen, USA), recombinant G48 was inoculated in 25 ml buffered glycerol-complex medium (BMGY) at 30 °C with shaking at 240 rpm for 16–18 h and then transferred into 100 ml buffered methanol-complex medium (BMMY) for 72 h induction. *Pichia* cells were centrifuged at 4000×*g* for 10 min for disruption. The pellets were washed with distilled water and resuspended in breaking buffer (50 mM sodium phosphate, pH 7.4, 1 mM EDTA, 5 % (v/v) glycerol, and freshly made 1 mM PMSF). An equal volume of acid-washed glass beads (0.5 mm, Sigma) and 0.2 % (w/v) AMP clay; glass beads only; or 0.2 % AMP clay only were added to the cell suspensions. In a primary experiment the concentration of 0.2 % was chosen from a serial of 0.2, 0.5 and 1 % as the most suitable amount of AMP clay added. The mixture was agitated as follows: a 30 s vortex followed by an interval of 30 s on ice and sample collection after every 2 min. The samples were centrifuged at 4000×*g* for 10 min at 4 °C, and protein concentration of the supernatant was measured by Bradford assay. The experiments were repeated 5 times and each figure was measured 3 times for average. As shown in Table 1, the starting concentrations of all samples (from 0 to 2 min) were too low to show any difference; as time went on, the results of AMP clay-assisted glass beads and glass beads mill only method displayed statistically significant difference ($p = 0.038$). In the combined method, the protein concentration increased and reached the highest level at 4.24 mg/ml after 4 min. With the beads mill only method, the highest protein concentration obtained was 3.81 mg/ml at 8 min. The disruption time assisted with AMP clay was half shorten, while the protein concentration extracted increased by 11.2 %. As expected, the methods using the negative control or AMP clay only did not yield proteins at a detectable level. Similar results were also observed when AMP clay was combined with sonication.

The supernatant samples were diluted ten times and checked by SDS polyacrylamide gel electrophoresis (SDS-PAGE, Bio-Rad Mini-PROTEAN 4-gel electrophoresis cell, 15 % polyacrylamide gel, 120 V for 2.5 h). As presented in Fig. 1, there was a significant increase in protein extraction from 0 to 2 mg/ml at 4 min using both the AMP clay-assisted beads mill and the beads mill only; however, all the bands from the method using AMP clay only were obscure. It's interesting to find that the amount of CCMV CP (approximate 20 kDa, boxed bands in Fig. 1) obtained from the combined method was much higher than that from the method using glass beads only: 0.82 mg/ml compared to 0.73 mg/ml (calculated by software BandScan v5.0). This indicated that AMP clay could preserve coat protein from degradation during disruption.

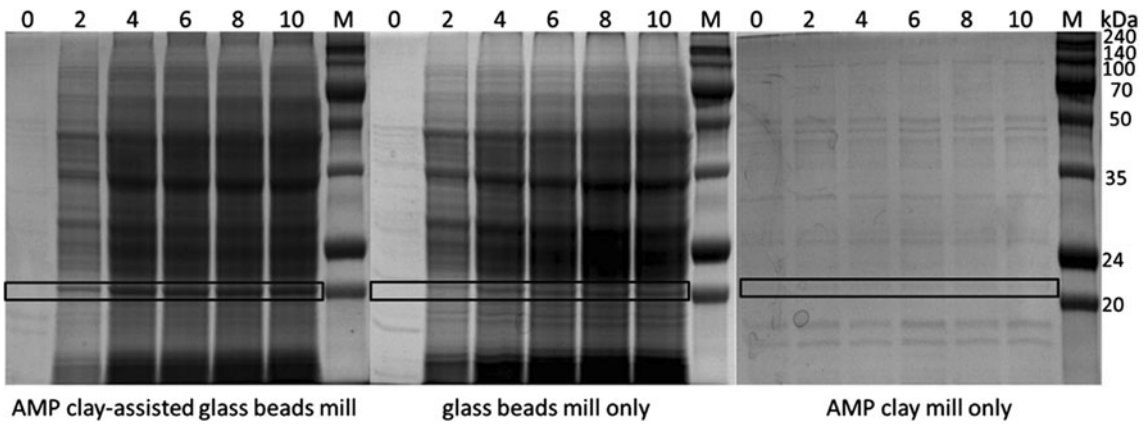

Fig. 1 Comparison of SDS-PAGE results by different cell disruption methods. Time 0, 2, 4, 6, 8, 10 min; the boxed band region was recombinant CCMV capsid protein; M, DokDo-MARK^{TM} Broad-range

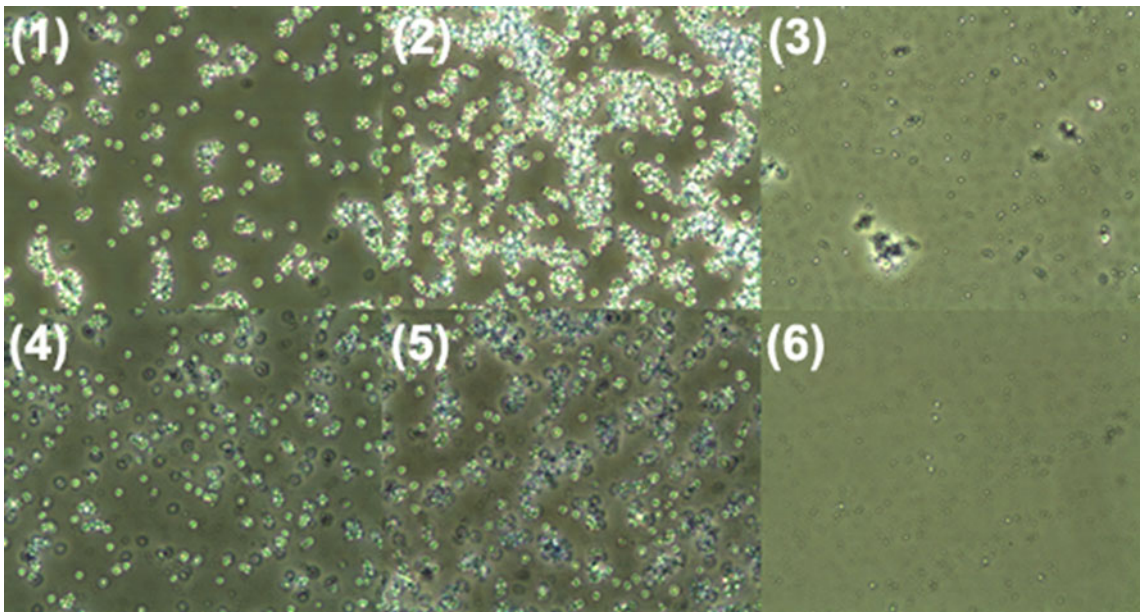

Fig. 2 Microscopy pictures of *Pichia* cell disruption by different methods. (1), (2), (3) were from AMP clay-assisted glass beads mill as time of 0, 4, and 10 min; (4), (5), (6) were from glass beads mill only as time of 0, 4, and 10 min as control

To check the influence of AMP clay on the lysis process, oil-immersion light microscopy was introduced to assess cell breakage and debris size using Nikon Eclipse TS100 microscope (Nikon, Japan). Samples were diluted to the equivalent of a 1 % cell slurry solution and examined at 400× magnification. From Fig. 2, the lysate from the AMP clay-assisted method showed a change from the initial aggregation to small cellular debris with large and irregular in shape. This change may be attributed to the binding of *Pichia* cells with AMP clay in the solution via electrostatic interactions. In contrast, the lysate from the glass beads only method revealed extensive fragmentation of cells with almost no large particles of aggregated cellular debris visible after the disruption.

Subsequently, a modified viral capsid purification procedure based on polyethylene glycol (PEG) precipitation and density gradient centrifugation was used to purify CCMV VLPs (Ali and Roossinck 2007). The concentration of purified CCMV CP by AMP clay assisted method was 0.28 mg/ml, which was a little higher compared to 0.23 mg/ml obtained by glass beads mill only. The recovery efficiency of target product by the combined method was 6.6 % of total protein (4.24 mg/ml) while it was 6.1 % of total protein (3.81 mg/ml) in the unmodified method. The purified CCMV VLPs were reassembled in sodium acetate buffer and analyzed by transmission electron microscopy (TEM) with High-Resolution Transmission Electron Microscope JEOL JEM 3010 (Electron Microscopy Laboratory, KAIST, Korea). CCMV CP reassembled into spherical VLPs with an average diameter of 28 nm as observed in Fig. 3. This result was identical to that of the control disrupted by the beads mill, implying that the assembly of viral capsids was not affected by AMP clay. Another recombinant GS115/pPICZ/lacZ (Mut^+) carried a fused lacZ gene was also disrupted by both methods to check whether AMP clay would affect the functionality of recombinant proteins in *P. pastoris*. Similar enzyme activity of crude β-galactosidase was observed in both methods. This suggested that AMP clay caused no denaturation or side effect on enzyme activity of recombinant proteins in *P. pastoris*.

As demonstrated by Lee et al. (2010), AMP clay was an organoclay-modified derivative in the form of nanocomposite $Si_8Mg_6O_{20}(OH)_4$. It was easy and inexpensive to synthesize and the amount added here was quite little which would not cause the increase of material cost. From the

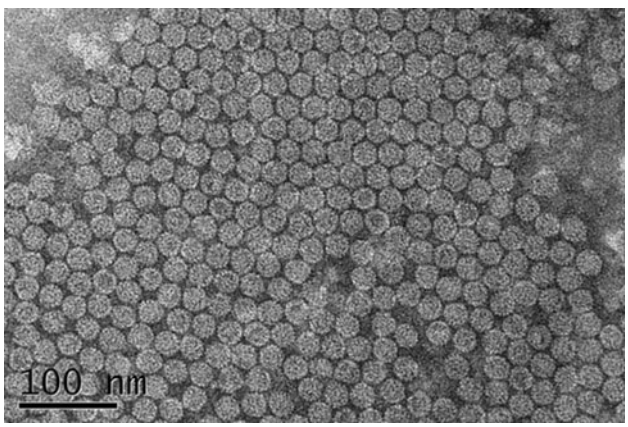

Fig. 3 TEM picture of CCMV VLPs by AMP clay combined glass beads mill. The spherical particles showed an average diameter of 28 nm

parent structure, AMP clay possesses hydrophilic and protonated groups (R-NH_2) which create a number of binding sites for ion exchange within the interlayer spaces and serve as surface groups on the lamella (Holmström et al. 2007). The interaction between AMP clay and the negatively charged layer of glucan, chitin and mannoproteins destroyed the rigidity of cell wall, encouraged cell wall leakage and increased permeability, which ultimately lead to cell lysis. Under the high shear stress resulting from the collision between cells and glass beads in vigorous agitation, the addition of AMP clay may enhance the lysis process significantly. Considering the higher yield of CCMV CP and well-assembled VLPs, the spaces between the clay sheets may shelter the proteins extracted from the cytoplasm in the buffer and preserve them from degradation caused by glass beads.

In conclusion, a modified AMP clay-assisted glass beads mill was provided for *Pichia* cell disruption at the laboratory scale without cost increase. The treatment time was shortened by half, while the yield of extracted proteins was 11.2 % higher. The stability of CCMV VLPs demonstrated this method to be a simple and reliable method for yeast cell lysis.

Acknowledgments This study was supported by the research fund from chosun university, 2010. We thank Dr. Young-Chul Lee (KAIST) for providing the TEM pictures.

References

Ali A, Roossinck MJ (2007) Rapid and efficient purification of Cowpea chlorotic mottle virus by sucrose cushion ultracentrifugation. J Virol Methods 141:84–86

Cereghino JL, Cregg JM (2000) Heterologous protein expression in the methylotrophic yeast *Pichia pastoris*. FEMS Microbiol Rev 24(1):45–66

Chandrasekaran G, Han HK, Kim GJ, Shin HJ (2011) Antimicrobial activity of delaminated aminopropyl functionalized magnesium phyllosilicates. Appl Clay Sci 53:729–736

Ferreira RB, da Silva CR, Pastore HO (2008) Aminopropyl-modified magnesium phyllosilicates: layered solids with tailored interlayer access and reactivity. Langmuir 24:14215–14221

Geciova J, Bury D, Jelen P (2002) Methods for disruption of microbial cells for potential use in the dairy industry–a review. Int Dairy J 12:541–553

Holmström SC, Patil AJ, Butler M, Mann S (2007) Influence of polymer co-intercalation on guest release from aminopropyl-functionalized magnesium phyllosilicate mesolamellar nanocomposites. J Mater Chem 17:3894–3900

Kollár R, Reinhold BB, Petráková E, Yeh HJ, Ashwell G, Drgonová J, Kapteyn JC, Klis FM, Cabib E (1997) Architecture of the yeast cell wall. β(1–6)-glucan interconnects mannoprotein, β(1–3)-glucan and chitin. J Biol Chem 272:17762–17775

Lee YC, Lee TH, Han HK, Go WJ, Yang JW, Shin HJ (2010) Optical properties of fluorescein-labeled organoclay. Photochem Photobiol 86(3):520–527

Smits GJ, van den Ende H, Klis FM (2001) Differential regulation of cell wall biogenesis during growth and development in yeast. Microbiology 147:781–794

Stowers CC, Boczko EM (2007) Reliable cell disruption in yeast. Yeast 24(6):533–541

Wenger MD, DePhillips P, Price CE, Bracewell DG (2007) An automated microscale chromatographic purification of virus-like particles as a strategy for process development. Biotechnol Appl Biochem 47:131–139

Wu Y, Yang H, Shin HJ (2011) Expression and self assembly of cowpea chlorotic mottle virus capsid proteins in *Pichia pastoris* and encapsulation of fluorescent myoglobin. MRS Proceedings 1317:mrsf10-1317-rr03-05

Korean J. Chem. Eng., **30**(7), 1359-1367 (2013)
DOI: 10.1007/s11814-013-0083-y

REVIEW PAPER

Viruses as self-assembled nanocontainers for encapsulation of functional cargoes

Yuanzheng Wu*,, Hetong Yang**, and Hyun-Jae Shin*,†**

*Department of Chemical and Biochemical Engineering, Chosun University,
#375, Seosuk-dong, Dong-gu, Gwangju 501-759, Korea
**Biotechnology Center of Shandong Academy of Sciences, No. 19 Keyuan Road, Jinan 250014, China
(*Received 21 March 2013 • accepted 9 May 2013*)

Abstract−Viruses naturally exhibit an incredible variety of sophisticated nanostructures, which makes them ideal biological building blocks for nanoengineered material research. By mimicking their spontaneous assembly process, tremendous advances have been made towards utilizing virus and virus-like particles (VLPs) as protein cages, scaffolds, and templates for nanomaterials in the last few years. This review outlines recent progress in the field of bionanotechnology in which viruses are introduced to encapsulate various functional cargoes in a precise and controlled fashion. The encapsulation mechanisms are summarized into three main strategies: electrostatic interaction, chemical conjugation, and covalent attachment by genetic manipulation. The combination with chemical modification and genetic engineering heralds a brilliant future for fabrication of functional nanomaterials. These well-defined architectures will find attractive applications in biosensing, drug delivery, enzyme confinement, light-harvesting system, and pharmaceutical therapy.

Key words: Virus, Virus-like Particles (VLPs), Encapsulation, Nanomaterials, Drug Delivery

INTRODUCTION

Bionanotechnology, or nanobiotechnology, has become a rapidly developing area of science research for its tremendous applications [1]. Biological materials that display an astonishing variety of highly sophisticated architectures are appropriate nanostructures for new material development. Their prescribed shape together with the chemical and physical functionality provides huge advantages over other inorganic and organic substances [2]. Since the last decade, self-assembled natural protein complexes, such as viruses and virus-based nanoparticles (VNPs), ferritins [3], small heat shock protein [4], and enzyme complexes [5], have been employed as building blocks and templates in bionanotechnology. These bionanoparticles (BNPs) can form robust biosynthetic machineries while still being capable of modification by genetic and chemical approaches.

Viruses and noninfectious virus-like particles (VLPs) exhibit the characteristics of ideal building blocks for their exquisite symmetry, uniformity of size and shape, and precise assembly of hundreds of molecules into highly organized scaffolds [6]. They can undergo a reversible disassembly/reassembly process *in vivo* and *in vitro*. Chemical and genetic manipulations on the surface of viral protein cages confer unique properties to VLPs as programmable scaffolds in bionanotechnology [7]. The enclosed space in the interior of VLPs can encapsulate and release various functional moieties. Due to the well-defined structure and self-assembling system, a large number of VLPs have been elaborated to function as constrained reaction vessels, imaging agents, drug/gene delivery vehicles, and other nanomaterials. From the viewpoint of material scientists, viruses provide another type of widely studied biological macromolecules in nanometer scale, i.e., organic nanoparticles, which are composed of nucleic acids, capsid proteins, and sometimes envelopes [8].

Recently there have been some detailed reviews which summarize the remarkable progress of viruses or protein cages in biomedicine and nanomaterial research [9-11]. In this review, we focus on the encapsulation of functional materials by these viruses to illustrate their utilizations in nanotechnology.

VIRUS CAPSIDS

Historically studied for their effects as pathogens, viruses play a key role in biological systems as the most abundant biological entities on earth. Viruses especially lacking genomic nucleic acid are widely used as emerging platforms in bionanotechnology. These viruses exhibit a distinctive diversity of shapes and sizes, from simple helical and icosahedral forms to more complex structures, ranging between 20 and 750 nanometers. In this part various viruses and VLPs that have been studied in the field of nanotechnology will be presented (Fig. 1).

Icosahedral virus particles are nearly spherical and exhibit icosahedral symmetry in their arrangement [12]. The icosahedron is composed of equilateral triangles fused together into a closed shell, which generally has 20 facets and 12 vertices formed by one or several identical coat protein (CP) subunits (known as capsomers). The spherical lattices are collections of two-, three-, and fivefold rotation axes (5 : 3 : 2 symmetry). The protein shell usually assembles from 60- and 180-comma structures of pentamers and hexamers. The quasi-equivalence principle of protein subunits and their three-dimensional arrangement is illustrated by the triangulation (*T*) number, which was originally proposed by Caspar and Klug in 1962 [13]. Icosahedral viruses can self-assemble spontaneously into capsids with diameter about 20-80 nm, and the size of capsids depends on the

†To whom correspondence should be addressed.
E-mail: shinhj@chosun.ac.kr
‡This paper is dedicated to commemorate Prof. Ji-Won Yang (KAIST) for his retirement.

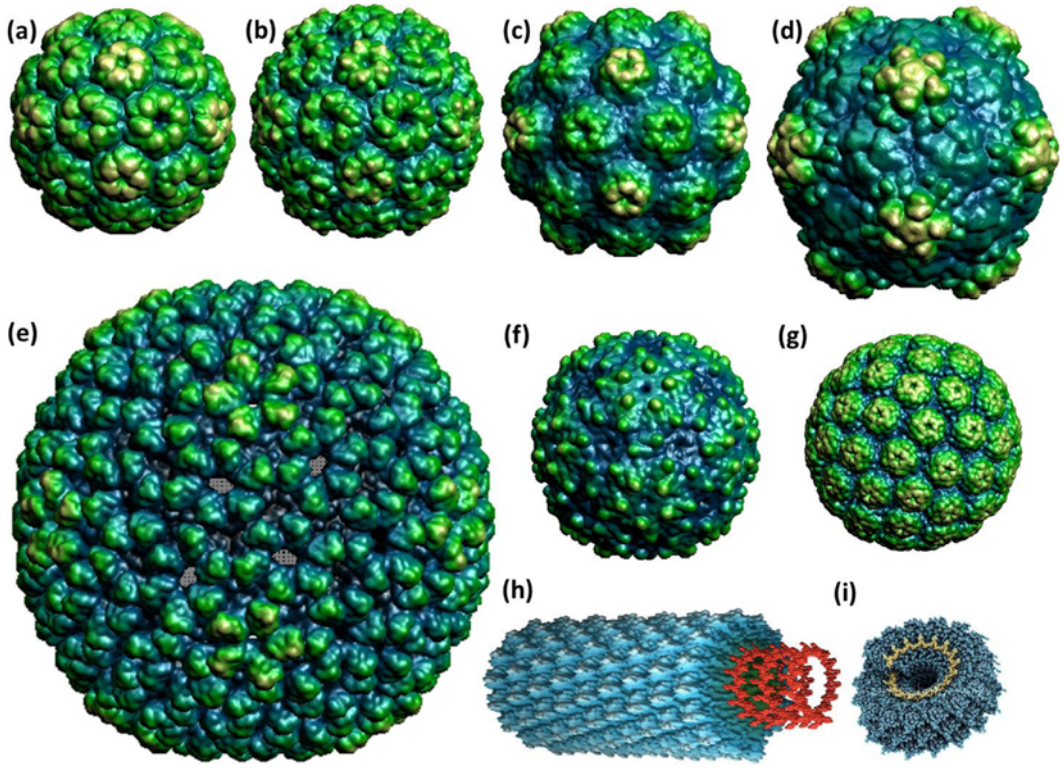

Fig. 1. Structures of virus particles used for nanotechnology. (a) Brome mosaic virus (BMV), 27 nm in diameter; (b) cowpea chlorotic mottle virus (CCMV), 28 nm in diameter; (c) turnip yellow mosaic virus (TYMV), 30 nm in diameter; (d) red clover necrotic mosaic virus (RCNMV), 36 nm in diameter; (e) bacteriophage P22, 58 nm in diameter; (f) bacteriophage MS2, 26 nm in diameter; (g) simian virus 40, 25 nm in diameter; (h) tobacco mosaic virus (TMV), 18 nm in diameter and variable in length; (i) top view of TMV. Structures (a)-(g) were obtained from the VIPER, URL: http://www.viperdb.scripps.edu/; TMV image by Jean-Yves Sgro, U. Wisconsin.

size and number of capsomers. The interior cavity of these cages offers the capacity to package genomic materials or encapsulate other particles.

Helical viruses are comprised of a single type of capsomer stacked around a central axis to form a helical structure, which results in a central cavity or hollow tube [12]. These viral helix arrangements are rod-shaped or filamentous, being either short and highly rigid or long and very flexible. The genetic material is enmeshed by the protein helix through interactions between the negatively charged nucleic acid and positive charged protein [14]. Helical particles are typically about 15-30 nm in diameter, and their lengths may range from 300 to 500 nm depending on the genome size.

Complex viruses usually have a combination of icosahedral and helical shape and contain extra appendages such as protein tails and/or complex exterior surfaces [12]. The head-tail structure comprising an icosahedral head bound to a helical tail is unique to bacteriophages that only infect bacteria. The poxvirus is one of the largest viruses and has a complex structure with an outer envelope with a thick layer of protein studded over its surface [15].

1. CCMV

Cowpea chlorotic mottle virus (CCMV) is a model plant virus belonging to the *Bromovirus* group of *Bromoviradea* family [16]. The capsid consists of 180 copies of a single protein (20 kDa, 190 amino acids) that form an icosahedral shell with an outer diameter of 28 nm and an inner diameter of 18 nm (T=3 symmetry). The quaternary structure of CCMV displays 32 prominent capsomers: 12 pentamers and 20 hexamers. CCMV was the first icosahedral virus to be reassembled *in vitro* into an infectious particle from wild-type purified components, i.e., the coat protein and genome RNA. The most profound property of CCMV is that the viral capsid can undergo a reversible structural transition depending on pH and ionic strength. The capsid expands into a radially swollen state around 10% when pH increases from 5.0 to 6.5 under low ionic strength (I<0.1 M). The swelling capsid with 60 separate open pores of 2-nm diameter permits ions to diffuse freely into and out of the cavity. The capsid then disassembles into protein dimers and RNA under high pH (above 7) and ionic strength (I~1 M). After removal of RNA and with a change in pH, the purified coat protein subunits will easily self-assemble and reform the capsids as shown in Fig. 2 [17]. This characteristic provides a unique molecular gating mechanism for entrapment of organic or inorganic materials and release of entrapped materials.

The high yield of CCMV capsid from natural infected leaf tissue (ca. 1-2 mg/g) capsid makes it suitable for the development of viral-based protein cage. Furthermore, heterologous expression of the coat protein in *Escherichia coli*, *Pseudomonas fluorescens*, and *Pichia pastoris* allows genetic alteration by site-directed mutagenesis. The wild and mutant-type of CCMV capsids are tolerant of high temperatures and various pH's, stable in organic solvents (e.g., DMSO), and nonpathogenic for mammals. These conspicuous properties enhance a wide range of chemical modification onto the capsid. The surface exposed amine (lysine), carboxylate (glutamate and aspartate), and thiol (cysteine) residues are accessible for attachment with

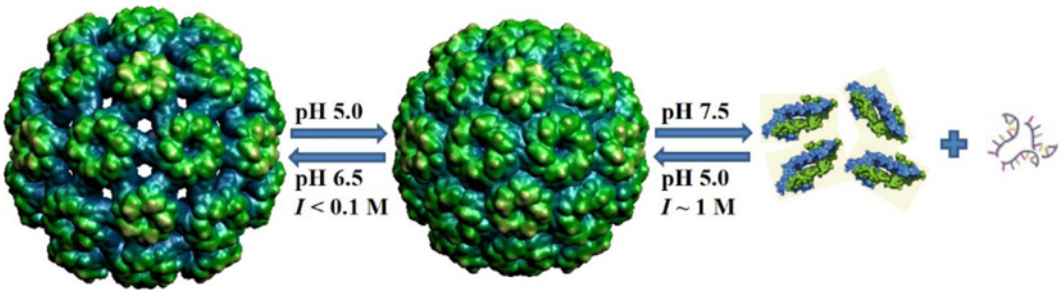

Fig. 2. Schematic representation of CCMV structure transition. With pH increasing from 5.0 to 6.5 under low ionic strength (I<0.1 M), CCMV capsid expands into a swollen state; when pH is increased to 7.5 under high ionic strength (I~1 M), the capsid disassembles into protein dimers and viral RNA. With/without the removal of RNA and pH lowering to 5.0, the protein dimers can be reassembled into empty/intact capsid.

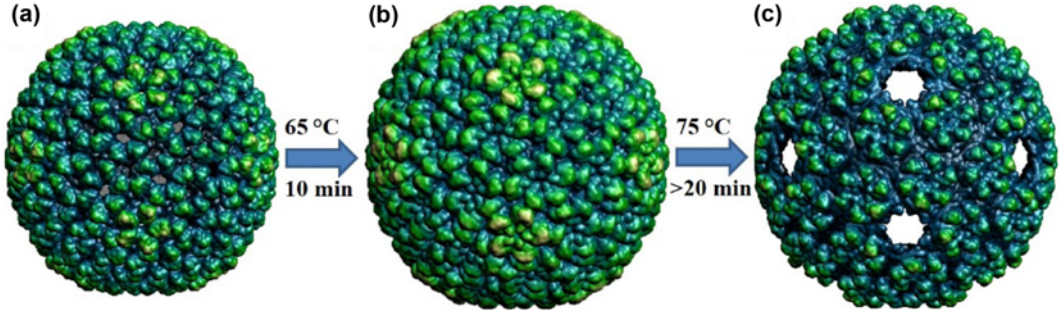

Fig. 3. Schematic representation of P22 structure transformation in three unique forms: (a) empty procapsid shell (ES) with a diameter of 58 nm; (b) mature capsid with a diameter of 64 nm after heating at 65 °C for 10 min; (c) wiffle-ball capsid (WB) after heating at 75 °C over 20 min.

specific ligands and small peptides via chemical interactions [16]. CCMV has feasible applications in biosensors, nanoelectric devices, and drug targeting and delivery.

2. Bacteriophage MS2

Bacteriophage MS2 is an icosahedral virus with an average diameter of 27 nm that infects *E. coli*. It contains one copy of maturation protein responsible for bacterial infection and 180 copies of coat protein (organized as 90 dimers) arranged into the phage head [18]. MS2 exhibits impressive stability to a broad range of temperature, pH, ionic strength, and organic solvent conditions. The coat protein can be propagated in multi-milligram quantities in bacteria by recombinant methods and afterwards be assembled to form empty VLPs. Genetically modified forms of MS2 are available for vaccine development and clinical diagnosis. Interestingly, MS2 also possesses 32 pores per capsid, each approximately 1.8 nm in diameter, which provides ready access to the interior space of moderately sized particles and reagents such as functionalized drug molecules for covalent attachment.

3. Bacteriophage P22

Salmonella typhimuriam bacteriophage P22 is an icosahedral virus assembled from 420 copies of coat protein with the assistance of approximately 300 copies of scaffolding protein (SP) [19]. The P22 capsid undergoes a structural transformation from the 58 nm empty procapsid shell (ES) to the mature capsid of 64 nm diameter (T=7) which is initiated by DNA packaging. The transformation can be mimicked *in vitro* by gentle heating (65 °C for 10 min). Further heating (75 °C over 20 min) produces a new form of wiffle-ball (WB) which has a 10 nm pore at each of the 12 icosahedral vertices caused by the release of subunits from the mature capsid (Fig. 3) [20]. The large pores of WB ensure free molecular exchange between the interior and exterior environments of the capsid. This unique characteristic makes the P22 capsid become a remarkable dynamic nanoplatform for synthetic utilization.

4. RCNMV

Red clover necrotic mosaic virus (RCNMV) is an icosahedral soil-transmitted virus with a diameter of 36 nm (T=3). The capsid of RCNMV is comprised of 180 copies of a 37 kDa coat protein packaging ssRNA [21]. The capsid has been demonstrated as a versatile container to entrap various nanoparticles in the diameter range 3-15 nm using RNA-dependent packaging based on the origin of assembly of RCNMV. Cryo-electron microscopy provides a molecular-level description of the mechanism whereby the RCNMV capsid undergoes a reversible opening and closure of pores at the pseudo-3-fold axes under control of divalent cations (Ca^{2+} and Mg^{2+}). Fluorescent dye and drug molecules have been incorporated into the interior cavity of RCNMV.

5. TMV

Tobacco mosaic virus (TMV), also known as tobamovirus, is a helical plant virus with a length of 300 nm and diameter of 18 nm. Its capsid is made from 2130 copies of coat protein arranged around the viral RNA [22]. The rod-like spiraling structure (16.3 proteins per helix turn) shows a distinct inner channel of 4 nm. Purified TMV coat protein undergoes a reversible states shift from micron-length rods in acetate buffer (pH 5.5) to double disks in phosphate buffer (pH 7.0). The internal and external surfaces of TMV capsid consist of repeated patterns of charged amino acid residues such as glutamate,

aspartate, arginine, and lysine that are viable for chemical ligation and bioconjugation [23]. TMV can be purified from infected tobacco plants in kilogram quantities. The particle is remarkably robust *in vitro*, remaining intact at temperatures up to 80 °C and pH values between 2 and 10. The assembled capsids have been used as templates to grow metal or metal oxide nanowires and coated conductive nanowires. TMV based materials offer a wide variety in the field of nanoelectronics, energy storage, and light harvesting.

MECHANISM OF ENCAPSULATION

The genomic RNA or DNA of virus is generally packaged within the capsid through a simple assembly and disassembly process *in vivo*. Scientists have discovered that a variety of phages, plant, and animal viruses can be assembled *in vitro* from their molecular components: proteins, nucleic acid, and sometimes lipids. Bancroft et al. first revealed the electrostatic interaction as the driving force for efficient packaging and assembly by encapsulation of polyanions instead of ssRNA inside icosahedral viruses [24]. The thermodynamic force during the assembly may include both specific and nonspecific interactions between the capsid and the genome, and there is no net delimitation to define these two mechanisms. The coat protein subunits themselves can spontaneously assemble into noninfectious VLPs under proper pH and ionic strength. From the viewpoint of material science, the highly uniform VLPs can be regarded as organic nanoparticles. The principle regulating the encapsidation of the genetic materials can also be utilized to load functional cargoes. The encapsulation occurs simply by mixing the protein subunits with cargo particles at specific ionic strength, temperature, and pH ranges. There have been numerous explorations in this respect, using viruses such as CCMV, brome mosaic virus (BMV), cucumber mosaic virus (CMV), RCNMV, hibiscus chlorotic ringspot virus (HCRSV) [25], simian virus 40 (SV40) [26], and bacteriophage MS2 (summarized in Table 1). The packaged functional cargoes include polymers, enzymes, liquid droplets, nucleic-acid functionalized particles, and even ligand-coated particles [27]. According to the encapsulation mechanisms, there are three main strategies, which will be discussed as follows.

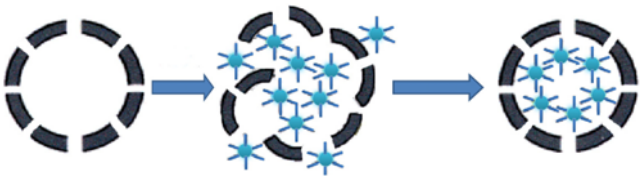

Fig. 4. Schematic diagram of encapsulation of foreign cargoes by viral capsids driven by electrostatic interaction. The negatively charged materials can act as the compressing genetic core to promote the assembly of a virus-like capsid as the natural type.

1. Electrostatic Interaction

The first strategy is to encapsulate the negatively charged species driven by electrostatic interaction (Fig. 4). The foreign material, for example, nanoparticles functionalized with anionic moieties or specific nucleic acid packaging signals and separated protein subunits, acts as the compressing genetic core to promote the assembly of a virus-like capsid like the natural type [28].

Douglas and Young first demonstrated the mineralization of two polyoxometalate species (paratungstate and decavanadate) and the encapsulation of an anionic polymer (poly-anetholesulphonic acid) inside CCMV capsids [29]. CCMV has been widely studied as a prominent example by several research groups for the ability to encapsulate various compounds. The exterior of the particle has a neutral charge, whereby the interior surface carries a high positive charge due to the presence of nine basic residues (arginine and lysine) on each subunit of coat protein. A straightforward way to entrap negatively charged molecules inside CCMV is to reversibly alter the pH to induce swelling and contraction of the capsid to facilitate the entry and sequestering of the foreign material. Nolte et al. further exploited the entrapment by CCMV with negatively charged polyelectrolytes including poly (styrene sulfonate) (PSS), polyferrocenylsilane (PFS), and poly[(2-methoxy-5-propyloxy sulfonate)-phenylene vinylene] (MPS-PPV) [30,31]. The encapsidation can lead to monodisperse or polydisperse formation of T=1, 2, and 3 VLPs. These

Table 1. Summary of viral capsids used for the encapsulation study

Encapsulation mechanism	Viral capsids	Encapsulated cargoes [Ref.]
Electrostatic interaction	CCMV	Polyoxometalate, polyelectrolytes, enzymes [29-31,35]
	TMV	CdS, PbS, silica, and iron oxide [32]
	BMV	PEGylated gold nanoparticles [33]
	RCNMV	Au and $CoFe_2O_4$ nanoparticles, Quantum dots (Qds) [34]
Chemical conjugation	TMV	The interior glutamate residues coupled by carbodiimide reaction [37]
	Bacteriophage MS2	The interior tyrosine residues coupled with diazonium salt of *p*-nitroaniline [38]
	Rotavirus VP6	The interior carboxyl groups coupled with the amine groups of DOX [39]
Covalent attachment by genetic manipulation	CCMV	The K-coil-modified capsids interacted with E-coil-EGFP by coiled-coil linkers [41]
	JC virus	The installed hexahistidine motif (His_6GFP) specifically binded with nitrilotriacetic acid-sulforhodamine (NTA-SR) by His_6-tag affinity [45]
	Bacteriophage P22	Cysteine residues introduced on valine 119 (V119C), lysine 110 (K110C) and lysine 118 (K118C), bioconjugated with maleimide-PEO_2-biotin (MPB) [42]
	Bacteriophage MS2	Cysteine residues introduced on asparagine 87 (N87C), bioconjugated with Alexa Fluor 488 maleimide [43]

approaches could be utilized for the encapsulation of negatively charged drug molecules for pharmaceutical applications in future.

Interestingly, the internal mineralization of CdS, PbS, silica, and iron oxide using TMV capsids, which led to the template-directed synthesis of inorganic-organic nanotubes, was also achieved [32]. The inner surface of TMV showed a high spatial density of glutamic acid residues, suggesting that nucleation within the 4 nm wide inner channel might have been expected under these conditions. The virus-based hybrid nanomaterials hold promise for development as platforms for the creation of hybrid materials with engineering applications such as nanowires and catalysts.

Dragnea et al. have shown that PEGylated gold nanoparticle could act as nucleating core for the self-assembly of BMV capsid, and the size of the formed hybrid VLPs was proportional to the size of anionic polymer cargoes [33]. The artificial core mimicked the process to promote the assembly of a symmetric viral protein structure around it in the absence of genomic RNA. The nonspecic core/capsid interactions were predominant during the assembly of forming capsid. The encapsulation efciency depended on the nanoparticle size, with a maximum efficiency occurring for 12 nm gold nanoparticles. The initial CP to Au particle ratio (CP/Au) with a threshold value above 100 protein subunits per gold nanoparticle was required for a complete capsid. VLPs of varying diameters were found to resemble three classes of viral particles (T=1, 2, and 3) the same way as the wild type of BMV: T=1 BMV capsids (60 CP) was obtained for 6 nm nanoparticle cores, while 12 nm particle cores promoted the formation of T=3 capsids (180 CP).

However, the encapsulation of various nanoparticles by RCNMV was found to yield uniform sized VLPs, independent of the composition and sizes of cores, which ranged from 3 to 15 nm [34]. Apart from the electrostatic interaction between coat protein and genomic RNA, the assembly of RCNMV requires a unique hairpin structure within RNA-2 hybridized with RNA-1 to form the origin of assembly (OAS) for selective recruitment and orientation of CP subunits. An oligonucleotide mimic of the OAS sequence was attached to Au and $CoFe_2O_4$ nanoparticles and Quantum dots (Qds), followed by addition of RNA-1 to form a synthetic OAS to initiate VLPs assembly. Despite the different type and size of packaged nanoparticles, the formed VLPs were homogeneous in size with an average diameter of 32.8 nm, less than that of the native virus at 36.6 nm.

Another fascinating exploration of virus encapsidation is to incorporate individual horseradish peroxidase (HRP) in the inner cavity of CCMV capsid for single enzyme studies [35]. Using the pH-dependent disassembly/reassembly process, HRP was loaded and immobilized in the capsid with only one or no enzyme present per capsid. The fluorogenic substrate dihydrorhodamine 6G diffused in the HRP-containing CCMV capsid where HRP catalyzed the oxidation of this non-fluorescent substrate to produce rhodamine 6G The release of fluorescent product through the pores on the capsid was easily monitored by confocal fluorescence microscope. The spatially confined virus capsid contributes to the understanding of the behavior and the interactions of enzymes at the single-molecule level.

2. Chemical Conjugation

The second strategy is to package the reagents or cargo molecules by chemical conjugation with the coat protein subunit as presented in Fig. 5. The foreign material is first transported and then sequestered inside the capsid by covalent bond such as peptide (amide) bonds between the carboxylate groups of amino acid residues and the amine groups of cargo molecules [36]. The chemically well-defined local environment of the viral cavity provides the circumstance to directly synthesize inside the capsid.

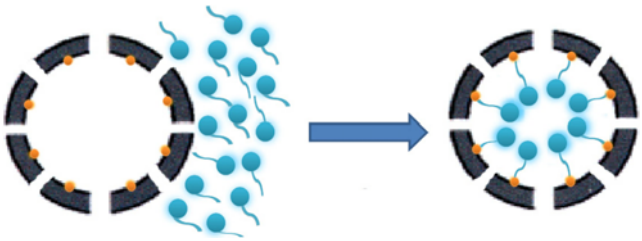

Fig. 5. Schematic diagram of encapsulation of foreign cargoes by viral capsids based on chemical conjugation. The cargo molecules (blue) interact with the functional groups of amino acid residues on the interior of capsids (orange) by covalent bond such as peptide (amide) bonds.

Francis et al. used rod-shaped TMV capsid as a robust and practical scaffold for the preparation of nanoscale materials [37]. Both the exterior and the interior surface of the virus were attached with new functionality strategies separately. As for the inner cavity of TMV, the modification strategy focused on glutamate residues as targets for amide bond by a carbodiimide coupling reaction with 1-ethyl-3-(3-dimethyl-aminopropyl) carbodiimide (EDC). Glu 97 exposed on the core surface was identified as the primary site of modification and Glu 106 was also found with appreciable reactivity, while there was no modification of exterior aspartic acids and carboxy terminus observed. After disassembly/reassembly process the internally modified TMV conjugates revealed rod-shape structures that were virtually identical to the native capsids. Importantly the interior surface could also be doubly modified by rhodamine derivative conjugation with azo-modified capsids, yielding ~650 internal chromophores per 300 nm rod. This method positioned the new functional groups as closely as 1 nm apart on the inside of TMV capsid. Different functional groups were eventually installed on the exterior and interior surfaces of the same capsid assemblies.

Bacteriophage MS2 was also modified using same covalent strategy to load drug molecules and imaging agents. The tyrosine 85 residue located on the interior face of each monomer after capsid assembly could be functionalized by a rapid and efficient coupling with the diazonium salt of *p*-nitroaniline. 50-70 copies of a fluorescent dye (5-amino-N-(2-[FAM-amido]-ethyl)-2-nitrobenzamide) were installed to the phenolic moiety of the tyrosine through the *ortho* azo linkage to serve as visualization probes for subsequent cell-based assays. After decoration of the exterior surface with PEG chains, biotin groups were then placed at the distal ends of the polymer chains to bind with streptavidin. Despite all these high levels of modification, MS2 capsids remained in the assembled state [38]. This modular strategy was developed to attach small targeting molecules on virus capsids for the potential therapeutic delivery.

More recently, the self-assembled rotavirus (RV) VLPs by the major viral protein VP6 were chemically conjugated with an anticancer drug doxorubicin (DOX) [39]. The formation of amide bond between the carboxyl group of VP6 and the amine group of DOX

was achieved in the presence of EDC and N-hydroxysuccinimide (NHS). There are six carboxylate groups on each VP6 subunit exposed on the exterior surface and seven carboxylate groups on the interior surface. For the DOX-loaded VLPs (DVLPs) it was estimated that about 12 DOX molecules were bound to each VP6 protein, meaning that most carboxylate groups on both surfaces were chemically occupied. DVLPs were further linked by lactobionic acid (LA) as target for hepatocytes or hepatoma cells bearing asialoglycoprotein receptors (ASGPRs). LA-modified DVLPs (DVLPLAs) showed specific immunofluorescence in HepG2 cells *in vitro*. The release of DOX from DVLPLAs was simulated under lysosomal conditions, and there was little release without protease in presence. This indicated it was suitable for transportation in the bloodstream (pH close to 7.4). The chemically functionalized VLPs may find practical applications in biomedicine.

3. Covalent Attachment by Genetic Manipulation

The third strategy is to integrate the cargo molecules based on covalent attachment with the site-specific residues on the capsid protein which is engineered through genetic manipulation (Fig. 6). The gene modification of coat protein results in the alteration of the amino acid residues displayed on the interior of the virus cage and even the charge change of the interior surface, which then offers functional versatility amenable to the chemical coupling with target peptides or other cargoes [40].

Making use of heterodimeric coiled-coil linkers, Cornelissen et al. reconstructed the interior cage of CCMV and encapsulated positively charged proteins inside it [41]. The K-coil $(KIAALKE)_3$ with positively charged lysine was introduced at the N-terminus of CCMV CP and E-coil $(EIAALEK)_3$ with negatively charged glutamic acid at the C-terminus of the enhanced green fluorescent protein (EGFP) and the modified proteins were expressed in *E. coli*, respectively. Specific heterodimerization between K-coil and E-coil led to the formation of EGFP-CP complex. After the assembly of EGFP-CP complex with wild-type CP, EGFP-filled capsids were obtained. Depending on the concentration and ratio of EGFP-CP/wt CP, up to 15 EGFP proteins were encapsulated per capsid. This provides a brand new approach of modification on virus capsids by gene manipulation.

Bacteriophage P22 is another virus that has been genetically manipulated to enhance the ability to package programmed cargoes [42]. Three residues of coat protein located on the interior surface were genetically substituted with cysteine residues: valine 119 (V119C) in the middle of the hydrophobic face, lysine 110 (K110C) in the middle of the hydrophilic face, and lysine 118 at the helical border (K118C). Maleimide-PEO_2-biotin (MPB), with a thiol reactive maleimide on one end and a biotin affinity tag to recruit reacting partners of streptavidin (StAv) on the other end, was site-specifically attached with the two morphological types (procapsid shell, ES form and wiffle-ball, WB form) of three mutants. Neither form of V119C was labeled with MPB, suggesting that C119 is not available in either form. While almost all subunits of K110C were labeled with MPB in ES form and completely blocked in WB form, indicating that C110 is only accessible in ES form. Only 35% of subunits of K118C in ES were labeled with MPB, whereas all the subunits were labeled in WB, showing that the partially exposed C118 becomes fully exposed to the interior surface during structural transformation from ES to WB.

Bacteriophage MS2 also presents a readily available scaffold for the construction of targeted delivery agents by genetic modification [43]. Wild type MS2 contains two native cysteines on the interior surface which are inaccessible under normal maleimide bioconjugation conditions. Therefore, a cysteine residue was introduced at asparagine 87 (N87C) of the coat protein. The mutation provided 180 sulfhydryl groups on the interior surface for cargo installation. Through the cysteine alkylation reaction, Alexa Fluor 488 maleimide was encapsulated as fluorescent label. 20-40 copies of 41-nucleotide DNA aptamers that target protein tyrosine kinase 7 (PTK7) receptor on Jurkat T cells were then installed on the outer surface of MS2 shell. The capsids bearing the cell-targeting sequence showed significant binding to Jurkat cells. These suggested that aptamer-labeled capsids could be used as convenient and evolvable targeting groups for drug delivery.

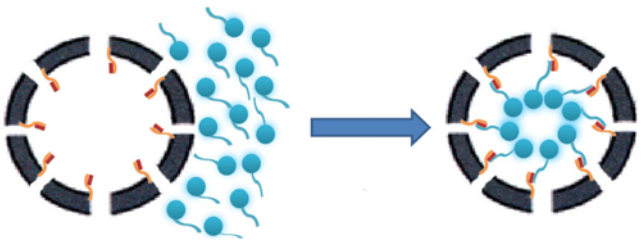

Fig. 6. Schematic diagram of encapsulation of foreign cargoes by viral capsids through genetic manipulation. The additional motifs (red) can be introduced inside virus cages by gene modification, which are amenable to cargo molecules (blue) by specific chemical coupling.

APPLICATIONS

1. Drug Delivery

With excellent biocompatibility and biodegradability, there are

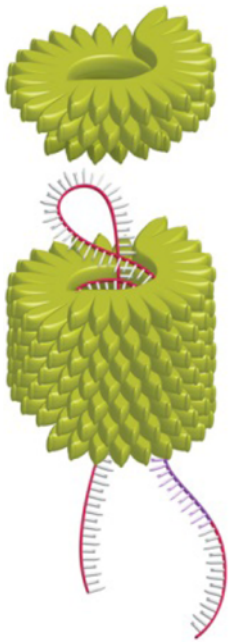

Fig. 7. Schematic representation of TMV-based siRNA formation for gene delivery.

various potential applications of functional self-assembled virus-based materials. Bentley's team has successfully utilized the hollow capsid of TMV as an RNAi carrier for gene delivery into mammalian and insect cells (Fig. 7) [44]. RNA interference (RNAi), which is a process in which RNA molecules reduce gene expression by causing the destruction of specific mRNA molecules, usually involves two small RNA molecules: microRNA (miRNA) and small interfering RNA (siRNA). There is an OAS within TMV genomic RNA which forms a unique hairpin structure and associates with coat protein to initiate the assembly. By incorporating TMV OAS into a siRNA which can program cells to destroy disease-causing proteins, the siRNA could assemble into "pseudo-virions" with coat protein. To deliver the siRNA to the targeted cells, pseudo virions are further modified with synthetic cell-penetrating peptides to facilitate cell endocytosis. The results showed pseudo virions targeting cyclin E (antisense cycE) were capable of arresting cells at G1 phase. TMV can be traced in the blood of most people from second-hand smoke and does not seem to cause irritation or obvious immune-system problems. This TMV-based siRNA packaging system protects the frail siRNA from degradation and provides a means of delivering RNAi constructs into various host cells. Through changing the types of siRNA, multiple diseases from cancers to genetic disorders could be targeted and treated by this therapeutic agent in the future.

A pH-dependent drug release system has been developed based on the JC virus, a type of human polyomavirus, by Ijiro et al. [45]. Green fluorescence protein with N-terminal hexahistidine motif (His_6GFP) was fused to the N-terminus of the inner core protein VP2 (His_6GFP-VP2) and co-expressed with the major coat protein VP1 in *E. coli*. VP1 and His_6GFP-VP2 associated with each other and formed His_6GFP-incorporated VLPs (His_6GFP-VLPs) with a diameter of 52.4±7.1 nm. Nitrilotriacetic acid-sulforhodamine (NTA-SR), containing both a His_6-tag-targeting NTA segment and a fluorescent sulforhodamine segment, could be encapsulated within His_6GFP-VLPs through the 1 nm holes at pH 7.4 and bind specifically to the His_6 tags. NTA was then released from the His_6GFP-VLPs at pH 5.0 due to a decrease in His_6-tag affinity, which has similar pH to the endosome and the lysosome. The process resulted in saturation of release within 20 min. The controlled release of GFP was further examined using NIH3T3 cells. In this system, VP2 acted as an anchoring unit for the protonation of histidines, which could offer specific and reversible attachment of drug molecules. The feasibility of the encapsulation-release system can be used as a cell-specific drug delivery vehicle.

2. Enzyme Nanocontainer

The virus capsid provides a well-defined structure to encapsidate the enzyme in a spatially confined way to observe the catalytic activity even in single-molecule level. The entrapment of enzymes in virus capsids has been done in CCMV, MS2, et al. A precise number of enzyme *Pseudozyma antarctica* lipase B (PalB) loaded into CCMV capsid were accomplished based on a coiled-coil linker described in Section 3.3 and EGFP was co-encapsulated as a non-catalytic protein to investigate the reaction rate [46]. The apparent overall reaction rate increased upon encapsulation and was almost independent of the number of enzymes in the capsid. The encapsulated PalB seemed to have a higher activity than non-encapsulated PalB. It was more likely caused by extremely high confinement molarity (M_{conf}=~1 mM) of the enzyme combined with an increased collision chance due to the spatial confinement leading to very rapid formation of the enzyme-substrate complex. These results highlight the importance of small volumes for efcient multi-enzyme cascade catalysis.

The RNA-removed MS2 capsids were also used to encapsulate *E. coli* alkaline phosphatase (PhoA) [47]. To increase the yield of encapsulation, PhoA was tagged with a 16 acidic peptide at C-terminus (PhoA-neg); trimethyl amine N-oxide (TMAO) was added as an osmolyte to decrease protein unfolding and increase the thermal stability. After incubation of PhoA-neg with disassembled coat protein dimers under presence of TMAO, intact capsids with the diameter of 27 nm were observed. About 1.6 PhoA-neg dimers were packaged per capsid. Enzyme assay was monitored by the hydrolysis of 4-methylumbelliferyl phosphate to yield fluorescent 4-methylumbelliferone. The value of K_m was equal to that of the free enzyme dimer and the K_{cat} was slightly reduced when the enzyme was encapsulated, possibly due to the constrained enzyme environment. This method provides a practical and potentially scalable way of studying the complex effects of encapsulating enzymes in protein-based compartments.

3. *In Vivo* Imaging

Near infrared (NIR) fluorescence imaging based upon virus capsids is particularly advantageous in optical imaging and therapy of disease. Indocyanine green (ICG), an FDA-approved NIR chromophore, was encapsulated into BMV for the utilization of mammalian intracellular optical imaging [48]. Instead of genomic RNA, the negatively charged ICG interacted with the positively charged arginine-rich motif in the N-terminus of BMV CP subunits to assemble into optical viral ghosts (OVGs). The mean diameter of OVGs was ~24.3 nm in T=1 symmetry. OVGs maintained stable at the absorption spectrum of ICG in the 600-900-nm NIR range and reduced by ~15% for 3 h at 37 °C. Human bronchial epithelial (HBE) cells were used to detect the intracellular optical imaging of OVGs, with the result that OVGs were internalized and localized at more than 90% of the HBE cells after 3 h. These constructs may serve as a potentially nontoxic and multifunctional nanoplatform for site-specific deep-tissue optical imaging and therapy of disease.

4. Light-harvesting System

A virus-based approach has been developed as light-harvesting systems through self-assembly. Recombinant TMV CP monomers with a reactive cysteine residue were constructed for the thiol-reactive chromophore attachment [49]. Three chromophores were installed on the interior surface of TMV including Oregon Green 488 maleimide as the primary donor, tetramethylrhodamine maleimide as an intermediate donor, and Alexa Fluor 594 maleimide as the acceptor. The conjugated TMV VLPs could be assembled into stacks of disks or rods under different buffers. Under both morphologies, there was efficient energy transfer (over 90% overall efficiency) observed using fluorescence spectroscopy, from numbers of donor chromophores to a single acceptor. Later, multiple porphyrin arrays were accomplished similarly in TMV, in which Zn-porphyrin (ZnP) was coordinated as donor and free-base porphyrin (FbP) as acceptor [50]. The photophysical properties of the arrayed porphyrins in the TMV assemblies were examined by time-resolved fluorescence spectroscopy, and the energy transfer rates were determined to be 3.1-6.4×10^9 s^{-1}. CCMV capsids were also employed to package and syn-

thesize TiO_2 nanoparticles, which showed similar structure to nanocrystalline anatase and photocatalytic activity [51]. This highly tunable method has emerged for the construction of photovoltaic devices.

CONCLUSION AND OUTLOOK

The ability to precisely encapsulate components into virus capsids by self-assembly, chemical conjugation, or genetic manipulation has inspired the creation of complex systems with novel functions. However, we should not just focus on one side of the coin. Today there are two main trends in the fabrication of modified virus capsids for nanotechnology: surface modification and encapsulation [52]. The selective chemical derivatization of viral exterior surface that allows the attachment of fluorescent dyes, gold clusters, and specific moieties has been demonstrated permissible in myriad viruses, e.g., cowpea mottle virus (CPMV) was exploited as addressable nanoblocks which can be imbued with a variety of chemical and physical properties [53].

As mentioned, the combination of two methods turns out to be more delicate and efficient for practical utilization. The chemical addressability of exterior and interior surfaces of virus capsids by covalent bioconjugation such as diazonium coupling and Cu(I)-catalyzed azide-alkyne cycloaddition (CuAAC) reaction [54] provides a diversity of functional moieties of versatile repertory. These dual modified VLPs can specifically recognize certain types of cells, attach with corresponding receptors, and deliver the packaged cargoes into the endosome.

Furthermore, quite a few plant viruses such as CCMV, CPMV, TMV, and rodlike phages have been shown to be noninfectious to humans and mammals in general, and will not induce obvious toxicity and immune response in human beings [55]. These will be quite promising nanocarriers with some issues concerning the toxicity and immunology to be fully evaluated. Virus particles have presented distinguished stability and flexibility for pharmaceutical application, biomaterial fabrication, and photovoltaic construction. More light will be cast upon these elegant and elaborate creations in the future.

ABBREVIATIONS

BMV : brome mosaic virus
BNPs : bionanoparticles
CCMV : cowpea chlorotic mottle virus
CMV : cucumber mosaic virus
CP : coat protein
CPMV : cowpea mottle virus
CuAAC : Cu(I)-catalyzed azide-alkyne cycloaddition
DOX : doxorubicin
EDC : 1-ethyl-3-(3-dimethyl-aminopropyl) carbodiimide
EGFP : enhanced green fluorescent protein
ES : empty procapsid shell
FbP : free-base porphyrin
HBE : human bronchial epithelial
HCRSV : hibiscus chlorotic ringspot virus
HRP : horseradish peroxidase
ICG : indocyanine green
LA : lactobionic acid
miRNA : microRNA
MPB : maleimide-PEO_2-biotin
MPS-PPV : poly[(2-methoxy-5-propyloxy sulfonate)-phenylene vinylene]
NHS : N-hydroxysuccinimide
NIR : near infrared
NTA-SR : nitrilotriacetic acid-sulforhodamine
OAS : origin of assembly
OVGs : optical viral ghosts
PalB : *Pseudozyma antarctica* lipase B
PFS : polyferrocenylsilane
PhoA : *E. coli* alkaline phosphatase
PSS : polystyrene sulfonate
PTK7 : protein tyrosine kinase 7
Qds : Quantum dots
RCNMV : red clover necrotic mosaic virus
RNAi : RNA interference
RV : rotavirus
siRNA : small interfering RNA
SP : scaffolding protein
StAv : streptavidin
SV40 : simian virus 40
TMAO : trimethyl amine N-oxide
TMV : tobacco mosaic virus
VLPs : virus-like particles
VNPs : virus-based nanoparticles
VP : viral protein
WB : wiffle-ball
ZnP : Zn-porphyrin

REFERENCES

1. C. M. Soto and B. R. Ratna, *Curr. Opin. Biotechnol.*, **21**, 426 (2010).
2. J. M. Kim, S. M. Chang, H. Muramatsu and K. Isao, *Korean J. Chem. Eng.*, **28**, 987 (2011).
3. T. Ueno, M. Suzuki, T. Goto, T. Matsumoto, K. Nagayama and Y. Watanabe, *Angew. Chem. Int. Ed.*, **43**, 2527 (2004).
4. K. K. Kim, R. Kim and S. H. Kim, *Nature*, **394**, 595 (1998).
5. G. J. Domingo, S. Orru and R. N. Perham, *J. Mol. Biol.*, **305**, 259 (2001).
6. J. Rong, Z. Niu, L. A. Lee and Q. Wang, *Curr. Opin. Colloid Interface Sci.*, **16**, 441 (2011).
7. J. K. Pokorski and N. F. Steinmetz, *Mol. Pharm.*, **8**, 29 (2011).
8. G. Lee, Y. S. Cho, S. Park and G. R. Yi, *Korean J. Chem. Eng.*, **28**, 1641 (2011).
9. T. Douglas and M. Young, *Science*, **312**, 873 (2006).
10. K. T. Kim, S. A. Meeuwissen, R. J. Nolte and J. C. van Hest, *Nanoscale*, **2**, 844 (2010).
11. K. J. Koudelka and M. Manchester, *Curr. Opin. Chem. Biol.*, **14**, 810 (2010).
12. D. M. Knipe and P. M. Howley, *Fields Virology*, 5th Ed., Lippincott Williams & Wilkins, Philadelphia (2007).
13. D. L. Caspar and A. Klug, *Cold Spring Harb Symp. Quant. Biol.*, **27**, 1 (1962).
14. M. A. Hemminga, W. L. Vos, P. V. Nazarov, R. B. Koehorst, C. J. Wolfs, R. B. Spruijt and D. Stopar, *Eur. Biophys. J.*, **39**, 541 (2010).
15. C. Gubser, S. Hué, P. Kellam and G. L. Smith, *J. Gen. Virol.*, **85**, 105

(2004).
16. J. A. Speir, S. Munshi, G. Wang, T. S. Baker and J. E. Johnson, *Structure*, **3**, 63 (1995).
17. F. Tama and C. L. Brooks III, *J. Mol. Biol.*, **318**, 733 (2002).
18. K. Valegard, L. Liljas, K. Fridborg and T. Unge, *Nature*, **36**, 345 (1990).
19. M. H. Parker, S. Casjens and P. E. Prevelige Jr., *J. Mol. Biol.*, **281**, 69 (1998).
20. C. M. Teschke, A. McGough and P. A. Thuman-Commike, *Biophys. J.*, **84**, 2585 (2003).
21. L. Tang, *Nat. Struct. Biol.*, **8**, 77 (2001).
22. A. Klug, *Philos. Trans. R. Soc. Lond. B Biol. Sci.*, **354**, 531 (1999).
23. M. Demir and M. H. Stowell, *Nanotechnology*, **13**, 541 (2002).
24. J. B. Bancroft, E. Hiebert and C. E. Bracker, *Virology*, **39**, 924 (1969).
25. F. Li, Z. P. Zhang, J. Peng, Z. Q. Cui, D. W. Pang, K. Li, H. P. Wei, Y. F. Zhou, J. K. Wen and X. E. Zhang, *Small*, **5**, 718 (2009).
26. Y. Ren, S. M. Wong and L. Y. Lim, *J. Gen. Virol.*, **87**, 2749 (2006).
27. Y. Ma, R. J. Nolte and J. J. Cornelissen, *Adv. Drug Deliv. Rev.*, **64**, 811 (2012).
28. S. E. Aniagyei, C. DuFort, C. C. Kao and B. Dragnea, *J. Mater. Chem.*, **18**, 3763 (2008).
29. T. Douglas and M. Young, *Nature*, **393**, 152 (1998).
30. F. D. Sikkema, M. Comellas-Aragonès, R. G. Fokkink, B. J. Verduin, J. J. Cornelissen and R. J. Nolte, *Org. Biomol. Chem.*, **5**, 54 (2007).
31. M. Brasch and J. J. Cornelissen, *Chem. Commun.*, **48**, 1446 (2012).
32. W. Shenton, T. Douglas, M. Young, G. Stubbs and S. Mann, *Adv. Mater.*, **11**, 253 (1999).
33. M. C. Daniel, I. B. Tsvetkova, Z. T. Quinkert, A. Murali, M. De, V. M. Rotello, C. C. Kao and B. Dragnea, *ACS Nano*, **4**, 3853 (2010).
34. L. Loo, R. H. Guenther, S. A. Lommel and S. Franzen, *J. Am. Chem. Soc.*, **129**, 11111 (2007).
35. M. Comellas-Aragonès, H. Engelkamp, V. I. Claessen, N. A. Sommerdijk, A. E. Rowan, P. C. Christianen, J. C. Maan, B. J. Verduin, J. J. Cornelissen and R. J. Nolte, *Nat. Nanotechnol.*, **2**, 635 (2007).
36. M. Uchida, M. T. Klem, M. Allen, P. Suci, M. Flenniken, E. Gillitzer, Z. Varpness, L. O. Liepold, M. Young and T. Douglas, *Adv. Mater.*, **19**, 1025 (2007).
37. T. L. Schlick, Z. Ding, E. W. Kovacs and M. B. Francis, *J. Am. Chem. Soc.*, **127**, 3718 (2005).
38. E. W. Kovacs, J. M. Hooker, D. W. Romanini, P. G. Holder, K. E. Berry and M. B. Francis, *Bioconjug. Chem.*, **18**, 1140 (2007).
39. Q. Zhao, W. Chen, Y. Chen, L. Zhang, J. Zhang and Z. Zhang, *Bioconjug. Chem.*, **22**, 346 (2011).
40. L. A. Lee, Z. Niu and Q. Wang, *Nano Res.*, **2**, 349 (2009).
41. I. J. Minten, L. J. Hendriks, R. J. Nolte and J. J. Cornelissen, *J. Am. Chem. Soc.*, **131**, 17771 (2009).
42. S. Kang, M. Uchida, A. O'Neil, R. Li, P. E. Prevelige and T. Douglas, *Biomacromolecules*, **11**, 2804 (2010).
43. G. J. Tong, S. C. Hsiao, Z. M. Carrico and M. B. Francis, *J. Am. Chem. Soc.*, **131**, 11174 (2009).
44. C. W. Hung, *RNA packaging and gene delivery using Tobacco mosaic virus pseudo virions*, Ph. D. Thesis, University of Maryland, U.S. (2008).
45. N. Ohtake, K. Niikura, T. Suzuki, K. Nagakawa, S. Mikuni, Y. Matsuo, M. Kinjo, H. Sawa and K. Ijiro, *Chembiochem.*, **11**, 959 (2010).
46. I. J. Minten, V. I. Claessen, K. Blank, A. E. Rowan, R. J. Nolte and J. J. Cornelissen, *Chem. Sci.*, **2**, 358 (2011).
47. J. E. Glasgow, S. L. Capehart, M. B. Francis and D. Tullman-Ercek, *ACS Nano*, **6**, 8658 (2012).
48. B. Jung, A. L. Rao and B. Anvari, *ACS Nano*, **5**, 1243 (2011).
49. R. A. Miller, A. D. Presley and M. B. Francis, *J. Am. Chem. Soc.*, **129**, 3104 (2007).
50. M. Endo, M. Fujitsuka and T. Majima, *Chemistry*, **13**, 8660 (2007).
51. M. T. Klem, M. Young and T. Douglas, *J. Mater. Chem.*, **18**, 3821 (2008).
52. Z. Su and Q. Wang, *Angew. Chem. Int. Ed. Eng.*, **49**, 10048 (2010).
53. Q. Wang, T. Lin, L. Tang, J. E. Johnson and M. G. Finn, *Angew. Chem. Int. Ed.*, **41**, 459 (2002).
54. Q. Wang, T. R. Chan, R. Hilgraf, V. V. Fokin, K. B. Sharpless and M. G. Finn, *J. Am. Chem. Soc.*, **125**, 3192 (2003).
55. N. F. Steinmetz, *Nanomedicine*, **6**, 634 (2010).